ROLE OF THE BAP1/ASXL1 COMPLEX IN MALIGNANT TRANSFORMATION AND THERAPEUTIC RESPONSE

by

Lindsay Marie LaFave

A Dissertation

Presented to the Faculty of the Louis V. Gerstner, Jr.

Graduate School of Biomedical Sciences,

Memorial Sloan Kettering Cancer Center

in Partial Fulfillment of the Requirements for the Degree of

Doctor of Philosophy

New York, NY

July, 2015

_____   _____
Ross L. Levine, MD   Date
Dissertation Mentor

DEDICATION

To my parents, without your endless support and dedication none of this would have been possible.

To my sister, for being the very best of friends and always making me laugh

To my loving husband, for the constant happiness you bring me. You are my everything.

ABSTRACT

Role of the BAP1/ASXL1 Complex in Malignant Transformation

and Therapeutic Response

Somatic mutations in epigenetic modifiers have recently been identified in hematopoietic malignancies and in other human cancers. However, the mechanisms by which these epigenetic mutations lead to changes in gene expression and disease transformation have not yet been well delineated. Epigenetic modifiers include chromatin regulators that modify post-translational modifications on histone molecules. Mutations in *ASXL1* (*Addition of sex combs-like 1*) are a common genetic event in a spectrum of myeloid malignancies and are associated with poor prognosis in acute myeloid leukemia (AML) and myelodysplastic syndromes (MDS). We investigated the role of *ASXL1* mutations on target gene expression and chromatin state in hematopoietic cell lines and mouse models.

We performed loss-of-function *in vitro* experiments in AML cell lines and conducted expression analysis. Loss of ASXL1 resulted in increased expression of the posterior *HOXA* cluster. *In vitro* analysis of histone modifications revealed a striking global loss of the repressive H3K27me3 mark, a modification placed by the enzymatic Polycomb Repressive Complex 2 (PRC2). Loss of H3K27me3 was identified locally at specific loci, including the posterior *HOXA* cluster. The data indicate that ASXL1 directly interacts with the PRC2 complex and has a key regulatory role in the placement of H3K27me3 in hematopoietic cells. ASXL1 mutations occur in concert with other classes of mutations in myeloid malignancies, including co-occurrence with mutations in the signaling molecule *JAK2* (*Janus Kinase 2*). We have modeled these co-occurring mutations *in vivo* and assessed changes in chromatin regulation.

ASXL1 interacts with another epigenetic regulator, termed BAP1 *(BRCA1 associated protein-1)* to form a deubiquitinase complex (Polycomb Repressive-Deubiquitinase Complex or PR-DUB) that can remove monoubiquitin from H2AK119. *BAP1,* a ubiquitin hydrolase that provides the catalytic activity for the PR-DUB complex, is frequently mutated in a spectrum of human cancers including metastatic uveal melanoma, mesothelioma, and renal cell carcinoma. However, *BAP1* and *ASXL1* are mutated in distinct cancer types and dysregulation of the PR-DUB complex has not been directly linked to transformation. We hypothesized that BAP1 and ASXL1 have distinct functions in the regulation of gene expression and chromatin state.

We generated a conditional murine *Bap1* loss-of-function model to study the effects of *Bap1* loss on gene expression and chromatin. Conditional deletion of *Bap1* in the hematopoietic system results in a one hundred percent penetrant myelodysplastic syndrome characterized by expansion and enhanced proliferation of myeloid progenitor cells. The majority of genes in *Bap1* KO myeloid progenitors are decreased in expression, including the posterior *HOXA* locus. In contrast to our *ASXL1* loss-of-function studies, we found a global increase of H3K27me3 in *Bap1*-deleted cells. We found that the myeloproliferative phenotype induced by loss of *Bap1* could be rescued by deletion of *EZH2 (Enhance of zeste homolog 2)*, the catalytic component of the PRC2 complex, or pharmacological inhibition of *EZH2* activity. We found that *Ezh2* mRNA and protein levels were upregulated likely due to transcriptional changes mediated by loss of H4K20me1 and identified a novel BAP1 DUB substrate, L3MBTL2, which regulates this mark. In mesothelioma xenograft model systems, *EZH2* inhibition in BAP1-mutant mesothelioma xenograft models was efficacious. Our data demonstrate that loss of *Bap1* leads to Ezh2-dependent malignant transformation and that EZH2 may represent a therapeutic target in *BAP1*-mutant malignancies.

BIOGRAPHICAL SKETCH

ACKNOWLEDGMENTS

The work in this thesis could not have been completed without the help and support of many individuals. I first have to thank my thesis mentor, Ross Levine. My mentorship from Ross began before I joined the lab, where he provided me with advice to choose Gerstner Sloan Kettering to complete my graduate education and helped me with the selection of rotations during my first year. Once joining the lab, Ross has endlessly supported me. While continuously supportive, he allowed me to independently pursue my own interests. Together, we approached important, yet risky, questions that put us in unfamiliar fields. I am forever indebted to Ross for his help in fostering my career as a scientist and helping me in the development of a sense of confidence in my abilities.

I also have to thank Omar Abdel-Wahab for his mentorship during my graduate career. During my rotation in the Levine lab, Omar guided me through experiments and also taught me how to approach research questions, and how to decide which research questions to ask. I am forever grateful to Omar for allowing me to work on the ASXL1 story with him, and his continuing mentorship and friendship.

I would like to thank the members of the Levine Lab for their constant support; I have been fortunate to have worked with such an inspiring and productive group of people. I appreciate the friendships I have made, and want to thank the current and past members for making the lab an enjoyable place to work. I want to highlight Efi Papalexi for her tremendous contributions to the mouse work described in this paper. I would also like to thank the tremendous technicians that have provided support for my thesis project during my time in the lab including Matthew Keller, Kaitlyn Shank, Young Rock Chung and Jihae Ahn. I would also like to thank Priya Koppikar and Neha Bhagwat who helped me get started in the Levine Lab and continue to offer advice. I would also like to thank

I would also like to thank my loving parents for their unending support. Thank you for always pushing me to be the best at whatever excites me. You are my role models and I appreciate all that you have done for me.

I would also like to thank my sister. You are my best friend and continue to inspire me daily.

Lastly, I would like to thank my loving husband Nathan. Your unending devotion and support has pushed me through the challenging times of graduate school and I am forever grateful for that. You constantly inspire me to do the best that I can. I could not have done this without you and I look forward to the adventures ahead.

TABLE OF CONTENTS

LIST OF FIGURES

LIST OF ABBREVIATIONS

CHAPTER I

INTRODUCTION

RATIONALE FOR STUDYING EPIGENETIC MODIFIERS IN HUMAN CANCERS

Before the advent of improved next generation sequencing technologies, cytogenetics and candidate gene sequencing led to the identification of recurrent alterations in myeloid malignancies, including myeloproliferative neoplasms (MPNs), myelodysplastic syndromes (MDS), and acute myeloid leukemia (AML). Functional studies suggested that a hit in each of two classes of mutations would lead to leukemogenesis: Class I mutations that activate downstream signaling cascades resulting in increased survival and Class II mutations that dysregulate the expression of transcriptional targets (*6*). However, improved sequencing technologies have confirmed that not all cases of AML have mutations in Class I and Class II genes (*7*). These studies have also identified novel somatic alterations in epigenetic modifiers, genes that regulate DNA methylation and post-translational histone modifications. Importantly, functional studies have shown that mutations in epigenetic modifiers can lead to aberrant self-renewal in hematopoietic stem and progenitor cells (HSPCs) and to myeloid disease transformation. All together, these data suggest that the two hit transformation model is not sophisticated enough to explain leukemogenesis and the model needs to be altered to include classes of mutations in epigenetic modifiers.

Epigenetics refers to heritable modifications that regulate gene expression but do not result in changes to the DNA sequence. There are numerous regulatory epigenetic modifications including DNA cytosine methylation, hydroxymethylation and histone methylation, acetylation, ubiquitination, and phosphorylation. The mechanisms by which

1

histone modifiers contribute to disease transformation are still not yet well-delineated; therefore, it is therapeutically valuable to understand the manner by which these alleles contribute to disease pathogenesis. Importantly, epigenetic modifications are reversible in contrast to somatic mutations, and are therefore potentially targetable with small molecule inhibitors. Mutations in some epigenetic modifiers, such as *EZH2*, are gain-of-function alterations and are more easily druggable by targeted small molecules (*8*). However, alterations in epigenetic modifiers are often loss-of-function and mechanistic inquiry is critical to understand how to therapeutically intervene in patients with these mutations. The work in this thesis primarily focuses on studying proteins that regulate chromatin modifications, namely histone methylation, in hematopoiesis and disease transformation. The goal of this thesis is to understand the mechanism by which loss-of-function mutations in the epigenetic modifiers ASXL1 and BAP1 contribute to hematopoietic disease pathogenesis and how these findings can inform therapeutic intervention.

MYELOID MALIGNANCIES

Myeloid malignancies are clonal disorders of hematopoiesis caused by alterations in hematopoietic stem and progenitor cells. Mutations contributing to these malignancies tend to cause aberrant differentiation, proliferation and/or self-renewal. These diseases include myleodysplastic syndromes (MDS), myeloproliferative neoplasms (MPN), and acute myeloid leukemia (AML) (*9*) (**Figure 1.1**). MDS are heterogenous disorders that are characterized by hematopoietic differentiation defects and peripheral blood cytopenias. Somatic mutations in epigenetic machinery and the spliceosome complex are common in MDS (*10*). Myeloproliferative neoplasms result in the increased

MPN

Increased proliferation of mature appearing cells

MDS

Impaired differentiation with decreased circulating mature cells

AML

Accumulation of cells with impaired differentiation
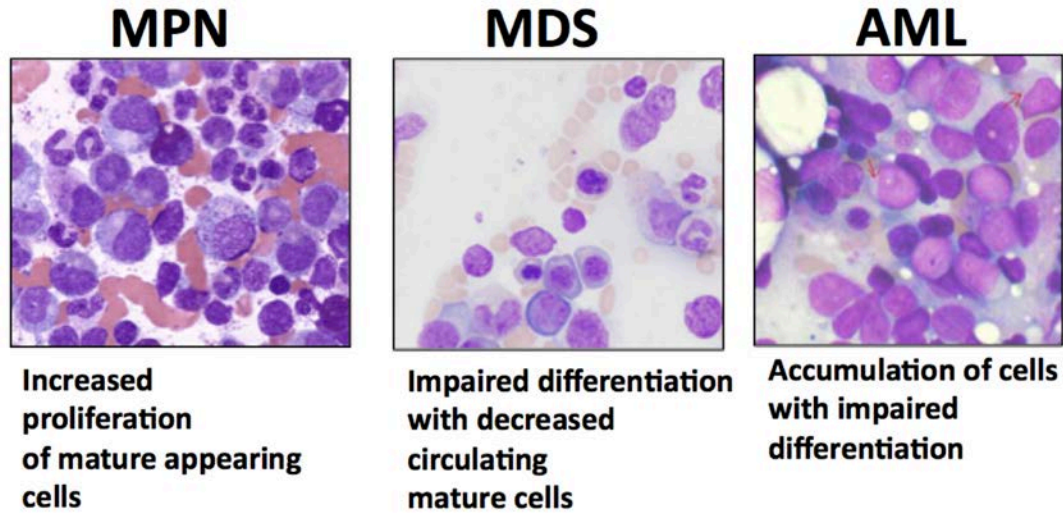
Figure 1.1. Schematic describing the pathology underlying myeloid malignancies.

production of mature blood cells including myelofibrosis (MF), polycythemia vera (PV, red blood cells), and essential thrombocytopenia (ET, platelets). Mutations in MPNs tend to occur in signaling molecules (such as Janus Kinase 2, JAK2) in cooperation with other alleles, such as epigenetic modifiers (*11*). Patients can also develop an MDS/MPN overlap disorder which is characterized by both dysplastic and proliferative symptoms, such as Chronic Myelomonocytic Leukemia (CMML). The standard of care for MDS and MPN patients is typically supportive care, including blood transfusions. Jakafi, an FDA approved drug for the treatment patients with JAK2 activating mutations, may also be beneficial to patients with MPN. However, JAK2 mutations co-occur with epigenetic modifications, and these mechanisms of disease transformation are poorly understood. MDS, MPN, and MDS/MPN patients risk transformation to acute myeloid leukemia (AML). AML is characterized by immature blasts in the peripheral blood and therapeutic options are limited, with bone marrow transplantation being the only curative treatment option (*12*). In this thesis, we utilize specific cell surface markers to identify HPSCs in our murine models as indicated in **Figure 1.2**.

CHROMATIN ALTERATIONS

C.H. Waddington developed the field of epigenetics about fifty years ago to describe the changes in organisms that could not be explained by changes in the DNA sequence (*13*). Modification of chromatin is an epigenetic event that is critical for DNA packaging/accessibility and the regulation of chromatin marks has critical implications for gene expression, DNA replication, and DNA damage repair. DNA is packaged around nucleosome octomers, composed of two H2A, H2B, H3, and H4 molecules. A fifth histone molecule, Histone H1, acts as a linker protein and serves to compact the higher
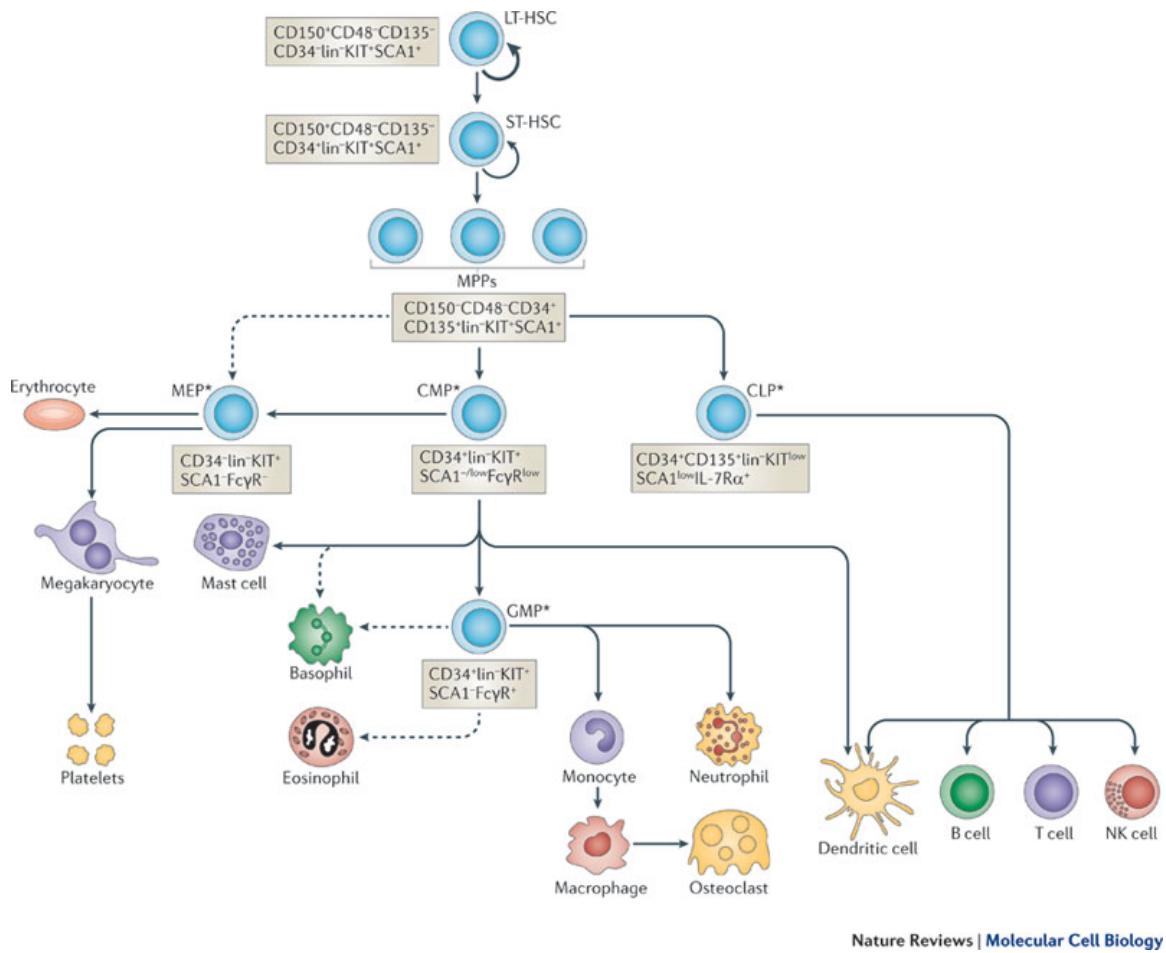
Figure 1.2. Hematopoietic hierarchy and murine HSPC markers (*1*).

order structure of chromatin (*14*). Nucleosomes serve as scaffolding platforms for effector molecules, termed epigenetics modifiers, which include chromatin writers, erasers, and readers. Histone writers are molecules that catalyze an enzymatic reaction to place a covalent modification (e.g. histone methyltransferases), histone erasers remove the modification (e.g. histone demethylases), and histone readers interpret these marks. All together, the balance of 'writing' and 'erasing' chromatin marks was classically thought of as the 'histone code hypothesis' (*15*).

While histones can be modified by various post-translation modifications, for the purpose of this thesis, the focus will be mainly on histone methylation. Repressive Polycomb and activating Trithorax Group proteins have a role in regulation of these methylation patterns. Histones can be methylated at lysine or arginine residues and methylation events are reversible. Histone modifications regulating the expression of specific target genes are typically cell type and context dependent, and can be regulated by differential expression and localization of epigenetic adaptor or modifying proteins. Aberrant activity of epigenetic modifiers in cancer can result in a disruption of the critical balance of marks placed by effector molecules (*7, 16*). This thesis will focus on the role(s) of the epigenetic modifiers in hematopoietic malignancies, specifically how they manipulate Polycomb protein activity. The goal of this thesis is to assess how the disruption of ASXL1 and BAP1 expression affects Polycomb activity.

ADDITION OF SEX COMBS-LIKE 1 (ASXL1)

ASXL family of proteins

ASXL1 belongs to the human *ASXL* gene family that has three members: *ASXL1*, *ASXL2*, and *ASXL3* (*17-19*). The ASXL proteins have a comparable domain architecture including an N-terminal ASXH homology domain, ASXM1 and ASXM2 domains in the middle of the protein and a C-terminal plant homology domain (PHD). The ASXH domain has only been identified in the ASXL family and is similar to the Forkhead-box (FOX) domain that is predicted to have a role in DNA binding (*20*). Other data have suggested that the N-terminal domain may be a unique DNA binding motif called the HARE-HTH (HB1, ASXL1, restriction endonuclease helix-turn-helix domain) (*21*). The ASXH domain facilitates protein-protein interactions, including the interaction of ASXL1 with BAP1 (*22, 23*). The PHD domain is also unique to the ASXL family and is predicted to recognize histone H3 tails via methylated lysines. The central ASXM1 and ASXM2 domains are also hypothesized to serve as modulators of protein-protein interactions and may coordinate interaction with NCOA1 and nuclear hormone receptors (*20*). The roles of these domains have not yet been fully elucidated. The sequence of ASXL1, ASXL2, and ASXL3 is divergent in regions not included in the conserved domain structures. The level of functional redundancy between the human ASXL family members has not yet been fully delineated and more work is warranted.

The ASXL family of proteins are homologs of *Drosophila Asx* (*Additional sex combs*). Deletion of *Asx* in *Drosophila* results in posterior and anterior homeotic transformations which phenocopies deletion of repressive PcG (Polycomb) and activating Trithorax genes, respectively (*24-26*). These data led to the hypothesis that *Asx* was involved in both the repression and activation of homeobox genes. However, data presented in this thesis and elsewhere suggest that human ASXL1 mainly regulates Polycomb activity in myeloid malignancies (*27, 28*). These data do not exclude the possibility that ASXL1 could activate homeobox genes in cell types and/or contexts. ASXL1 has also been

shown to have functions in non-hematopoietic systems including cooperation with HP1a and LSD1 to repress retinoic acid activity and peroxisome proliferation-activated receptorγ to inhibit lipogenesis (*29-31*).

ASXL1 mutations in human malignancies

Constitutive heterozygous mutations in *ASXL1* (20q11.21) have been found in about 54% of patients with Bohring-Opitz syndrome, a developmental disorder that results in distinctive craniofacial abnormalities and failure to thrive (*32*). Recurrent somatic mutations in *ASXL1* have been identified in hematopoietic malignancies including in myelodysplastic syndromes (MDS), CMML, myelofibrosis, MDS/myeloproliferative neoplasm overlap disorders (MDS/MPN), and acute myeloid leukemia (AML) transformed from MDS. *ASXL1* mutations are found in about 45% of CMML (*33, 34*), 35% of myelofibrosis (*33*), 15-20% of MDS (*34-36*), 40-60% of MDS/MPN overlap syndrome (*37*), 30% of AML transformed from MDS (*38*), and 6% of *de novo* AML cases (*39, 40*). Many studies in hematopoietic malignancies have found that *ASXL1* mutations are associated with adverse overall survival (*2, 35, 39, 41*).

ASXL1 mutations are commonly heterozygous frameshift or nonsense mutations that cluster in the C-terminal domain and can result in truncation before the PHD domain (*33*). *ASXL1* missense mutations are also scattered throughout the protein consistent with the tumor suppressor activity of *ASXL1* and the likelihood that the mutations lead to a loss of activity of the mutant allele. The hypothesis that *ASXL1* mutations are loss-of-function mutations, however, remains controversial. Because many *ASXL1* mutations are nonsense and frameshift, the *ASXL1* mutant allele could code for a truncated protein product with a gain of activity. Data to support this notion include the development of a murine bone marrow transplant model where retroviral expression of an ASXL1 C-

8

terminal truncated mutant protein (ASXL-MT) develops MDS-like symptoms (*42*). Recent work has indicated that expression of truncated ASXL1 proteins in conjunction with its interacting partner BAP1 results in an MDS-like disease (*43*). The authors propose that the C-terminal domain of ASXL1 has autoinhibitory capabilities and loss of this functionality results in a hyperactive protein. About 88% of the ASXL1 mutations in the COSMIC database are frameshift mutations which could mean that it is advantageous to lose the C-terminal (*43*). However, to date, no one has yet been able to show that mutant truncated proteins are expressed endogenously in cell lines or patient samples. Further, the activity of knockdown or deletion of *ASXL1* has not been compared side-by-side to activity of truncated ASXL1 products. Data presented in this dissertation suggest that ASXL1 mutations are most commonly loss-of-function.

Modeling loss of *Asxl1* in murine models

Asxl1 shares 81% sequence homology with human *ASXL1* and maintains the key conserved domains of the human ASXL family (*44*). The first murine loss-of-function model studying the role of *Asxl1* in hematopoiesis was developed utilizing targeted insertion of a neo cassette into the *Asxl1* locus. Constitutive deletion of *Asxl1* resulted in partial perinatal lethality, and the remaining viable mice develop B and T cell abnormalities in addition to myeloid differentiation defects. However, hematopoietic repopulating assays with *Asxl1* knockout (KO) cells did not lead to differences in long-term reconstitution (*45, 46*). Germline homozygous deletion of *Asxl1* in another murine model (utilizing *EIIa*-Cre) results in embryonic lethality at day E19.5 (*47*). Knockout mice had developmental abnormalities, consistent with those seen in Bohring-Opitz syndrome patients, including microcephaly, cleft palates, and skeletal abnormalities. Hematopoietic specific deletion of Asxl1 in adult animals utilizing *Vav*-cre or *Mx1*-cre results in a

9

progressive hematopoietic disorder that is accelerated with serial transplantation into secondary and tertiary recipients. *Asxl1* KO mice developed leukopenia and anemia at 6-12 months of age, consistent with an MDS-like disease (*47*). Subsequently, a novel constitutive whole body *Asxl1* knockout model was generated, and surviving mice also developed a progressive hematopoietic malignancy (*28*).

Asxl1 KO animals have increased HSPCs but impaired self-renewal (*28, 47*). Loss of *Asxl1* results in a stem cell deficiency as indicated by decreased *in vitro* replating capacity and defective reconstitution in *in vivo* competition assays. Because loss of *Asxl1* results in defective self-renewal, *Asxl1* mutations likely co-occur with other mutations that compensate for these stem cell defects. Consistent with this, concomitant deletion of *Asxl1* and *Tet2*, an epigenetic modifier commonly mutated in myeloid malignancies, rescues the *Asxl1* stem cell defect and results in a worsened disease as compared to deletion of either single allele (*47*). Truncated *Asxl1* proteins also cooperate with loss of *Tet2* to induce a worsened myelodysplastic syndrome (*43*).

In a massive sequencing study, 483 European patients and 396 Mayo Clinic primary myelofibrosis patient samples were assessed for mutation status and prognosis of the identified somatic alterations. *ASXL1* mutations were identified in about 22% of patients; *JAK2* activating mutations were found in about 60% of patients. As indicated by the described Circos plot, *ASXL1* and *JAK2* mutations were the most common somatic alterations to co-occur in primary myelofibrosis patients. Strikingly, a majority of these patients were determined to be high risk. In this large cohort of patients, the only significant indicator of poor prognosis was ASXL1 mutational status. These data have been validated by other studies (*2*) (**Figure 1.3**). In this thesis we examine the role of ASXL1 in cooperating with other alleles, specifically *JAK2V617F*. *JAK2V617F* itself has

10
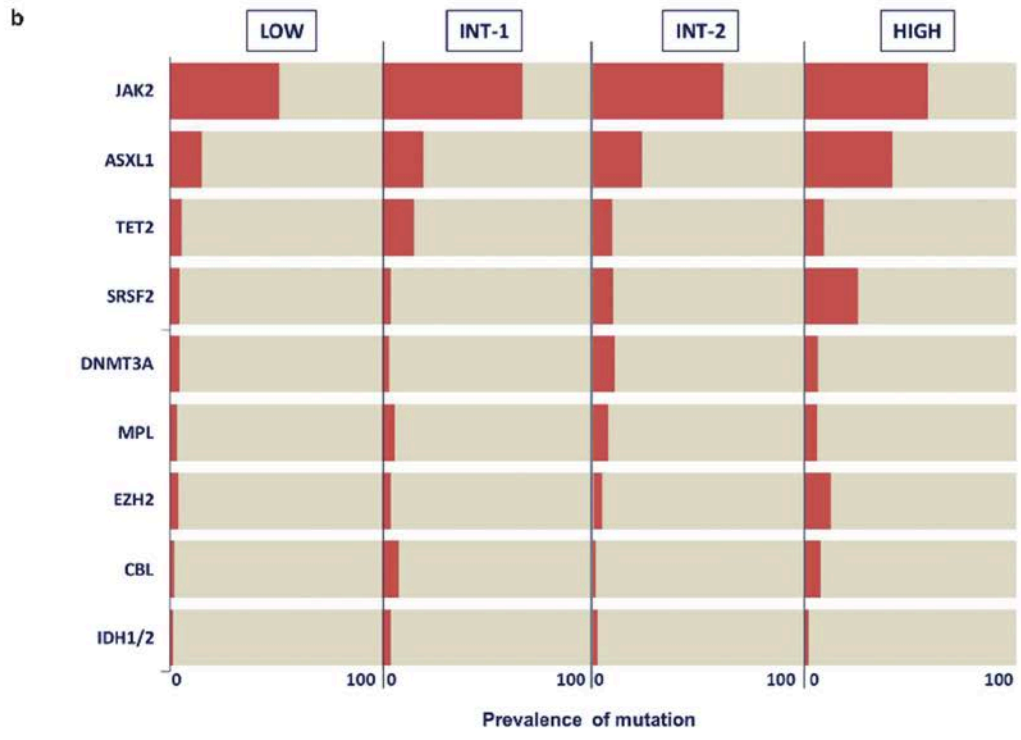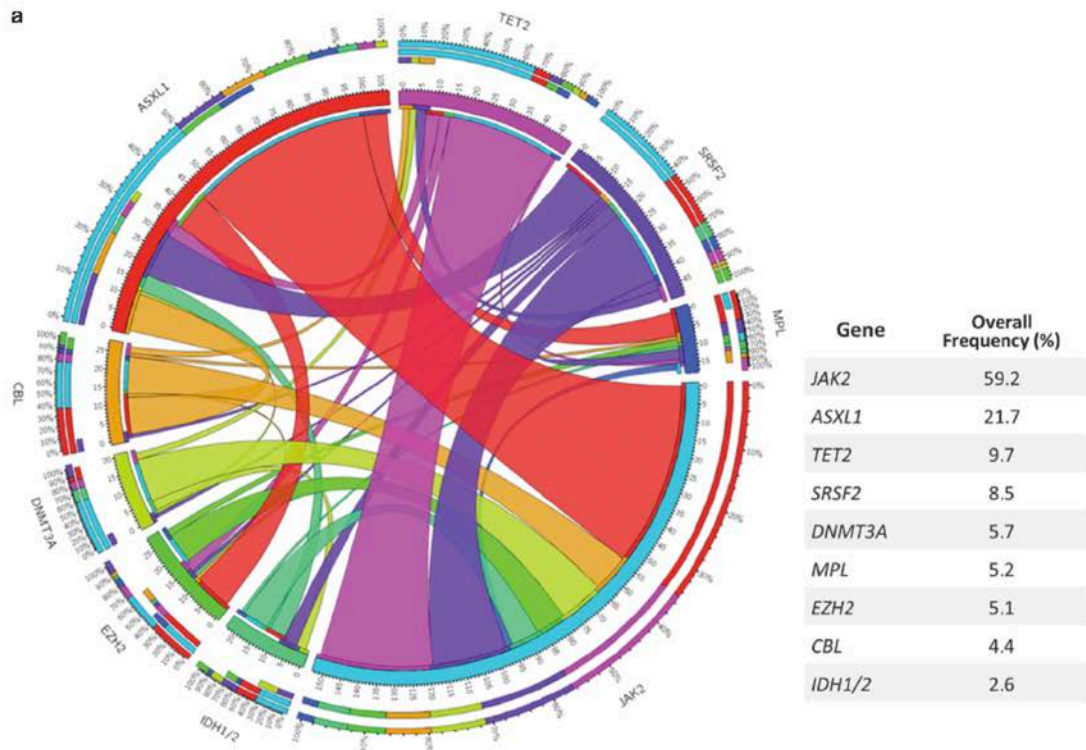
Figure 1.3. JAK2V617F and ASXL1 collaborate in primary myelofibrosis (*2*).

11

been linked to chromatin regulation, as JAK2 is thought to phosphorylate histone H3 at tyrosine 41 (*48*).

BRCA1 ASSOCIATED PROTEIN-1

BAP1 protein structure

BAP1 was initially discovered in a BRCA1 yeast two hybrid screen due to its interaction with the RING finger domain of BRCA1 (*49*). BAP1, a tumor suppressor, is a dequbiquitinase that is a part of the ubiquitin C-terminal hydrolase (UCH) family (*50*). Ubiquitination is a post-translation modification that marks proteins for degradation via the cellular degradation machinery, and deubiquitinases (DUBs) remove this mark. Dysregulation of the ubiquitination machinery in human malignancies has implications for cellular regulatory pathways including protein stability, signaling and cellular localization. BAP1 shares a high degree of sequence similarity with another ubiquitin hydrolase DUB, UCHL5. The BAP1 protein has three critical domains: a UCH N-terminal catalytic domain which contains the enzymatic active site, a central linker region (HBM) which modulates binding to Host cell factor-1 (HCF-1), and a C-terminal ULD domain which potentially coordinates protein-protein interactions (*23, 51*). Three key residues in the UCH domain—cysteine 91, alanine 95, and glycine 178—are required for removal of ubiquitin from target substrates (*52*). *BAP1 C91A* and *BAP1 C91S* have been established as catalytically dead mutants and are frequently used in *in vitro* assays as a control. BAP1 has two nuclear localization signals (NLSs) located in the C-terminal of the protein (*53*). BAP1 is ubiquitinated by UBE2O on an NLS, inducing cytoplasmic sequestration. BAP1 is typically nuclear localized and counteracts UBE2O-mediated

cytoplasmic sequestration by autodeubiquitination. This regulatory process can be disrupted by loss-of-function mutations in BAP1 (*54*).

BAP1 mutations in human malignancies

The BAP1 gene (3p21.1) is located in a chromosomal tumor suppressor hot spot that is commonly deleted in many human malignancies. Several alterations have been identified in *BAP1* that contribute to malignancy including deletions of exons leading to loss of the UCH domain or premature protein truncation, focal deletions, frameshift mutations, splice site mutations, nonsense mutations and missense mutations (*50*). Constitutive mutations in *BAP1* were initially identified in benign atypical melanocytic tumors (ASTs) which were later termed melanocytic *BAP1*-mutated atypical intradermal tumors (MBAITS) (*55-57*). These mutations tend to co-occur with mutations in *BRAF* and typically have biallelic loss of BAP1 which is indicative of loss of nuclear staining (*57*). Germline mutations in *BAP1* lead to a cancer syndrome which leads to an increased likelihood of mesothelioma, uveal melanoma, cutaneous melanoma and other cancers in affected families (*58, 59*). Families with germline *BAP1* mutations have an overall greater risk of developing a malignancy (about 70% of *BAP1* mutation carriers). *BAP1* mutation carriers also develop other cancers including renal, breast, lung meningioma and other types of carcinomas (*60*). Conversely, germline deletion of *ASXL1* does not result in a predisposition to cancer syndromes.

Unlike *ASXL1* mutations, *BAP1* somatic mutations are more common in solid tumors than hematopoietic malignancies. Loss-of-function mutations have been identified in uveal melanomas and *BAP1* mutations clearly mark out metastatic cases (26 of 31

13

cases, 84%) (*61*). *BAP1* mutations in sporadic melanomas occur in about 5% of cutaneous melanomas (*55*). The *BAP1* mutations again co-occurred with *BRAF* mutations, but the *BAP1* mutations were only present in the melanocytic portion while *BRAF* mutations were found in the nevus and melanoma components (*55*). These data suggest *BAP1* mutations may have a role in melanocytic transformation. Loss of BAP1 in melanoma cell lines results in reversion to a de-differentiated state, suggesting that BAP1 status contributes to stemness of the cells (*62*).

BAP1 mutations are found in sporadic mesotheliomas. About 50% of mesothelioma tumors have chromosomal loss of 3p21.1. Somatic mutations in *BAP1* occur in about 20% of mesothelioma patients overall, suggesting that BAP1 loss is a key genetic event in mesothelioma (*63*). Another study found that *BAP1* gene alterations occur in 61% of mesotheliomas and that *BAP1* mutations do not correspond to asbestos exposure or cell type (*64*). Inactivating mutations and 3p21 chromosomal deletions are also common in renal clear cell carcinoma (8-14% of patients) (*65*). *BAP1* expression acts as an independent indicator of poor patient prognosis in renal cell carcinoma (*66*). About 25 percent of patients with cholangiocarcinoma also have inactivating mutations in *BAP1* (*67*). Rare mutations have also been identified in bladder, liver, prostate, stomach, breast, ovary and lung carcinomas (*60*). It is unclear how these alterations contribute to carcinogenesis.

While germline and somatic mutations in *BAP1* are prevalent in human disease, there are no established treatment protocols for patients with these mutations. *BAP1* is a tumor suppressor gene and, therefore, is not a candidate for small molecule targeted inhibition. Rather, it is critical to elucidate pathways that can be hijacked to indirectly target BAP1 activity. Histone deacetylase inhibitors have shown some activity in BAP1

mutant cells *in vitro,* potentially due to the importance of BAP1 in chromatin regulation (*68*). BAP1 mammalian models, specifically in solid tumors, are currently lacking. The challenge with developing these reagents is likely due to the requirement of BAP1 mutations to co-occur with other oncogenic alleles, such as *BRAF* in cutaneous melanoma and *GNAQ* in uveal melanoma. The development of more sophisticated murine models will allow for further study of BAP1 transformation in solid tumors and efficacy of therapeutic candidates *in vivo.*

BAP1 in the BRCA1/BARD1 complex, DNA repair and the cell cycle

BAP1 was initially identified as a BRCA1 interaction partner, a protein that is involved in repair of double-stranded DNA breaks (*49*). Further functional studies, however, have clouded the relevance of BAP1 in BRCA1 regulation. BAP1 has been shown to interact with the BRCA1-BARD1 complex that has important roles in DNA repair (*69, 70*). However, there are conflicting reports about whether BAP1 regulates the stability of BRCA1. Some studies report that BAP1 does not deubiquitinate the BRCA1-BARD1 complex and BAP1-mediated tumor suppressive activity is independent of wild-type BRCA1 (*70*). A more recent study has shown that BAP1 interacts with BARD1 to modulate the E3 ligase activity of BARD1 and that these proteins may coordinately regulate ubiquitination in the DNA response pathway (*69*). These data suggest that BAP1 likely has BRCA1-dependent and –independent functions.

Recent work has further implicated BAP1 in the DNA damage response. A cell line based RNA interference screen demonstrated that BAP1 was required for efficient recruitment of BRCA1 and RAD51 to DNA damage foci (*71*). Cells with depleted BAP1 have defective repair and have more chromosomal breaks in response to ionizing

15

radiation. Further, mutation of six phosphorylation sites of BAP1 result in defective recruitment of repair machinery. BAP1 has also been shown to phosphorylate the DNA damage response kinase ATM (*72*). BAP1 has a role in cell cycle regulation that may be linked to the regulation of the DNA damage response. Reintroduction of BAP1 into the cell line H226, a mesothelioma cell line that lacks BAP1 expression, results in faster passage through the G1/S checkpoint (*52*). These cells have impaired repair leading to the induction of cell death. H226 cells with BAP1 re-expression grow more slowly in tumor xenograft models than either the wild-type cell line or the catalytic dead mutant. This mechanism appears to be independent of BRCA1 (*52*). These data suggest that BAP1 is a tumor suppressor that has multifaceted roles in cell regulation.

Known BAP1 interaction partners

BAP1 has been shown to interact *in vitro* with the host cell factor 1 (HCF-1) in the nucleus. HCF-1 is a transcriptional regulator that acts as a scaffolding protein to recruit histone modifying complexes to target loci, including at E2F responsive promoters, and has a key role in cell proliferation (*52*). BAP1 binds HCF-1 via the HBM domain of BAP1. HCF-1 is a direct target DUB substrate of BAP1 and BAP1 hydrolyses its K48 linked ubiquitin chains. It is thought that ubiquitinated HCF-1 cannot bind E2F responsive promoters and that BAP1 activity removes this inhibition and stimulates cell proliferation by regulating target gene expression (*51, 73, 74*). The BAP1/HCF-1 complex may be critical for progression through G1/S-phase and for regulation of gene expression during the cell cycle. YY1 is a transcription factor that interacts with the BAP1/HCF-1 complex and may regulate gene expression by recruiting the complex to target loci (*75*).

To define the Bap1 interaction network *in vivo*, Dey et al. generated a FLAG-tagged Bap1 knock-in (KI) mouse (*76*) and hematopoietic cells from the Bap1 KI model were utilized for mass spectrometry experiments. *In vivo* Bap1 interacts with HCF-1, OGT, ASXL1, ASXL2, and KDM1B. Levels of HCF-1 were decreased in *Bap1* KO cells, consistent with the proposition that protein stability of HCF-1 is regulated by Bap1(*73*). *Bap1* KO cells also had decreased OGT, an enzyme that adds the sugar O-GlcNAc to protein. O-GlcNAc was coordinately decreased in *Bap1* KO cells compared to controls (*76*). The biological consequence of the O-GlcNAc mark is still unclear, as is the importance of Bap1 in the modulation of this mark. It is possible that the increased O-GlcNAc mark activates HCF-1 and promotes its regulatory activity (*77*) (**Figure 1.4**). OGT is thought to have a role in providing nutrient availability to chromatin structure (*78*). Chromatin immunoprecipitation experiments also indicated that HCF-1 and OGT were located at many sites bound by BAP1 (*76*). Yu et al. has proposed that most cellular BAP1 protein is found in a core complex composed of HCF1, ASXL1, ASXL2, OGT, FOXK1 and FOXK2. This core complex could potentially interact with various transcription factors resulting in differential regulatory activities (*75*). The effects of BAP1-associated transcriptional complexes are also likely context dependent.

The BAP1-ASXL1 interaction has been validated in several reports (*73, 76, 79*). Studies in *Drosophila* have demonstrated that BAP1 and ASXL1 can function as a complex to remove the H2KA119Ub mark from chromatin. The Polycomb Repressive 1 Complex (PRC1) places the H2AK119Ub mark to effectively fix chromatin in a repressed state. The H2AK119Ub mark can be removed by the BAP1-ASXL1 complex, with BAP1 contributing the catalytic activity. This complex has been termed the Polycomb Repressive Deubiquitinase Complex (PR-DUB) (*22*). These data suggest that PR-DUB
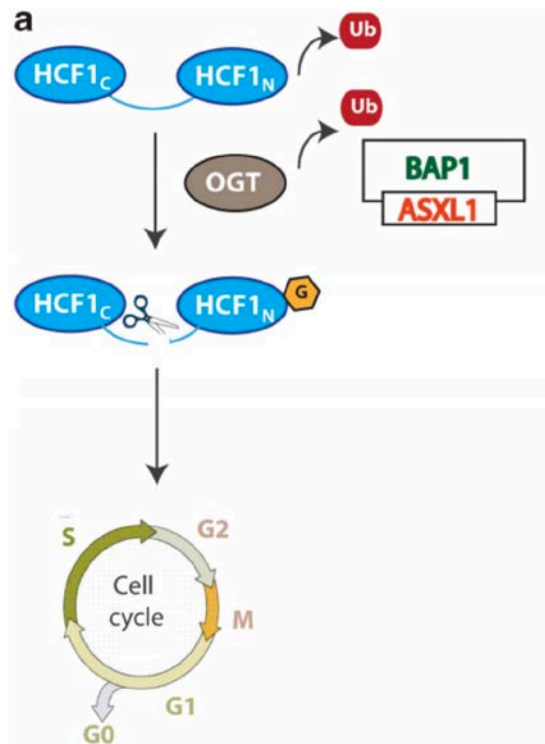
Figure 1.4. BAP1-dependent regulation of HCT and OGT.

could have a role in the regulation of Polycomb target genes (**Figure 1.5**). However, changes in H2AK119Ub in BAP1 knockdown and knockout models have been inconsistent and more work needs to be done to functionally characterize this complex in mammalian systems.

BAP1 loss-of-function *in vivo* models

Constitutive loss of Bap1 results in embryonic lethality at embryonic day 8.5 due to developmental retardation, including cardiac defects (*76*). Dey et al. generated a whole body conditional knockout model of *Bap1* utilizing a creERT2 tamoxifen inducible Cre system. Four weeks after induction of excision with tamoxifen, *Bap1*-null mice developed a hematopoietic phenotype characterized by splenomegaly due to extramedullary hematopoiesis. Histopathological analyses of these animals revealed a syndrome similar to an MDS/MPN overlap disorder such as human chronic myelomonocytic leukemia. Heterozygous deletion of Bap1 resulted in a mild hematopoietic phenotype in comparison to complete loss of Bap1. *Bap1* KO mice were characterized as having high white cell counts and anemia in addition to thrombocytopenia. Conditional deletion of *Bap1* results in an expansion of hematopoietic stem cells and myeloid progenitor cells in the bone marrow. However, these stem cells have defective self-renewal in colony assays and in *in vivo* competitive assays. These data suggest that Bap1 loss may lead to defects in stem cell homing or engraftment and more work is necessary to understand this (*77*). Further, single copy or complete loss of Bap1 may need to be coupled with another hematopoietic alteration that promotes self-renewal to propagate the disease.
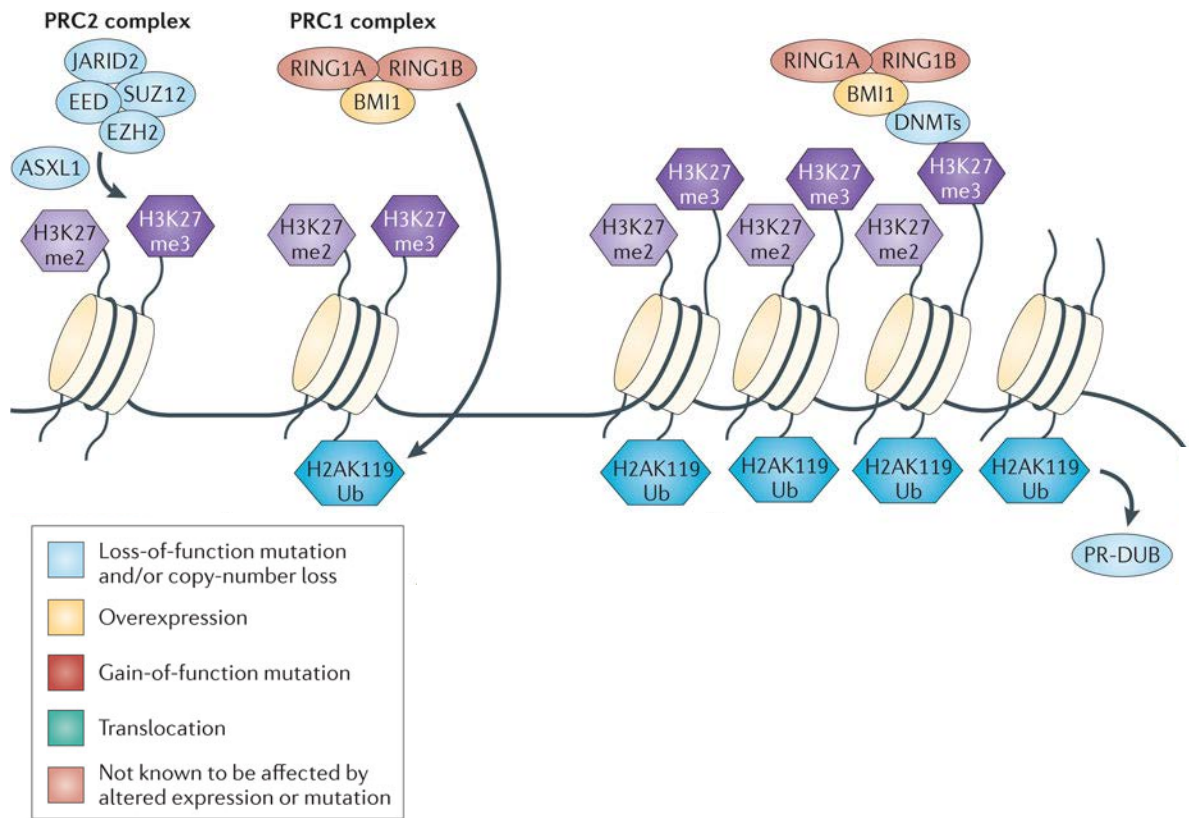
Figure 1.5. BAP1 and ASXL1 are implicated in regulation of repressive polycomb machinery. Reprinted by permission from Macmillan Publishers Ltd: NATURE REVIEWS CANCER 12(9), copyright 2012**.**

Others have attempted to model *Bap1* loss-of-function in solid tumor murine models. Mice with deletion of a single copy of *Bap1* have increased susceptibility to mesothelioma after chronic exposure to asbestos; however, spontaneous mesotheliomas were not seen in these models (*80*). Wild-type mice require the loss of *Cdkn2a* to develop asbestos-induced mesothelioma, while mice with heterozygous loss of *Bap1* did not. Xu et al. found that *Bap1* loss led to downregulation of Rb via a p16(Ink4a)-independent mechanism.

Bap1 loss was also assessed in a morpholino DUB screen in zebrafish (*81*). Deletion of *bap1* led to the development of increased neurons. The Notch pathway is involved in this process and loss of Notch leads to premature differentiation of neural progenitors. More analysis is warranted here to understand the role of BAP1 and the regulation of Notch signaling. Overall, the development of *Bap1* loss-of-function models is in its infancy and the development of new reagents will allow for further elucidation of the roles of Bap1 loss in disease transformation.

ENHANCER OF ZESTE 2 (EZH2) AND POLYCOMB COMPLEXES

Polycomb expression and EZH2 catalytic activity

In *Drosophila*, Polycomb and Trithorax genes maintain gene expression patterns. Polycomb genes are repressed with two regulatory complexes, the Polycomb repressive complex 1 (PRC1) and the ESC-E(Z) complex (*82*). The ESC-E(Z) complex represses key development genes in *Drosophila* which maintain appropriate patterning in adult animals. EZH2 is the catalytic component of the human Polycomb Repressive Complex 2 (PRC2), analogous to the *Drosophila* ESC-E(Z) complex, which is responsible for

placing the repressive H3K27me2/3 mark on chromatin. The PRC2 complex has been established as a key chromatin regulatory complex that modulates transcriptional silencing (*83*). EZH2 has four protein domains: two SANT domains, a CXXC domain, and the catalytic SET domain. EZH2 also contains a non-coding RNA binding domain (*84*). The canonical PRC2 complex is composed of EZH2, SUZ12, EED, and RBBP4. JARID2, AEBP2, and PCL are accessory proteins that regulate the activity of the PRC2 complex in different contexts (*85, 86*). Histone methylation by EZH2 is mediated by a conserved NHS catalytic triad that is responsible for recognition of the histone peptide and for binding of S-adenosyl-methionine (SAM) in the active site (*87*). EZH2 activity is regulated by several post-translational modification events. These include phosphorylation at serine 21 by AKT1 which reduces EZH2 activity (*88*) and phosphorylation at threonine 345 by CDK1 and CDK2 which helps to maintain H3K27me3 marks at promoters (*89*). Two demethylases have been identified, UTX and JMJD3, that remove the H3K27me3 placed by EZH2 (*90*). EZH2 may also have non-canonical roles in breast and prostate cancer, including involvement in a B-catenin/TCF complex at the promoter of c-Myc in ER positive breast cancer cells (*91*).

EZH2 and EZH1 redundancy

In some contexts, EZH1 can replace EZH2 as the catalytic component in the PRC2 complex. This redundancy complicates the understanding of PRC2 regulation, and the role of the EZH1-PRC2 complex is still somewhat elusive. In embryonic stem cells, both EZH1 and EZH2 have a role in maintenance of H3K27me3 on repressed chromatin and regulation of stem cell related transcriptional programs (*92, 93*). However, EZH1 can mark active promoters in muscle cells and hippocampal neurons (*94, 95*). Recent work has shown that EZH1 and EZH2 expression are inversely correlated during normal

22

hematopoiesis and that they are not always functionally redundant. The authors suggest that EZH1 can bind SUZ12 in the absence of EED, a sort of non-canonical PRC2 complex. This complex may sequester SUZ12 from the canonical PRC2 complex or it could be directly activating transcription via regulation of the transcriptional machinery (*3*). EZH2 was shown to be highly expressed in progenitors cells and is downregulated in more mature hematopoietic lineages, while EZH1 is very lowly expressed in progenitor populations (**Figure 1.6**). EZH1 tends to be more highly expressed in non-proliferating cells while EZH2 is more highly expressed in proliferating cells (*96*). *Ezh1* knockout mice have no changes in fetal hematopoiesis but conditional knockout mice severely disrupt adult hematopoiesis (*97*), while the reverse is true for *Ezh2* (*98*).

Other evidence supports the EZH2/EZH1 redundancy in some contexts. A study in MLL-AF9 leukemia revealed that EZH2 was required for leukemic progression although some H3K27me3 was still found in cells with deleted EZH2 (*99*). Therefore, the authors proposed that there is some potential redundancy in Polycomb complexes, potentially with an EZH1-PRC2 complex. Conditional deletion of *Eed* in hematopoietic cells results in a more severe phenotype than *Ezh2* deletion alone. In HSPCs, fewer genes change in response to *Ezh2* deletion compared to *Eed* deletion, meaning there may be some redundancy with another protein (*100*). There have also been reports of the formation of EZH1/EZH2 heterodimers, but studies in the hematopoietic system did not show evidence of this (*96*).

EZH2 alterations in human malignancies: dual oncogene and tumor suppressor

Oncogene

23
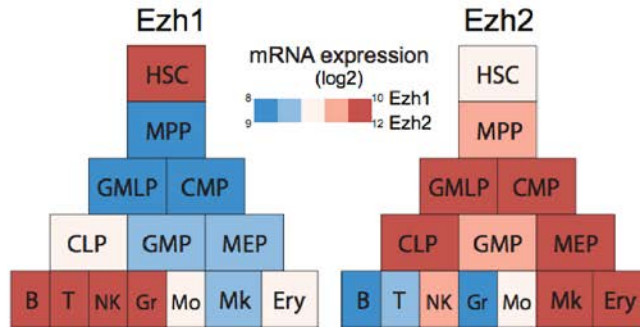
Figure 1.6. EZH2 and EZH1 expression in sorted murine hematopoietic populations (*3*) Reprinted from Molecular Cell, 57(2), Jian Xu,Zhen Shao,Dan Li,Huafeng Xie,Woojin Kim, et al., Developmental Control of Polycomb Subunit Composition by GATA Factors Mediates a Switch to Non-Canonical Functions, 304-316. Copyright 2015, with permission from Elsevier**.**

PRC2-dependent gene regulation varies based on cell-type and context, and a multitude of target genes are disrupted by dysregulation of Polycomb. Therefore, it is not surprising that EZH2 alterations have dual roles in human carcinogenesis, with reports of EZH2 acting as an oncogene and tumor suppressor. Heterozygous mutations in EZH2 have been identified in B-cell lymphomas of germinal center origin such as diffuse large B-cell lymphomas (DLBCL) and follicular lymphoma (FL). EZH2 point mutations typically occur in the SET domain of EZH2 at residue Tyr641 (Y641). EZH2 mutations are found in about 21% of DLBCLs and 7% of FLs (*8, 101*). The Y641N mutation is thought to alter the substrate binding pocket, allowing for accommodation of the trimethyl group. Two other rare mutations have been detected in B-cell malignancies, A677G and A687V, which are also believed to be activating mutations (*102*). Initially, these mutations were thought to reduce EZH2 enzymatic activity while later studies showed that they were in fact activating mutations. EZH2 Y646 activating point mutations have also been identified in cutaneous melanoma models (*103*).

EZH2 has also been found to be overexpressed in metastatic prostate cancer and loss of EZH2 represses the growth of prostate cancer cells. EZH2 silencing has a greater effect on androgen independent growth *in vitro* and *in vivo*. Further, androgen receptor signaling pathways modulate EZH2 activity levels and androgens have been found to repress EZH2 expression (*104, 105*). EZH2 is also overexpressed in breast cancers and may be indicative of a more aggressive phenotype (*106*). EZH2 may regulate genes involved in the E2F-Rb, PI3K/Akt and estrogen signaling pathways. Further, overexpression of EZH2 has been reported in non-small cell lung cancers also related to activation of the E2F-Rb pathway (*107*). EZH2 overexpression has also been identified in bladder cancer and ovarian cancer (*91*). High EZH2 expression was linked to poorer

overall survival in cutaneous melanoma patients (*103*). Therefore, EZH2 has been implicated as an oncogene in several cellular contexts.

Tumor Suppressor

Inactivating/hypomorphic mutations in EZH2 have also been identified in hematopoietic malignancies. Ernst et al. found that about 8% of patients with myeloid malignancies had mutations in EZH2 (with a third of these being loss-of-function, which is indicative of a tumor suppressor). Many of these patients had myelofibrosis and MDS/MPN overlap syndromes (*108*). Another study identified loss-of-function mutations in patients with MDS. EZH2 mutations tend to be indicative of poorer prognosis in patients with MDS/MPN and myelofibrosis (*109*). Mutations in splicing machinery, including U2AF1 and SRSF2, result in aberrant pre-mRNA processing and reduction in EZH2 expression (*110*). HOXA9 has been shown to be a key downstream target of EZH2 and is typically increased in patients where EZH2 expression is lost. HOXA9 tends to also be increased in patients with losses at chromosome 7 including the EZH2 locus. Therefore, loss-of-function mutations in EZH2 may lead to changes in self-renewal mediated by HOXA9 (*91*). EZH2 inactivating mutations have also been identified in about 25% of primary T-acute lymphoblastic leukemias (T-ALLs). Knockdown of EZH2 in T-ALL xenograft models results in increased cell growth, suggestive of EZH2 acting as a tumor suppressor in this context (*111*).

EZH2 in EMT and Metastasis

Overexpression of EZH2 has been reported in several cancers including prostate and breast cancer. Expression of EZH2 has also been linked to metastasis in these tumor types. One mechanism by which EZH2 regulates metastasis and invasion is by

transcriptional silencing of the E-cadherin gene, a gene critical for EMT. E-Cadherin has been shown to be a Polycomb target gene resulting in the recruitment of histone deaceytlase machinery. Histone deacetylase inhibitors can counteract the invasion of cancer cell lines induced by repression of E-Cadherin signaling (*112*).

Ezh2 murine models

Gain-of-function

An Ezh2 knock-in mouse model was generated to test the effect of conditional overexpression of Ezh2 in the hematopoietic lineages (*113*). Overexpression of EZH2 led to the development of an MPN characterized by an expanded hematopoietic stem cell compartment with increased self-renewal capacity. These data suggest that EZH2 regulates HSPCs and has a smaller effect in more mature lineages (*113*). MLL-AF9 transformed AML cells have been studied with and without *Ezh2* knockout. Deletion of *Ezh2* resulted in increased differentiation in MLL-AF9 mice and a reversion to a less severe phenotype that resembled MDS/MPN. Therefore, Ezh2 may have an oncogenic effect in this leukemia by inhibition of differentiation (*99*). Conditional expression using Cγicre of *EZH2 Y641N* resulted in increased proliferation of the germinal B cell compartment. While these mice did develop B cell hyperplasia, they do not develop overt lymphomas. The authors demonstrate that EZH2 has a role in the suppression of differentiation in this model (*114*). In various tumor types, EZH2 expression is required for disease progression, including in melanoma (*103*).

Loss-of-function

Interestingly, Ezh2 is required for fetal hematopoiesis in mice, but not in adult stem cell maintenance (*115*). Mx1-Cre mediated conditional deletion of Ezh2 results in defective

27

pro-B and immature B cells (*116*). Ezh2 hematopoietic KO mice do not develop myeloid malignancies, but over time mice develop T-ALLs (*117*). Conditional deletion of Ezh2 in germinal center B-cells demonstrated that Ezh2 activity was essential for germinal center proliferation (*114*). The epigenetic modifiers *EZH2* and *TET2* are commonly co-mutated in myelodysplastic syndromes. Co-deletion of *EZH2* and *TET2* in mice leads to a more severe myelodysplastic syndrome (*118*); therefore, loss of Ezh2 may cooperate with other alleles to cause transformation. Homozygous conditional deletion of *Eed* results in stem cell exhaustion. Conversely, heterozygous loss of *Eed* results in a stem cell advantage *in vitro* and *in vivo.* Serial transplantation assays *in vivo* with *Eed f/+* cells do not result in leukemic transformation (*100*). Depletion of *Suz12* in the hematopoietic system also results in a severe hematopoietic defect, demonstrating that *Eed* and *Suz12* components are essential and non-redundant (*119*). Overall, the PRC2 complex plays diverse roles in normal hematopoiesis and disease transformation. Therefore, the clinical utility of PRC2 inhibitors will need to be carefully evaluated.

Small molecule inhibitors of EZH2

S-adenosylhomocysteine hydrolase inhibitors
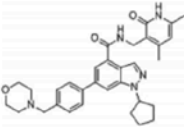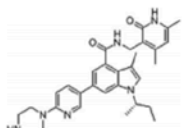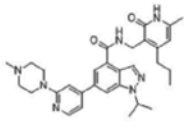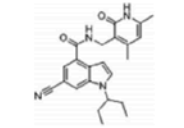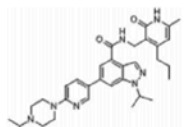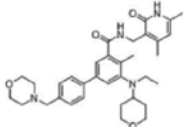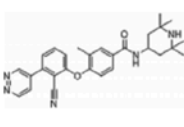
The first drug that was found to inhibit EZH2 was 3-Deazaneplanocin (DZNep) which indirectly targets S-adenosylhomocysteine (SAH) hydrolase, inhibiting methyltransferases and targeting EZH2 for degradation (*120*). However, DZNep was later considered to be a poor EZH2 inhibitor due to its broad effect on histone methyltransferases.

SAM-competitive inhibitors

Since the discovery of EZH2 gain-of-function mutations in lymphoma, significant advances have been made in the development of small molecule EZH2 inhibitors. The structures of these inhibitors are included in **Figure 1.7**. Most of these inhibitors utilize a similar structure and act via a competitive mechanism to bind the S-adenosylmethionine (SAM) pocket of the SET domain in EZH2. Most of these inhibitors have some selectivity of EZH2 over EZH1. Novartis, GlaxoSmithKline, and Epizyme all identified small molecule inhibitors of EZH2, termed EI1 (*121*), EPZ005687(*122*), and GSK126 (*123*). These inhibitors were shown to induce apoptosis in lymphoma cell line models with the *EZH2Y641* mutation. *In vivo* activity was also described in lymphoma xenograft models utilizing GSK126 and later EPZ-6438 (*124*), a variant of EPZ005687 with improved pharmacodynamics properties. Another clinical tool compound, EPZ011989 (*125*), was recently described. UNC1999 is a derivative of GSK126 and is orally available, unlike GSK126. Furthermore, unlike the other inhibitors described above, UNC1999 does not have selectivity of EZH2 over EZH1 (*126*). From these data, the hypothesis was proposed that patients with activating mutations in EZH2 would be more sensitive to EZH2 inhibition. However, initial clinical trials presented by Epizyme have shown that patients with wild-type EZH2 are also sensitive to EZH2 inhibition, suggesting that EZH2 inhibitors may prove to be more efficacious in the clinic than initially realized.

Inhibition of the EZH1/2-EED Interface

An alternate mechanism to inhibit PRC2 is to disrupt the EZH2-EED binding interface. To this end, hydrocarbon-stapled peptides were utilized to generate SAH-EZH2 peptides that contained non-natural amino acids inserted into the EZH2 alpha-helical sequence. These peptides could sequester EED and impair catalyzation of the H3K27me3 mark. The SAH-EZH2 peptides induced growth arrest and differentiation, phenotypes

Compound	Structure	In vitro activity, IC$_{50}$ (nmol/L)[b]					In vivo activity?	Orally bioavailable?	Fold selectivity for EZH2
		WT	Y641N	A677G	A687V	EZH1			
EPZ005687		54	41	10	ND	2713	No	No	50
GSK126		10	29	24	441	680	Yes	No	150
GSK343		4	ND	ND	ND	240	No	No	60
EI1		9	ND	ND	ND	1340	No	No	140
UNC1999		10	46	ND	ND	45	Yes	Yes	5
EPZ6438		11	38	2	2	392	Yes	Yes	35
Constellation Compound 3		21	197	ND	ND	213	No	No	10

ND = not determined.
[a]Compounds appear in the order they were disclosed in the literature. All compounds except Constellation compound 3 bear a dimethylpyridone motif that is requisite for activity. Additionally, all compounds remain active against EZH2 gain-of-function mutants tested and are fairly selective for EZH2 over EZH1, with UNC1999 displaying the most EZH1 inhibition. GSK126 exhibited the first activity in vivo, and UNC1999 was the first EZH2/1 inhibitor to exhibit oral bioavailability.
[b]IC$_{50}$ values were calculated on the basis of the Cheng–Prusoff equation for competitive inhibitors.

Figure 1.7. Small molecule EZH2 inhibitors (4).

comparable to knockdown or small molecule inhibition of EZH2 (*127*). This rationale may lead to a secondary approach to clinically target EZH2.

POLYCOMB REPRESSIVE COMPLEX 1

The role of the Polycomb Repressive Complex 1 (PRC1) is to functionally lockdown silenced genes after PRC2-mediated methylation. Unlike the PRC2 complex, the PRC1 complex is functionally diverse and five independent PRC1 complexes (**Figure 1.8**) have been classified to date. All of these complexes contain the RING1 E3 ligase that catalyzes the placement of the ubiquitin mark of H2AK119 (*128*). The canonical PRC1 complex contains the protein BMI1 and CBX proteins, which maintain the ability to bind PRC1. An atypical PRC1 complex contains the protein L3MBTL2, which may maintain repressive chromatin. L3MBTL2 can bind H2AK119ub, but loss of L3MBTL2 *in vivo* did not grossly alter this mark (*129*). L3MBTL2 has been shown to bind to H4K20me1 (*130*), a finding that we follow up on in this study. The ASXL1-BAP1 complex is hypothesized to regulate the activity of the PRC1 complex, with BAP1 being implicated in removal of this mark. However, more work needs to be done to further understand the role of the myriad PRC1 complexes in transcriptional and chromatin regulation.

CONCLUSION OF INTRODUCTION

The PRC2 machinery is highly conserved and plays key roles in development, hematopoiesis, and transformation. Because the PRC2 complex broadly controls the expression of a panel of Polycomb target genes, tight regulation of the PRC2 members is critical to maintain normal gene expression patterning. In many cancer types, the PRC2 complex is hijacked by mutation or loss of key components resulting in aberrant
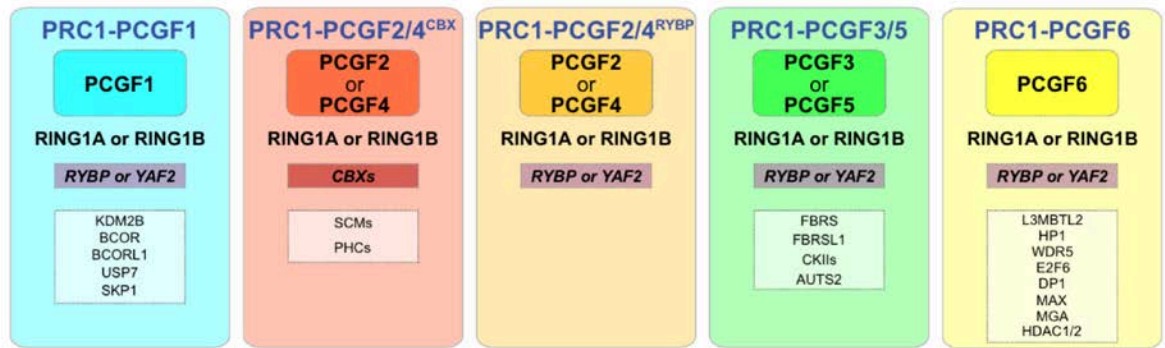
Figure 1.8. Varied composition of the five described PRC1 complexes (*5*).

transcription. This necessity to maintain a fine balance of PRC2 activity is evidenced by the fact that EZH2 can act as an oncogene and tumor suppressor in different settings. Therefore, greater mechanistic understanding of how the PRC2 complex regulates gene expression and how it contributes to disease transformation is key to understand how to therapeutically intervene in patients with PRC2-related alterations.

We are becoming increasingly aware of the complexity of epigenetic complexes. Many proteins, such as BAP1 and ASXL1, are key interactors in these complexes. Further, it is becoming apparent that these epigenetic modifiers are promiscuous and therefore may be interactors with multiple epigenetic complexes. This regulation may vary based on the expression and localization of specific adaptor proteins in different cell types. The goal of this thesis is to understand the complex relationships of BAP1 and ASXL1 with the PRC2 complex and other cellular machinery. To do this, we utilized varied *in vitro* and *in vivo* systems to manipulate BAP1 and ASXL1 expression and to understand how these changes affect PRC2 activity. Our goal was to use this information to understand the roles of ASXL1 and BAP1 in normal and malignant hematopoiesis. We also aimed to determine if we could broadly extend these findings to relevant settings in solid tumors.

CHAPTER II

ASXL1 Mutations Promote Myeloid Transformation through Loss of PRC2-Mediated Gene Repression

SUMMARY

Recurrent somatic *ASXL1* mutations occur in patients with myelodysplastic syndrome, myeloproliferative neoplasms, and acute myeloid leukemia, and are associated with adverse outcome. Despite the genetic and clinical data implicating *ASXL1* mutations in myeloid malignancies, the mechanisms of transformation by *ASXL1* mutations are not understood. Here, we identify that *ASXL1* mutations result in loss of polycomb repressive complex 2 (PRC2)-mediated histone H3 lysine 27 (H3K27) tri-methylation. Through integration of microarray data with genome-wide histone modification ChIP-Seq data, we identify targets of ASXL1 repression, including the posterior *HOXA* cluster that is known to contribute to myeloid transformation. We demonstrate that ASXL1 associates with the PRC2, and that loss of ASXL1 *in vivo* collaborates with *NRASG12D* to promote myeloid leukemogenesis.

INTRODUCTION

Recent genome-wide and candidate-gene discovery efforts have identified a series of novel somatic genetic alterations in patients with myeloid malignancies with relevance to pathogenesis, prognostication, and/or therapy. Notably, these include mutations in genes with known or putative roles in the epigenetic regulation of gene transcription. One such example are mutations in the gene *Addition of sex combs-like 1* (*ASXL1),* which is mutated in ≈15–25% of patients with myelodysplastic syndrome (MDS) and ≈10–15% of patients with myeloproliferative neoplasms (MPN) and acute

myeloid [1]leukemia (AML) (*33, 34, 36*). Clinical studies have consistently indicated that mutations in *ASXL1* are associated with adverse survival in MDS and AML (*35, 36, 39, 131*). *ASXL1* is the human homologue of *Drosophila Additional sex combs (Asx)*. *Asx* deletion results in a homeotic phenotype characteristic of both Polycomb (PcG) and Trithorax group (TxG) gene deletions (*132*) which led to the hypothesis that Asx has dual functions in silencing and activation of homeotic gene expression. In addition, functional studies in *Drosophila* suggested that *Asx* encodes a chromatin-associated protein with similarities to PcG proteins (*24*). More recently, it was demonstrated that *Drosophila* Asx forms a complex with the chromatin deubiquitinase Calypso to form the Polycomb-repressive deubiquitinase (PR-DUB) complex, which removes monoubiquitin from histone H2A at lysine 119. The mammalian homologue of Calypso, BAP1, directly associates with ASXL1, and the mammalian BAP1-ASXL1 complex was shown to possess deubiquitinase activity *in vitro* (*22*).

The mechanisms by which *ASXL1* mutations contribute to myeloid transformation have not been delineated. A series of *in vitro* studies in non-hematopoietic cells have suggested a variety of activities for ASXL1 including physical cooperativity with HP1a and LSD1 to repress retinoic acid-receptor activity and interaction with peroxisome proliferator-activated receptor gamma (PPARg) to suppress lipogenesis (*29-31*). In addition, a recent study using a gene-trap model reported that constitutive disruption of *Asxl1* results in significant perinatal lethality, however the authors did not note alterations in stem/progenitor numbers in surviving Asxl1 gene trap mice (*45, 46*).

Importantly, the majority of mutations in *ASXL1* occur as nonsense mutations and insertions/deletions proximal or within the last exon prior to the highly conserved PHD domain. It is currently unknown whether mutations in *ASXL1* might confer a gain-of-function due to expression of a truncated protein, or whether somatic loss of ASXL1 in hematopoietic cells leads to specific changes in epigenetic state, gene expression, or hematopoietic functional output. The goals of this study were to determine the effects of *ASXL1* mutations on ASXL1 expression as well as the transcriptional and biological effects of perturbations in ASXL1 which might contribute towards myeloid transformation.

MATERIALS AND METHODS

Cell culture

HEK293T cells were cultured in Dulbecco's modified Eagle's medium (DMEM) supplemented with 10% fetal bovine serum (FBS) and nonessential amino acids. Human leukemia cell lines were cultured in RPMI-1640 medium supplemented with 10% FBS+1mM hydrocortisone+10% horse serum (UKE1 cells), RPMI-1640 supplemented with 10% FBS (K562, MOLM13, KCL22, KU812 cells), RPMI-1640 supplemented with 20% FBS (SET2, NOMO1, Monomac-6 cells), or IMDM + 20% FBS (KBM5 cells). For proliferation studies, 1×10^3 cells were seeded in 1mL volume of media in triplicate and cell number was counted manually daily for 7 days by Trypan blue exclusion.

Plasmid constructs, mutagenesis protocol, short hairpin RNA (shRNA) and small interfering RNA (siRNA)

The cDNA clone of full-length mouse ASXL1 (NM_001039939) was purchased from Kazusa DNA Research Institute (http://www.kazusa.or.jp/huge/) and human ASXL1

36

(NM_015338) with an N-terminal FLAG tag was a generous gift from Daniel Birnbaum. The *ASXL1 591X, 629X, 710X,* and *936X* mutations were generated using site-directed mutagenesis (Quickchange-XL; Stratagene) and confirmed by full-length DNA sequencing. A MSCV vector encoding NRASG12D was a generous gift of Rubaio Ren. Wild-type sequences were then subcloned into MIGR1 or MSCV-IRES-Puromycin vectors. All sequences were confirmed by direct sequencing before expression in 293T cells and retrovirus generation. shRNAs for knockdown of human ASXL1 (TRC Oligo IDs: TRCN0000134690 and TRCN0000135296), human BAP1 (TRC Oligo IDs: TRCN0000078702 and TRCN0000078698), and mouse BAP1 (TCR Oligo IDs: TRCN0000030719 and TRCN0000030720) were obtained from the The RNAi Consortium (TRC) in a pLKO.1 puromycin vector. pLKO.1-puromycin empty vector or pLKO.1-puromycin vector encoding an shRNA for luciferase (shLUC) were used as controls. Oligonucleotide sequences targeting murine ASXL1 (NM_001039939) were selected on the basis of BIOPREDsi algorithms (http://www.biopredsi.org; (*133*)) as described previously and are available upon request. Individual shRNAs for validation were synthesized as 97 bp oligos (Sigma Genosys), PCR-amplified, cloned into LMS (MSCV-based vectors encoding GFP) (*134*)and verified by sequencing. For shRNA-mediated knockdown of Asxl1 in Ba/F3 and mouse bone marrow cells, cells were infected with retroviruses bearing Asxl1 shRNA constructs and cells were then sorted for GFP-positive cells 48 hours after infection. Knockdown of hASXL1 in CD34+ cells from cord blood was performed by transfection of Dharmacon ON-TARGETplus SMARTpool ASXL1 siRNA pool (ThermoScientific L-012856-00-0005) or p-MaxGFP vector using a Nucleofector II device (Lonza).

Primary AML patient samples and *ASXL1, BAP1, EZH2, SUZ12 and EED* genomic DNA sequencing analysis

37

Approval was obtained from the institutional review boards at Memorial Sloan-Kettering Cancer Center and at the Hospital of the University of Pennsylvania for these studies, and informed consent was provided according to the Declaration of Helsinki. Genomic DNA was extracted from all cell lines used in this manuscript and select AML patient samples for *ASXL1* genotyping prior to Western blot and ChIP-qPCR analysis. Patient samples were obtained from the Stem Cell and Xenotransplantation Core Facility of the University of Pennsylvania. Approval was obtained from the institutional review boards at Memorial Sloan Kettering Cancer Center (IRB protocol 06-107) and the University of Pennsylvania (IRB protocol 703185), and informed consent was provided according to the Declaration of Helsinki. All samples were collected after de-identification for these studies. High-throughput DNA sequence analysis was used to screen for *ASXL1, BAP1, EZH2, SUZ12*, and *EED* mutations. We performed high throughput PCR amplification followed by DNA sequence analysis using an ABI 3730 capillary sequencer (Agencourt Bioscience, Beverly, MA). Bidirectional sequence traces were analyzed for mutations using Mutation Surveyor (Softgenetics, Inc., State College, PA), and all traces with putative mutations were reviewed manually. Any potential missense alleles were censored from analysis without validation in paired germline material, whereas all frameshift and nonsense alleles were scored somatic in origin.

Western Blot and Immunoprecipitation Analysis

Western blots were carried out using the following antibodies: ASXL1 (Clone N-13; Santa Cruz (sc-85283); N-terminus directed), ASXL1 (Clone 2049C2a; Santa Cruz (sc-81053); C-terminus directed), BAP1 (clone 3C11; Santa Cruz (sc-13576)), BMI1 (Abcam ab14389), EED (Abcam ab4469), EZH2 (Active Motif 39933 or Millipore 07-689), FLAG (M2 FLAG; Sigma A2220), Histone H3 lysine 27 trimethyl (Abcam ab6002), Histone H2A Antibody II (Cell Signaling Technologies 2578), Ubiquityl-Histone H2AK119 (Clone

D27C4; Cell Signaling Technologies 8240), RING1A (Abcam ab32807), SUZ12 (Abcam ab12073), and total histone H3 (Abcam ab1791), and tubulin (Sigma, T9026). Antibodies different from the above used for immunoprecipitation include: ASXL1 (clone H105X; Santa Cruz (sc- 98302)), FLAG (Novus Biological Products; NBP1-06712), and EZH2 (Active Motif 39901). IP and pull-down reactions were performed in IP buffer (150 mM NaCl, 20mM Tris (pH 7.4–7.5), 5mM EDTA, 1% Triton, 100mM sodium orthovanadate, protease arrest (Genotec), 1mM PMSF, and phenylarsene oxide). To ensure nuclease-free IP conditions, IP's were also performed using the following methodology (*135*): cells were lysed in BC-300 buffer (20mM Tris-HCl (pH 7.4), 10% glycerol, 300mM KCl, 0.1% NP-40) and the cleared lysate was separated from the insoluble pellet and treated with $MgCl_2$ to 2.5mM and benzonase (EMD) at a concentration of 1250 U/ml. The lysate was then incubated for 1–1.5 hours at 4 degrees. The reaction was then stopped with addition of 5mM EDTA. DNA digestion in confirmed on an ethidium bromide agarose gel. We then set up our IP by incubating our lysate overnight at 4 degrees.

Histone Extraction and Histone LC/MS analysis

Histones were extracted using either standard overnight acid extraction protocol or using Histone Purification MiniKit (Active Motif 40026). Acid-extracted proteins were resolved in SDS-PAGE, in-gel trypsin digested, and analyzed by reversed-phase LC-MS/MS as described previously (*136*).

Gene Expression Analysis

Total RNA was extracted from cells using Qiagen's RNeasy Plus Mini kit (Valencia, CA). cDNA synthesis, labeling, hybridization and quality control were carried out as previously described (*137*). Ten micrograms of RNA was then used for generation of labeled cRNA according to the manufacturer's instructions (Affymetrix, Santa Clara, CA). Hybridization

of the labeled cRNA fragments and washing, staining, and scanning of the arrays were carried out as per instructions of the manufacturer. Labeled cRNA from CD34+ cells treated with either ASXL1 siRNA or controls were analyzed using the Affymetrix HG-U133-Plus2.0 platform and from UKE1 cells using the Illumina Href8 array. All expression profile experiments were carried out using biological duplicates. Raw expression values from the Affymetrix platform were pre-processed using the MAS 5.0 algorithm where probeset values having "Present" calls in ≥80% of samples were captured and quantile normalized across all samples on a per-chip basis. Raw expression values generated by Genome Studio (Illumina) were filtered to exclude probesets having expression values below negative background in ≥80% of samples. Probesets remaining after background filtering were log-2 transformed and quantile normalized on a per-chip basis. qRT-PCR was performed on cDNA using SYBR green quantification in an ABI 7500 sequence detection system.

Chromatin Immunoprecipitation and Antibodies

ChIP experiments for H3K4me3, H3K27me3, and H3K36me3 were carried out as described previously (*138, 139*). Cells were crosslinked in 1% formaldehyde, lysed and sonicated with a Branson 250 Sonifier to obtain chromatin fragments in a size range between 200 and 700 bp. Solubilized chromatin was diluted in ChIP dilution buffer (1:10) and incubated with antibody overnight at 4°C. Protein A sepharose beads (Sigma) were used to capture the antibody-chromatin complex and washed with low salt, LiCl, as well as TE (pH 8.0) wash buffers. Enriched chromatin fragments were eluted at 65°C for 10 min, subjected to crosslink reversal at 65°C for 5 hrs, and treated with Proteinase K (1 mg/ml), before being extracted by phenol-chloroform-isoamyl alcohol, and ethanol precipitated. ChIP DNA was then quantified by QuantiT Picogreen dsDNA Assay kit (Invitrogen). ChIP experiments for ASXL1 were carried out on nuclear preps.

Crosslinked cells were incubated in swelling buffer (0.1 M Tris pH 7.6, 10 mM KOAc, 15 mM MgOAc, 1% NP40), on ice for twenty minutes, passed through a 16G needle 20 times and centrifuged to collect nuclei. Isolated nuclei were then lysed, sonicated and immunoprecipitated as described above. Antibodies used for ChIP include anti-H3K4me3 (Abcam ab8580), anti-H3K27me3 (Upstate 07-449), anti-H3K36me3 (Abcam ab9050), and anti-ASXL1 (clone H105X; Santa Cruz (sc-98302)), and Ubiquityl-Histone H2AK119 (Clone D27C4; Cell Signaling Technologies 8240).

Sequencing Library Preparation, Illumina/Solexa Sequencing, and Read Alignment and Generation of Density Maps

Library preparation and ultra high-throughput sequencing were carried out as described (*139*). Briefly, one to ten nanograms (ng) of ChIP DNA were end-repaired and 59phosphorylated using ENDIt DNA End-Repair Kit (Epicentre). We then followed steps four through seven of Illumina standard sample prep protocol (v1.8) using Genomic DNA Sample Prep Kit (Illumina) with minor modifications. A single Adenine was added to 39 ends by Klenow (39*R*59 exo2), and double-stranded Illumina Adapters were ligated to the ends of the ChIP fragments. Adapter-ligated ChIP DNA fragments between 275 bp to 700 bp were gel-purified and subjected to 18 cycles of PCR. Prepared libraries were quantified using PicoGreen and sequenced on the Illumina Genome Analyzer per standard operating procedures. Sequence reads (36 bases) from each ChIP experiment were compiled, post-processed and aligned to the appropriate reference genome using a general purpose computational pipeline as described previously (*139*). Aligned reads are used to estimate the number of end-sequenced ChIP fragments that overlap any given genomic position (at 25-bp resolution). For each position, we counted the number of reads that are oriented towards it and closer than the average length of a library fragment (300 bp). The result is a high-resolution density map that can be viewed

through the UCSC Genome Browser [62] and is used for downstream analyses. Prior comparisons to microarray analysis and quantitative real-time PCR have shown that ChIP-Seq density maps accurately reflect enrichment (*139*).

HOXA Nanostring nCounter Gene Expression CodeSet

Direct digital mRNA analysis of *HOXA* cluster gene expression was performed using a Custom CodeSet including each *HOXA gene* (NanoString Technologies). Synthesis of the oligonucleotides was done by NanoString Technologies, and hybridization and analysis was done using the Prep Station and Digital Analyzer purchased from the company.

Animal Use, Retroviral Bone Marrow Transplantation, Flow Cytometry and Colony Assays

Animal care was in strict compliance with institutional guidelines established by the Memorial Sloan-Kettering Cancer Center, the National Academy of Sciences Guide for the Care and Use of Laboratory Animals, and the Association for Assessment and Accreditation of Laboratory Animal Care International. All animal procedures were approved by the Institutional Animal Care and Use Committee (IACUC) at Memorial Sloan-Kettering Cancer Center. NRasG12D plus MIGR1 EV or mASXL1 shRNA bone marrow transplantation assays were performed using donor cells from 5FU-conditioned mice as described previously (*140*). Animal care was in strict compliance with institutional guidelines established by the Memorial Sloan-Kettering Cancer Center, the National Academy of Sciences Guide for the Care and Use of Laboratory Animals, and the Association for Assessment and Accreditation of Laboratory Animal Care International. For surface flow cytometry of mouse bone marrow and spleen, cells were washed in phosphate-buffered saline (PBS) plus 1% BSA and stained with monoclonal

42

antibodies in PBS plus 1% BSA for 20 minutes on ice. Antibodies used were CD11b (PECy7), Gr1 (APCCy7), CD71 (PE), and Ter119 (PECy7; all from BD Pharmingen). Files were analyzed in FlowJo (TreeStar). Bone marrow was harvested from the femurs of C57/Black/6 mice transplanted with NRasG12D in combination with a MIGR1 EV or ASXL1 shRNA after sacrifice$1x10^4$ whole bone marrow cells were plated in duplicate in methylcellulose with complete cytokine mix (MethoCult GF M3434; StemCell Technologies). Colonies were scored at 14 days after seeding and followed by flow cytometric analysis of the population of cells plated in methylcellulose. Cytospins were made from 10-30,000 mouse bone marrow cells collected from liquid culture using a Cytospin 4 slide centrifuge (Thermo). Cells were then stained with Wright-Giemsa stain. Digital images were acquired using a Nikon Eclipse E400 microscope equipped with a digital camera and analyzed using Spot Advanced software.

Protein half-life and proteasome-mediated degradation of H2K119Ub studies and densitometry

HEK-293T cells were transfected with cDNA constructs and then treated with 100ug/mL cycloheximide (Sigma-Aldrich). Cells were harvested at 0 and 4 hours and prepped for Western blots, as previously described (see above). For proteasome inhibitor studies, SET2 cells were pretreated with 5 µM MG-132 (EMD Chemicals) or DMSO for 2 hours (as previously described (*141*) followed by harvesting of cells for histone extraction and subsequent Western blotting using anti-total H2A and anti-H2AK119Ub antibodies. Western blots were scanned using Adobe Photoshop CS4 11.0.1, and quantitative densitometry was analyzed using ImageJ (http://rsbweb.nih.gov/ij/). Quantitative densitometry was expressed as the proportion of the protein of interest relative to loading control or input (as specified in the accompanying Figure Legend and/or manuscript text).

Statistical Analysis

Statistical significance was determined by Mann-Whitney U test and Fisher's exact test using Prism GraphPad software; Significance of survival differences was calculated using Log-rank (Mantel-Cox) test. $p < 0.05$ was considered statistically significant. Normalized expression data from CD34+ cord blood was used as a Gene Set Enrichment Analysis query of the C2 database (MSig DB) where 1,000 permutations of the genes was used to generate a null distribution. A pre-ranked gene list, containing genes up-regulated at least $\log^2$ 0.5-fold where the highest ranked genes corresponds to the genes, with the largest fold-difference between Asxl1 hairpin treated UKE1 cells and those treated with empty vector was used to query the C2 MSig DB as described above.

RESULTS

ASXL1 Mutations Result in Loss of ASXL1 Expression

ASXL1 mutations in patients with myeloproliferative neoplasms, myelodysplastic syndrome, and acute myeloid leukemia most commonly occur as somatic nonsense mutations and insertion/deletion mutations in a clustered region adjacent to the highly conserved PHD domain. To assess whether these mutations result in loss of ASXL1 protein expression or in expression of a truncated isoform, we performed western blots using N- and C-terminal anti-ASXL1 antibodies in a panel of human myeloid leukemia cell lines and primary acute myeloid leukemia samples, which are wild-type or mutant for *ASXL1*. We found that myeloid leukemia cells with homozygous frameshift/nonsense mutations in *ASXL1* (NOMO1 and KBM5) have no detectable ASXL1 protein expression (**Figure 2.1A**). Similarly, leukemia cells with heterozygous *ASXL1* mutations have reduced or absent ASXL1 protein expression. Western blot analysis of ASXL1 using an

N-terminal anti-ASXL1 antibody in primary acute myeloid leukemia samples wild-type

and mutant for *ASXL1* revealed reduced/absent full-length ASXL1 expression in

samples with *ASXL1* mutations compared to *ASXL1* wild-type samples (**Figure 2.2A**).

Importantly, we did not identify truncated ASXL1 protein products in mutant samples
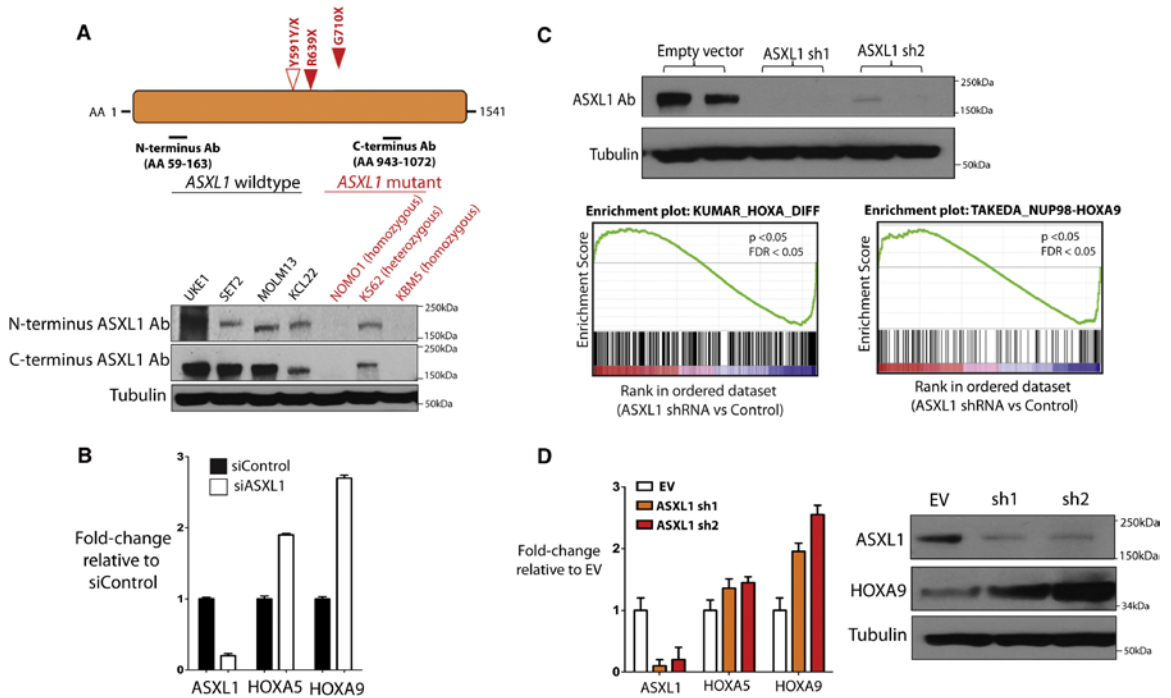
Figure 2.1. Leukemogenic ASXL1 Mutations Are Loss-of-Function Mutations and ASXL1 Loss is Associated with Upregulation of HOXA Gene Expression. (**A**) Characterization of ASXL1 expression in leukemia cells with nonsense mutations in ASXL1 reveals loss of ASXL1 expression at the protein level in cells with homozygous ASXL1 mutations as shown by western blotting using N- and C-terminal anti-ASXL1 antibodies. (**B**) Displayed are the ASXL1-mutant cell line lines NOMO1 (homozygous ASXL1 R639X), K562 (heterozygous ASXL1 Y591Y/X), and KBM5 (homozygous ASXL1 G710X) and a panel of ASXL1-wild-type cell lines. ASXL1 siRNA in human primary CD34+ cells form cord blood results in upregulation of HOXA5 and HOXA9 with ASXL1 knockdown (KD) as revealed by quantitative real-time PCR (qRT-PCR) analysis. (**C** and **D**) Stable KD of ASXL1 in ASXL1-wild-type transformed human myeloid leukemia UKE1 cells (as shown by western blot) followed by GSEA reveals significant enrichment of gene sets characterized by upregulation of 50 HOXA genes (**C**) as was confirmed by qRT-PCR (**D**). Statistical significance is indicated in (**D**) by the p value and false-discovery rate (FDR). Similar upregulation of HOXA9 is seen by the western blot following stable ASXL1 KD in the ASXL1-wild-type human leukemia SET2 cells. Error bars represent standard deviation of expression relative to control.
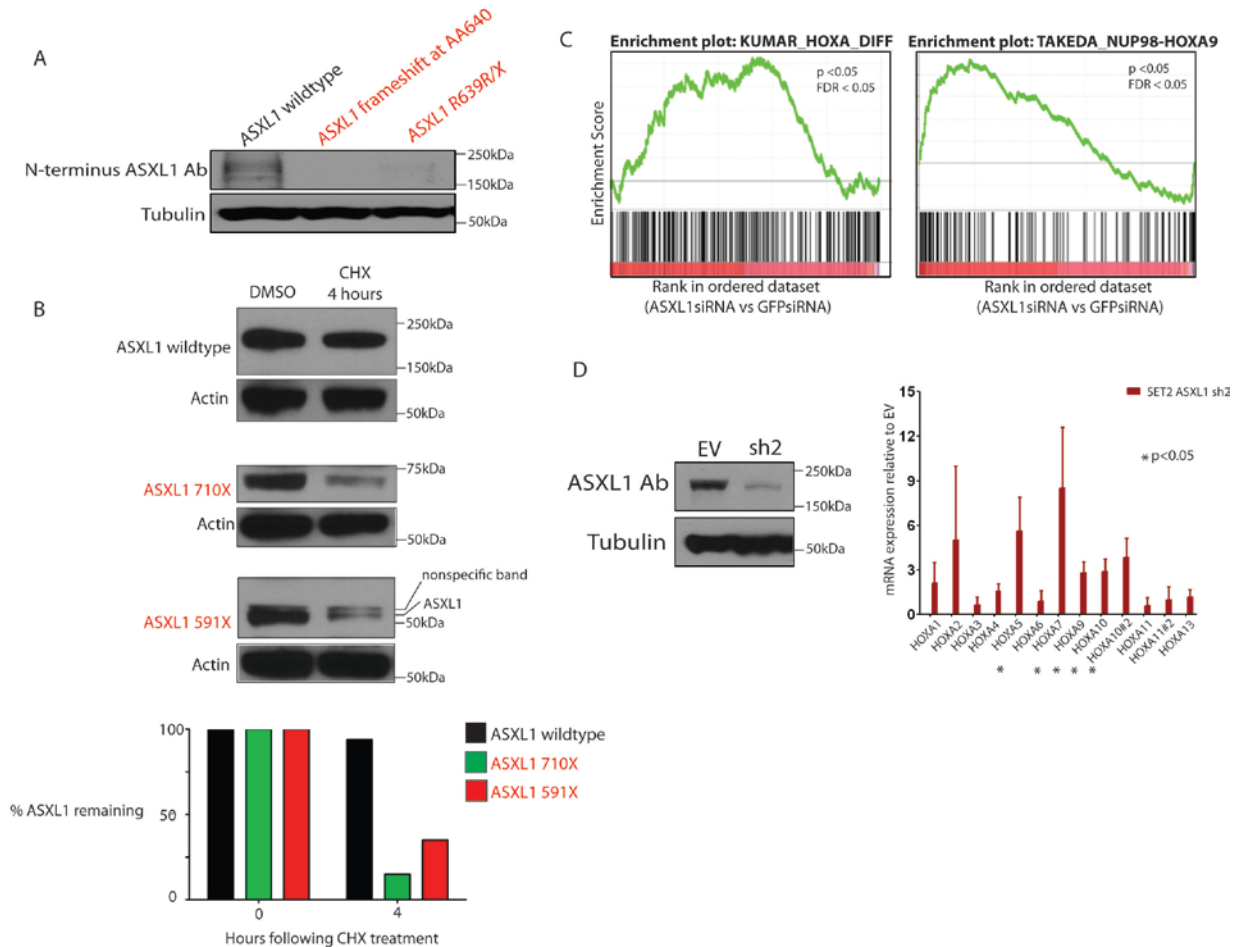
Figure 2.2. Leukemogenic *ASXL1* mutations are loss-of-function mutations and ASXL1 loss is associated with upregulation of *HOXA* gene expression. Minimal ASXL1 protein expression in mononuclear cell lysates from primary AML samples from patients with *ASXL1* mutations compared to those which are *ASXL1* wildtype. (**A**). Use of an N-terminal anti-ASXL1 antibody failed to detect a truncated form of ASXL1 in full-length Western blot confirming loss of ASXL1 protein expression with *ASXL1* mutations. Transfection of HEK293T cells with wildtype ASXL1 cDNA or ASXL1 cDNAs bearing *ASXL1* mutations (ASXL1 591X and ASXL1 710X) followed by treatment with DMSO or cycloheximide (100ug/mL) reveals a larger time-dependent decrease in ASXL1 protein expression in cells bearing mutant forms of ASXL1 cDNA compared with wildtype forms (**B**). Western blotting was performed after 4 hours of DMSO or cycloheximide exposure using an N-terminal anti-ASXL1 antibody. Loss of ASXL1 in primary CD34+ cells from cord blood revealed a significant enrichment of genes seen with *MLL-AF9* and *NUP98-*

46

HOXA9 overexpression as seen by Gene Set Enrichment Analysis (GSEA) (**C**). Statistical significance is indicated by the p-value and false-discovery rate (FDR). Stable shRNA-mediated knockdown of ASXL1 in the human myeloid leulemia cell line SET2 followed by direct quantitative mRNA measurement of *HOXA* genes expression by Nanostring reveals significant upregulation of multiple HOXA genes including *HOXA5, 7, 9,* and *HOXA10* (**D**). Error bars represent standard deviation of mRNA quantity relative to control. Asterisks indicate *p*<0.05.

using N- or C-terminal directed antibodies in primary acute myeloid leukemia samples or leukemia cell lines. Moreover, expression of wild-type ASXL1 cDNA or cDNA constructs bearing leukemia-associated mutant forms of ASXL1 revealed reduced stability of mutant forms of ASXL1 relative to wild-type ASXL1, with more rapid degradation of mutant ASXL1 isoforms following cycloheximide exposure (**Figure 2.2B**). These data are consistent with ASXL1 functioning as a tumor suppressor with loss of ASXL1 protein expression in leukemia cells with mutant *ASXL1* alleles.

ASXL1 Knockdown in Hematopoietic Cells Results in Upregulated *HOXA* Gene Expression

Given that *ASXL1* mutations result in loss of ASXL1 expression, we investigated the effects of ASXL1 knockdown in primary hematopoietic cells. We used a pool of small interfering RNAs (siRNA) to perform knockdown of ASXL1 in primary human CD34+ cells isolated from umbilical cord blood. ASXL1 knockdown was performed in triplicate and confirmed by qRT-PCR analysis (**Figure 2.1B**), followed by gene-expression microarray analysis. Gene-set enrichment analysis (GSEA) of this microarray data revealed a significant enrichment of genes found in a previously described gene expression signature of leukemic cells from bone marrow of *MLL-AF9* knock-in mice (*142*), as well as highly significant enrichment of a gene signature found in primary human cord blood CD34+ cells expressing *NUP98-HOXA9* (**Figure 2.2C**) (*143*). Specifically, we found that ASXL1 knockdown in human primary CD34+ cells resulted in

47

increased expression of 145 genes out of the 279 genes, which are overexpressed in the *MLL-AF9* gene expression signature ($p < 0.05$, FDR < 0.05). These gene expression signatures are characterized by increased expression of posterior *HOXA* cluster genes, including *HOXA5-9.*

In order to ascertain whether loss of ASXL1 was associated with similar transcriptional effects in leukemia cells, we performed short hairpin RNA (shRNA)-mediated stable knockdown of *ASXL1* in the *ASXL1*-wild-type human leukemia cell lines UKE1 (**Figure 2.1C,D**) and SET2 (**Figure 2.1D**) followed by microarray and qRT-PCR analysis. Gene expression analysis in UKE-1 cells expressing ASXL1 shRNA compared to control cells revealed significant enrichment of the same *HOXA* gene expression signatures as were seen with ASXL1 knockdown in CD34+ cells (**Figure 2.1C**). Upregulation of 5′ *HOXA* genes was confirmed by qRT-PCR in UKE1 (**Figure 2.1D**) cells and by western blot analysis (**Figure 2.1D**) in SET2 cells expressing ASXL1 shRNA compared to control. Quantitative mRNA profiling (Nanostring nCounter) of the entire *HOXA* cluster revealed upregulation of multiple *HOXA* members, including *HOXA5, 7, 9,* and *10*, in SET2 cells with ASXL1 knockdown compared to control cells (**Figure 2.2D**). These results indicate consistent upregulation of *HOXA* gene expression following ASXL1 loss in multiple hematopoietic contexts.

ASXL1 Forms a Complex with BAP1 in Leukemia Cells, but BAP1 Loss Does Not Upregulate *HoxA* Gene Expression in Hematopoietic Cells

Mammalian ASXL1 forms a protein complex *in vitro* with the chromatin deubiquitinase BAP1, which removes monoubiquitin from histone H2A at lysine 119 (H2AK119) (*22*). In *Drosophila* loss of either Asx or Calypso resulted in similar effects on genome-wide H2AK119 ubiquitin levels and on target gene expression. Recent studies have revealed recurrent germline and somatic loss-of-function *BAP1* mutations in mesothelioma and

uveal melanoma (*58, 61, 63*). However, we have only identified rare *BAP1* mutations in patients with myeloproliferative neoplasms or acute myeloid leukemia (*76*). Co-immunopreciptation studies revealed an association between ASXL1 and BAP1 in human myeloid leukemia cells wild-type for *ASXL1* but not in those cells mutant for *ASXL1* due to reduced/absent ASXL1 expression (**Figure 2.3A**). Immunoprecipitation of FLAG-tagged wild-type ASXL1 and FLAG-tagged leukemia-associated mutant forms of ASXL1 revealed reduced interaction between mutant forms of ASXL1 and endogenous BAP1 (**Figure 2.4A**). Despite these findings, BAP1 knockdown did not result in upregulation of *HOXA5* and *HOXA9* in UKE1 cells, although a similar extent of ASXL1 knockdown in the same cells reproducibly increased *HOXA5* and *HOXA9* expression (**Figure 2.3B**). We obtained similar results with knockdown of Asxl1 or Bap1 in the Ba/F3 murine hematopoietic cell line (**Figure 2.3C**). In Ba/F3 cells, knockdown of *Asxl1* resulted in upregulated *Hoxa9* gene expression commensurate with the level of Asxl1 downregulation, whereas knockdown of Bap1 does not impact *Hoxa* expression (**Figure 2.3C**). ASXL1 knockdown in SET-2 cells failed to reveal an effect of ASXL1 loss on H2AK119Ub levels as assessed by western blot of purified histones from shRNA control and ASXL1 knockdown cells (**Figure 2.4B**). By contrast, SET2 cells treated with MG132 (25 µM) had a marked decrease in H2AK119Ub, as has been previously described (*141*). These data suggest that ASXL1 loss contributes to myeloid transformation through a BAP1-independent mechanism.

Loss of ASXL1 Is Associated with Global Loss of H3K27me3

The results described above led us to hypothesize that ASXL1 loss leads to BAP1-independent effects on chromatin state and on target gene expression. To assess the genome-wide effects of ASXL1 loss on chromatin state, we performed chromatin immunoprecipitation followed by next generation sequencing (ChIP-seq) for histone

49

modifications known to be associated with PcG [histone H3 lysine 27 trimethylation (H3K27me3)] or TxG activity [histone H3 lysine 4 trimethylation (H3K4me3)] in UKE1
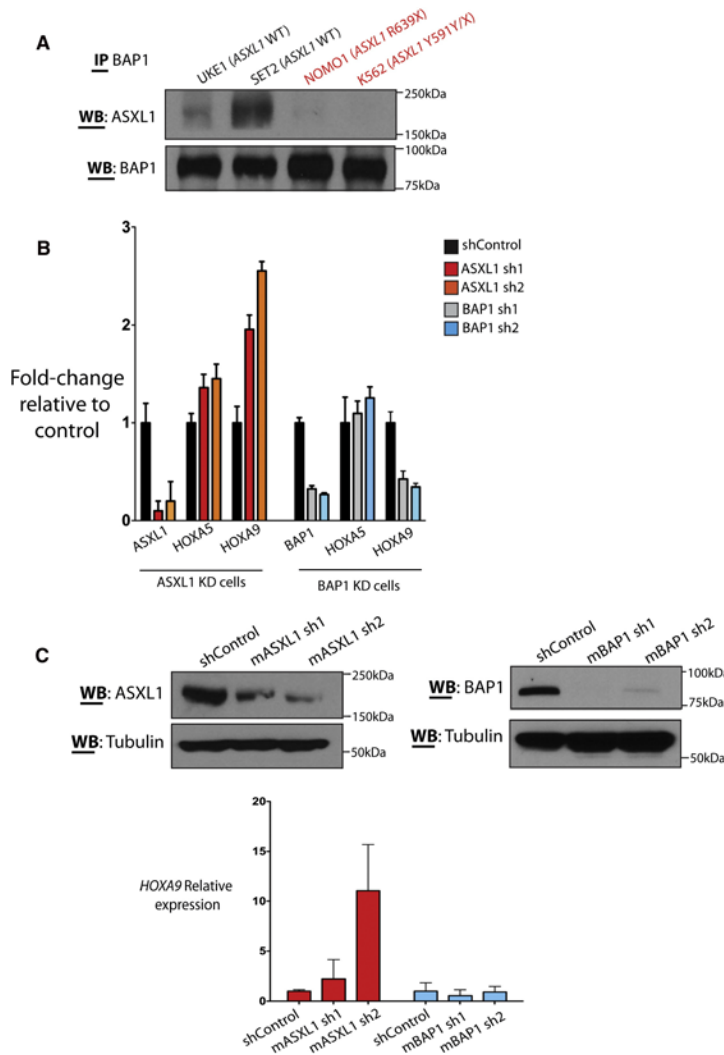
Figure 2.3. ASXL1 and BAP1 Physically Interact in Human Hematopoietic Cells but BAP1 Loss Does Not Result in Increased HoxA Gene Expression. (**A**) Immunoprecipitation of BAP1 in a panel of ASXL1-wild-type and mutant human myeloid leukemia cells reveals co-association of ASXL1 and BAP1. (**B**) Cells with heterozygous or homozygous mutations in ASXL1 with reduced or absent ASXL1 expression have minimal interaction with BAP1 in vitro. BAP1 knockdown in the ASXL1/BAP1 wild-type human leukemia cell line UKE1 fails to alter HOXA gene expression. In contrast, stable knockdown of ASXL1 in the same cell type results in a significant upregulation of HOXA9. (**C**) Similar results are seen with knockdown of Asxl1 or Bap1 in murine precursor-B lymphoid Ba/F3 cells. Error bars represent standard deviation of expression relative to control.
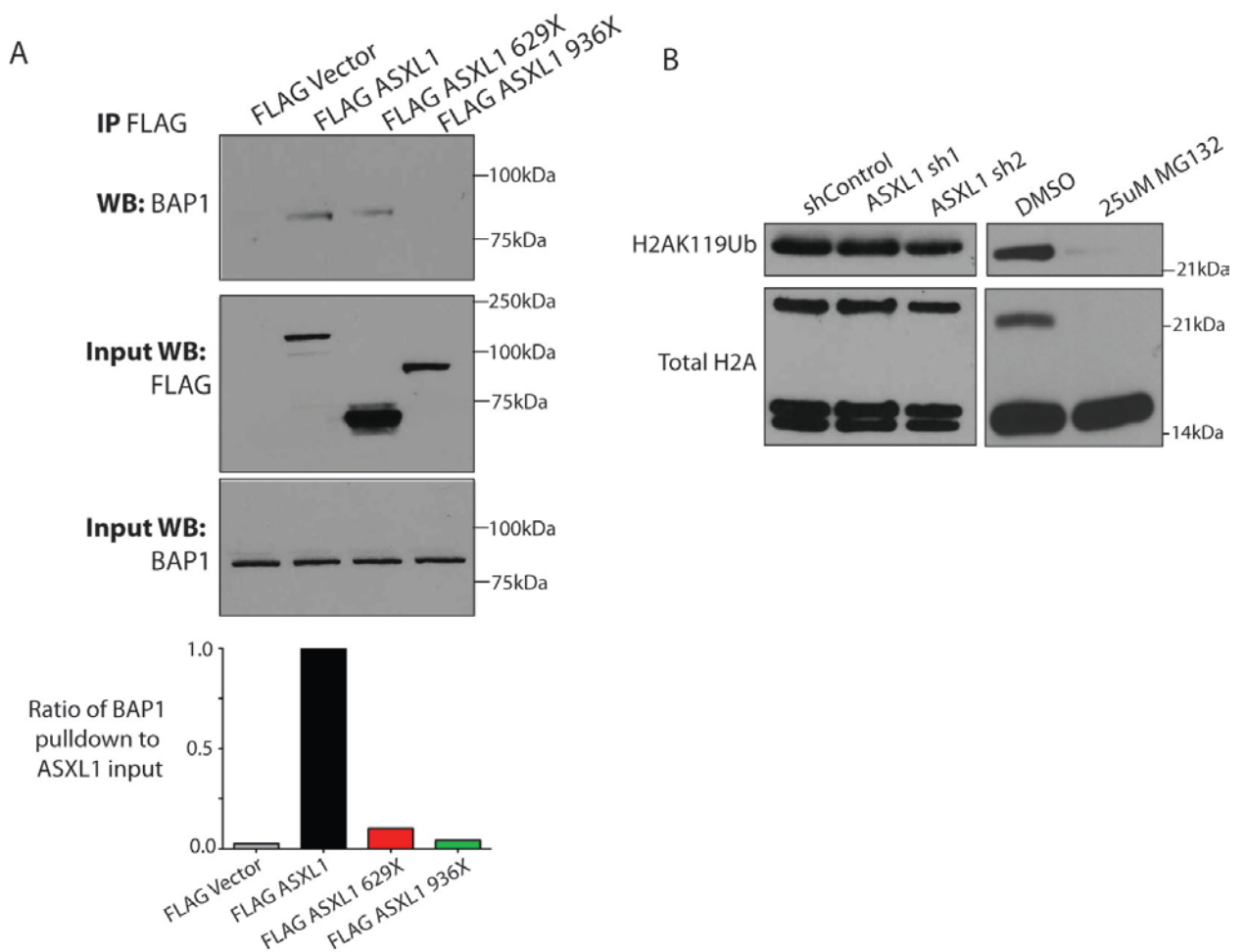
Figure 2.4. Leukemia-associated mutations in *ASXL1* affect ASXL1 binding to BAP1 but loss of ASXL1 has minimal global effects on H2AK119 ubiquitin (H2AK119Ub) in myeloid leukemia cells. Immunoprecipitation of FLAG-tagged empty vector, ASXL1 wildtype or 2 mutant forms of ASXL1 (ASXL1 629X, ASXL1 936X) in HEK293T cells followed by Western blotting using an anti-BAP1 antibody reveals specific binding of ASXL1 to endogenous BAP1 and decreased ASXL1 pulldown of endogenous BAP1 by mutant forms of ASXL1 (**A**). Protein quantitative densitometry is also shown displaying the proportion of immunoprecipitated BAP1 relative to input ASXL1. Western blotting of H2AK119Ub and total H2A in purified histones from SET2 cells treated with shRNA control or one of 2 shRNAs against ASXL1 fails to reveal global alterations in H2AK119Ub levels with ASXL1 knockdown (**B**). As a control to indicate the ability to detect alterations in global H2AK119Ub levels, Western blotting of histones from SET2 cells treated with DMSO or MG132 (25uM) is shown revealing a decrease in H2AK119Ub in blots performed with anti-H2AK119Ub and anti-total H2A antibodies.

cells expressing empty vector or two independent validated shRNAs for ASXL1. ChIP-Seq data analysis revealed a significant reduction in genome-wide H3K27me3 transcriptional start site occupancy with ASXL1 knockdown compared to empty vector ($p = 2.2 \times 10^{-16}$; **Figure 2.5A**). Approximately 20% of genes (n = 4,686) were initially marked by H3K27me3 in their promoter regions (defined as 1.5 kb downstream and 0.5 kb upstream of the transcriptional start site). Among these genes, ~27% had a 2-fold reduction in H3K27me3 (n = 1,309) and ~66% had a 1.5-fold reduction in H3K27me3 (n = 3,092), respectively, upon ASXL1 knockdown. No significant effect was seen on H3K4me3 transcriptional start site occupancy with ASXL1 depletion (**Figure 2.5A**). We next evaluated whether loss of ASXL1 might be associated with loss of H3K27me globally by performing western blot analysis on purified histones from UKE1 cells transduced with empty vector or shRNAs for ASXL1 knockdown. This analysis revealed a significant decrease in global H3K27me3 with ASXL1 loss (**Figure 2.5B**), despite preserved expression of the core polycomb repressive complex 2 (PRC2) members EZH2, SUZ12, and EED. Similar effects on total H3K27me3 levels were seen following Asxl1 knockdown in Ba/F3 cells (**Figure 2.6A**). These results demonstrate that ASXL1 depletion leads to a marked reduction in genome-wide H3K27me3 in hematopoietic cells.

Detailed analysis of ChIP-seq data revealed that genomic regions marked by large H3K27me3 domains in control cells displayed more profound loss of H3K27me3 upon loss of ASXL1. Genome-wide analysis of the ChIP-Seq data from control and ASXL1 shRNA treated cells revealed that the sites that lose H3K27me3 in the ASXL1 knockdown cells were on average ~6.6 kb in length, while the sites that maintained H3K27me3 were on average ~3.1 kb in length ($p < 10^{-16}$) (**Figure 2.6B**). This is visually illustrated by the reduction in H3K27me3 at the posterior *HOXA* cluster (**Figure 2.5C**)
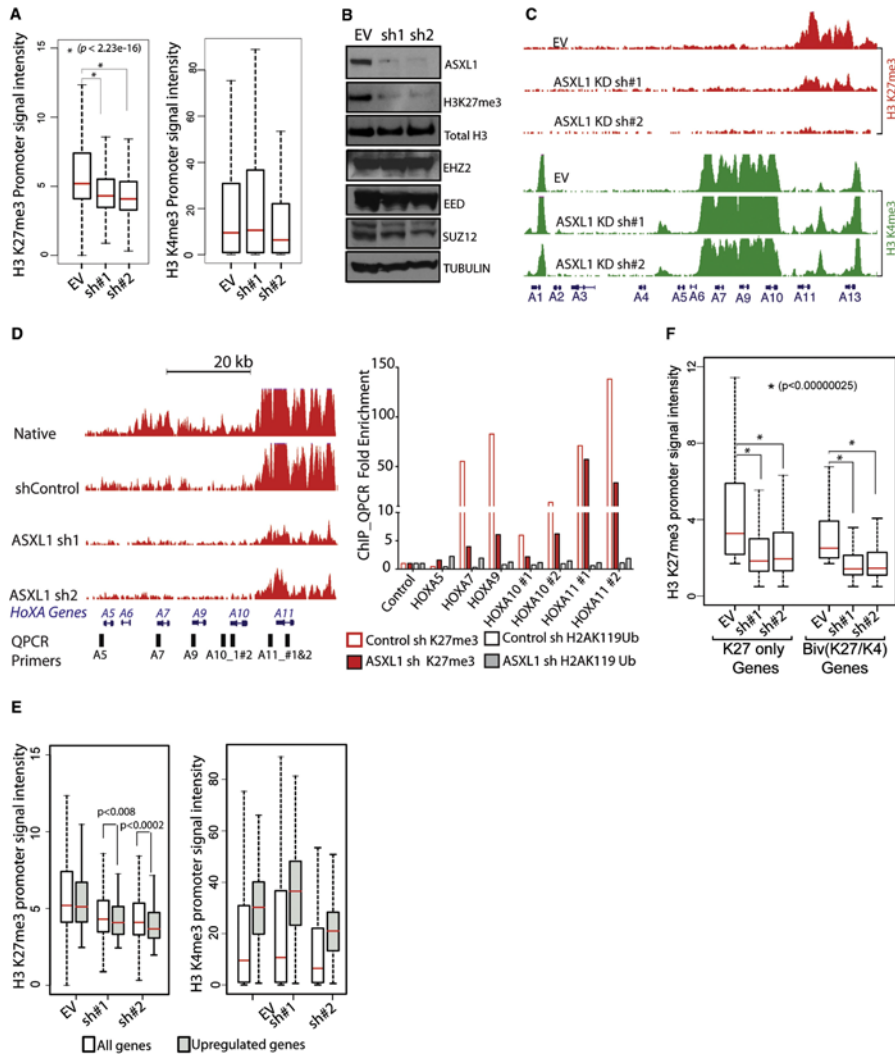
Figure 2.5. ASXL1 Loss Is Associated with Loss of H3K27me3 and with Increased Expression of Genes Poised for Transcription. (**A**) ASXL1 loss is associated with a significant genome-wide decrease in H3K27me3 as illustrated by box plot showing the 25th, 50th, and 75th percentiles for H3K27me3 and H3K4me3 enrichment at transcription start sites in UKE1 cells treated with an empty vector or shRNAs directed against ASXL1. The whiskers indicate the most extreme data point less than 1.5 interquartile range from box and the red bar represents the median. (**B**) Loss of ASXL1 is associated with a global loss of H3K27me3 without affecting PRC2 component expression as shown by western blot of purified histones from cells with UKE1 knockdown and western blot for core PRC2 component in whole cell lysates from ASXL1 knockdown UKE1 cells.
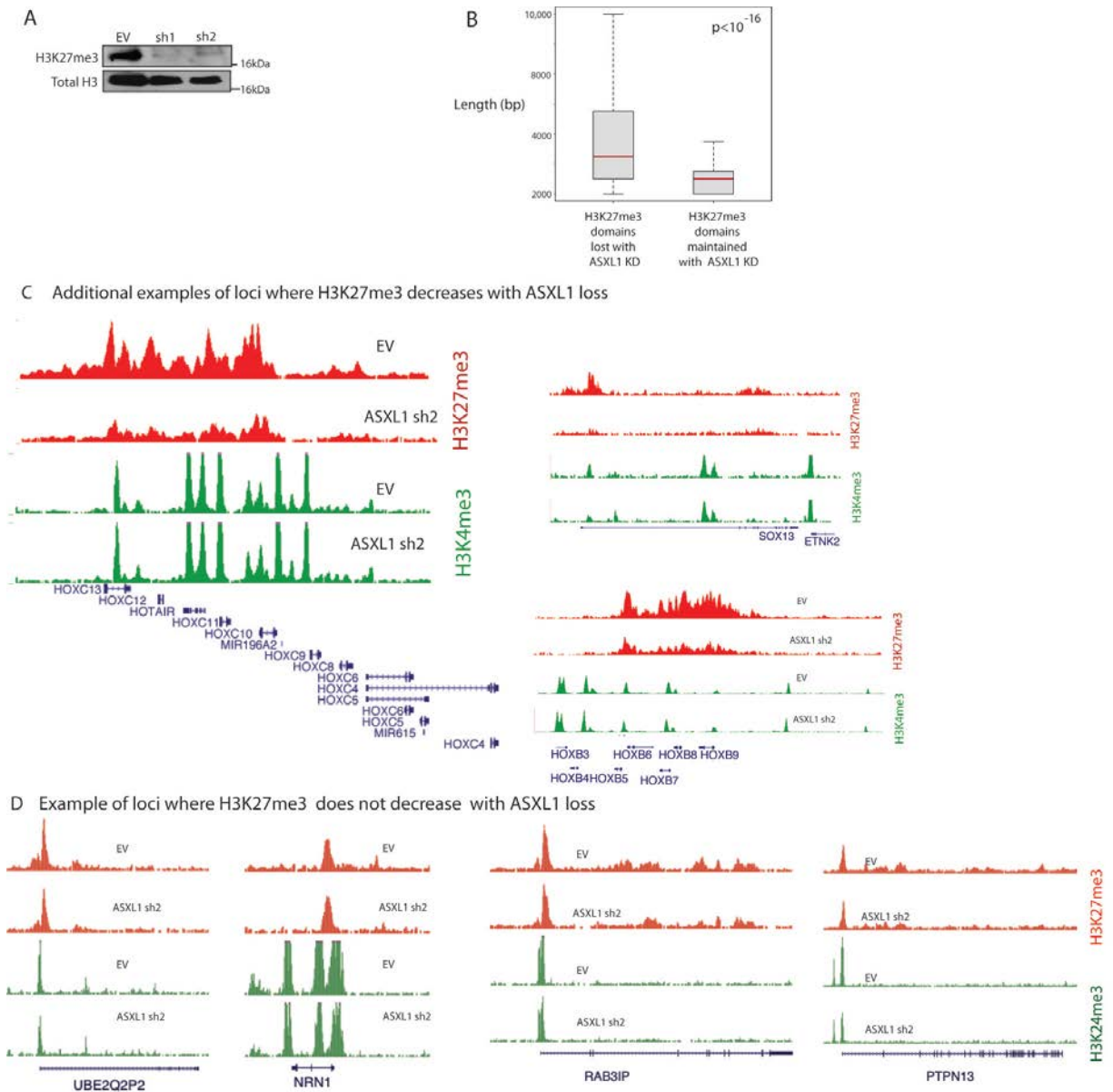
Figure 2.6. ASXL1 loss is associated with significant loss of global H3K27me3 in hematopoietic cells. Global loss of H3K27me3 following ASXL1 loss in murine precursor-B lymphoid Ba/F3 cells as shown by Western blot of purified histones (**A**). The association of ASXL1 loss with loss in H3K27me3 is most evident at genes normally marked by wide-regions of H3K27me3 occupancy as illustrated by box-and-whisker plots showing the length of the regions of DNA where H3K27me3 is lost following ASLX1 knockdown compared with the regions of DNA where H3K27me3 is maintained (**B**). The boxes represent the 25th and 75th quartiles, whiskers indicate most extreme data point less than 1.5 interquartile range from box and red bar represents the median. Additional examples of genes where H3K27me3 is decreased with ASXL1 loss are shown in (**C**). Examples of genes where H3K27me3 abundance is unchanged despite loss of ASXL1 are also shown (**D**).

and at the *HOXB and HOXC* loci (**Figure 2.6C**). The association of ASXL1 loss with loss of H3K27me3 abundance at the *HOXA* locus was confirmed by ChIP for H3K27me3 in control and ASXL1 knockdown cells followed by qPCR (ChIP-qPCR) across the *HOXA* locus (**Figure 2.5D**). ChIP-qPCR in control and knockdown cells revealed a modest increase in H2AK119Ub with ASXL1 loss at the *HOXA* locus (**Figure 2.5D**), in contrast to the more significant reduction in H3K27me3. In contrast to the large decrease in H3K27me3 levels at the *HOXA* locus with ASXL1 knockdown, a subset of loci had much less significant reduction in H3K27me3, in particular at loci whose promoters were marked by sharp peaks of H3K27me3 (**Figure 2.6D**). Intersection of gene expression and ChIP-Seq data revealed that genes overexpressed in ASXL1 knockdown cells were simultaneously marked with both activating (H3K4me3) and repressive (H3K27me3) domains in control cells (**Figure 2.5E,F**). This finding suggests that the transcriptional repression mediated by ASXL1 in myeloid cells is most apparent at loci poised for transcription with bivalent chromatin domains. Indeed, the effects of ASXL1 loss on H3K27me3 occupancy were most apparent at genes whose promoters were marked by the dual presence of H3K27me3 and H3K4me3 (**Figure 2.5F**). We cannot exclude the possibility that H3K4me3 and H3K27me3 exist in different populations within the homogeneous cell lines being studied, but the chromatin and gene expression data are consistent with an effect of ASXL1 loss on loci with bivalent chromatin domains (*138, 139*).

Enforced Expression of ASXL1 in Leukemic Cells Results in Suppression of *HOXA* Gene Expression, a Global Increase in H3K27me3, and Growth Suppression

We next investigated whether reintroduction of wild-type ASXL1 protein could restore H3K27me3 levels in *ASXL1* mutant leukemia cells. We stably expressed wild-type

ASXL1 in NOMO1 and KBM5 cells, homozygous *ASXL1* mutant human leukemia cell lines, which do not express ASXL1 protein (**Figure 2.7A** and **Figure 2.8A**). ASXL1 expression resulted in a global increase in H3K27me3 as assessed by histone western blot analysis (**Figure 2.7A**). Liquid chromotography/mass spectrometry of purified histones in NOMO1 cells expressing ASXL1 confirmed a ~2.5-fold increase in trimethylated H3K27 peptide and significant increases in dimethylated H3K27 in NOMO1 cells expressing ASXL1 compared to empty vector control (**Figure 2.7B**). ASXL1 add-back resulted in growth suppression (**Figure 2.7C**) and in decreased *HOXA* gene expression in NOMO1 cells (**Figure 2.7D**). ASXL1 add-back similarly resulted in decreased expression of *HOXA* target genes in KBM5 cells (**Figures 2.8A**,**B**). ChIP-qPCR revealed a strong enrichment in ASXL1 binding at the *HOXA* locus in NOMO1 cells expressing ASXL1, demonstrating that the *HOXA* locus is a direct target of ASXL1 in hematopoietic cells (**Figure 2.7E**).

ASXL1 Loss Leads to Exclusion of H3K27me3 and EZH2 from the HoxA Cluster Consistent with a Direct Effect of ASXL1 on PRC2 Recruitment

We next investigated whether the effects of ASXL1 loss on H3K27me3 was due to inhibition of PRC2 recruitment to specific target loci. ChIP-qPCR for H3K27me3 in SET2 cells with ASXL1 knockdown or control revealed a loss of H3K27me3 enrichment at the posterior *HoxA* locus with ASXL1 knockdown (**Figure 2.9A**,**B**). We observed a modest, variable increase in H3K4me3 enrichment at the *HOXA* locus with *ASXL1* depletion in SET2 cells (**Figure 2.9C**). We similarly assessed H3K27me3 enrichment in primary bone marrow leukemic cells from acute myeloid leukemia patients, wild-type and mutant for *ASXL1,* which likewise revealed decreased H3K27me3 enrichment across the *HOXA* cluster in primary acute myeloid leukemia
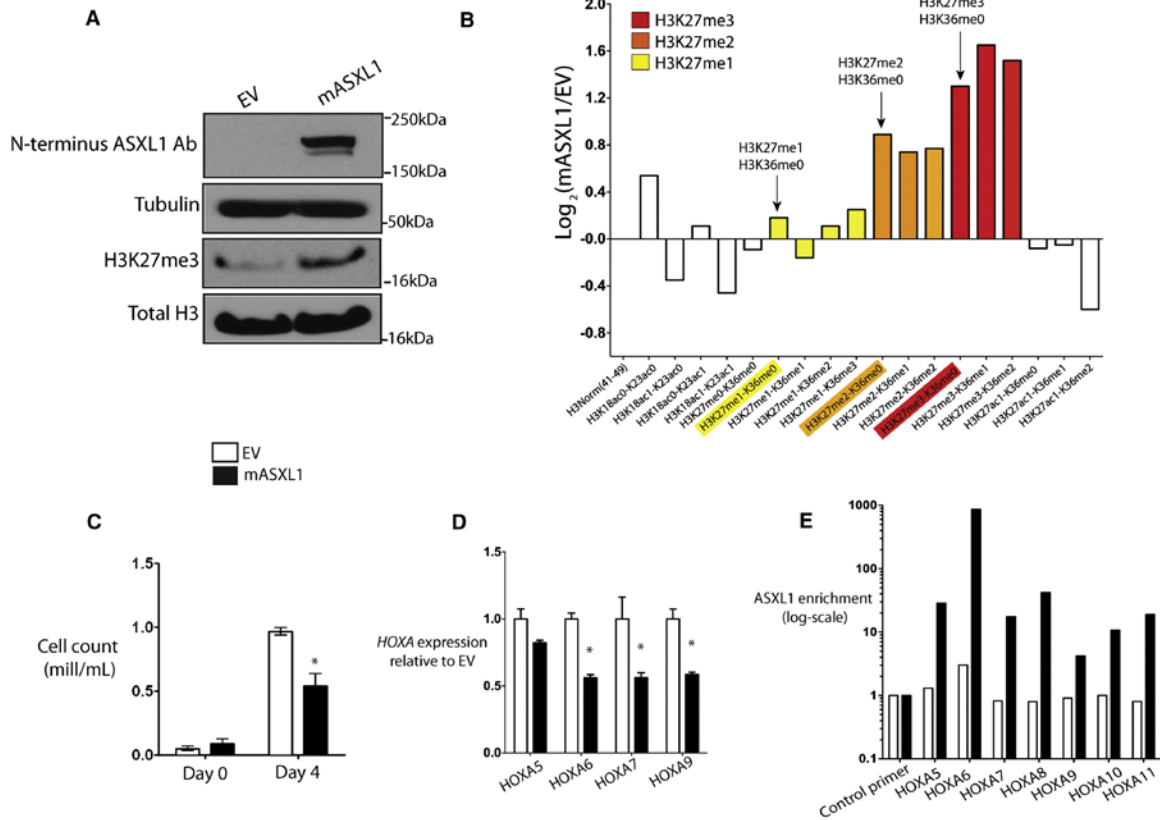
Figure 2.7. Expression of ASXL1 in ASXL1-Null Leukemic Cells Results in Global Increase in H3K27me2/3, Growth Suppression, and Suppression of HoxA Gene Expression. (**A** and **B**) ASXL1 expression in ASXL1 null NOMO1 cells is associated with a global increase in H3K27me3 as detected by western blot of purified histones (**A**) as well as by quantitative liquid-chromatography/mass spectrometry of H3 peptides from amino acids 18–40 (**B**) (arrows indicate quantification of H3K27me1/2/3). (**C**) ASXL1 overexpression results in growth suppression in 7-day growth assay performed in triplicate. (**D**) Overexpression of ASXL1 was associated with a decrement in posterior HoxA gene expression in NOMO1 cells as shown by qRT-PCR for HOXA5, 6, 7, and 9. (**E**) This downregulation in HOXA gene expression was concomitant with a strong enrichment of ASXL1 at the loci of these genes as shown by chromatin immunoprecipitation of ASXL1 followed by quantitative PCR with BCRRP1 as a control locus. Error bars represent standard deviation of target gene expression relative to control.
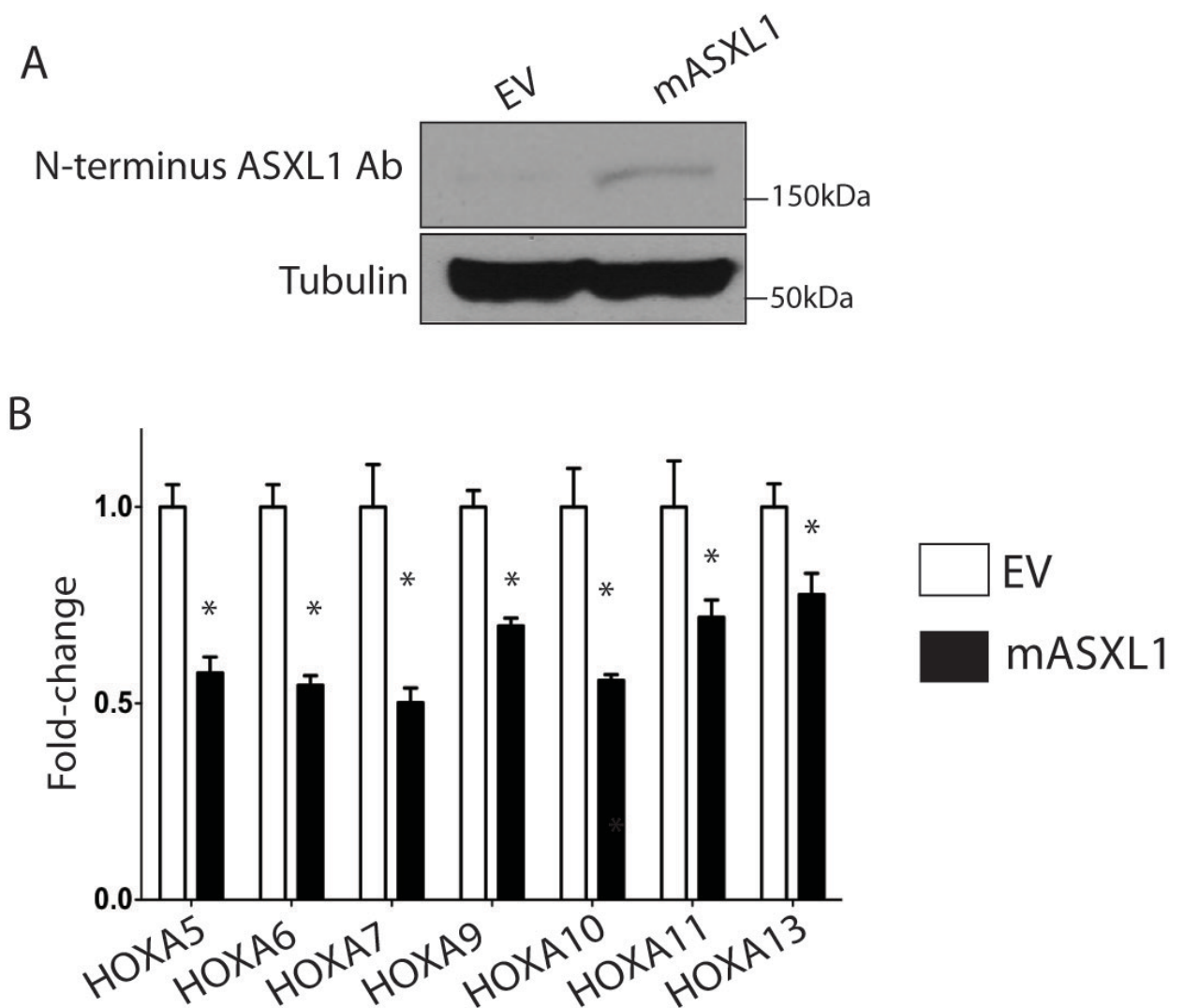
Figure 2.8. Reintroduction of ASXL1 in ASXL1-null leukemic cells results in a global increase in H3K27me3 and downregulation of *HOXA* gene expression. Murine Asxl1 cDNA (mASXL1) or an empty vector (EV) was expressed in human leukemia KBM5 cells, null for ASXL1 (**A**). ASXL1 expression in KBM5 cells is associated with a strong downregulation of *HoxA* gene expression as shown by qRT-PCR for *HOXA5-13* (**B**). Error bars represent standard deviation of mRNA expression relative to control. Asterisks indicate *p*<0.05 (two-tailed, Mann Whitney U test).

samples with *ASXL1* mutations compared to *ASXL1*-wild-type acute myeloid leukemia samples (**Figure 2.9D**).

Given the consistent effects of ASXL1 depletion on H3K27me3 abundance at the *HOXA* locus, we then evaluated the occupancy of EZH2, a core PRC2 member, at the *HoxA* locus. ChIP-Seq for H3K27me3 in native SET2 and UKE1 cells identified that H3K27me3 is present with a dome-like enrichment pattern at the 5′ end of the posterior *HOXA* cluster (**Figure 2.9A**); ChIP-qPCR revealed that EZH2 is prominently enriched in this same region in parental SET2 cells (**Figure 2.9E**). Importantly, ASXL1 depletion resulted in loss of EZH2 enrichment at the *HOXA* locus (**Figure 2.9E**), suggesting that ASXL1 is required for EZH2 occupancy and for PRC2-mediated repression of the posterior *HOXA* locus.

ASXL1 Physically Interacts with Members of the PRC2 in Human Myeloid Leukemic Cells

Given that ASXL1 localizes to PRC2 target loci and ASXL1 depletion leads to loss of PRC2 occupancy and H3K27me2, we investigated whether ASXL1 might physically interact with the PRC2 complex in hematopoietic cells. Co-immunoprecipitation studies using an anti-FLAG antibody in HEK293T cells expressing empty vector, hASXL1-FLAG alone, or hASXL1-FLAG plus hEZH2 cDNA revealed a clear co-immunoprecipitation of FLAG-ASXL1 with endogenous EZH2 and with ectopically expressed EZH2 (**Figure 2.10A**). Similarly, co-immuniprecipitation of FLAG-ASXL1 revealed physical association between ASXL1 and endogenous SUZ12 in 293T cells (**Figure 2.10A**). Immunoprecipitations were performed in the presence of benzonase to ensure that the protein-protein interactions observed were DNA-independent (**Figure 2.10B**) (*135*). We then assessed whether endogenous ASXL1 formed a complex with PRC2 members in
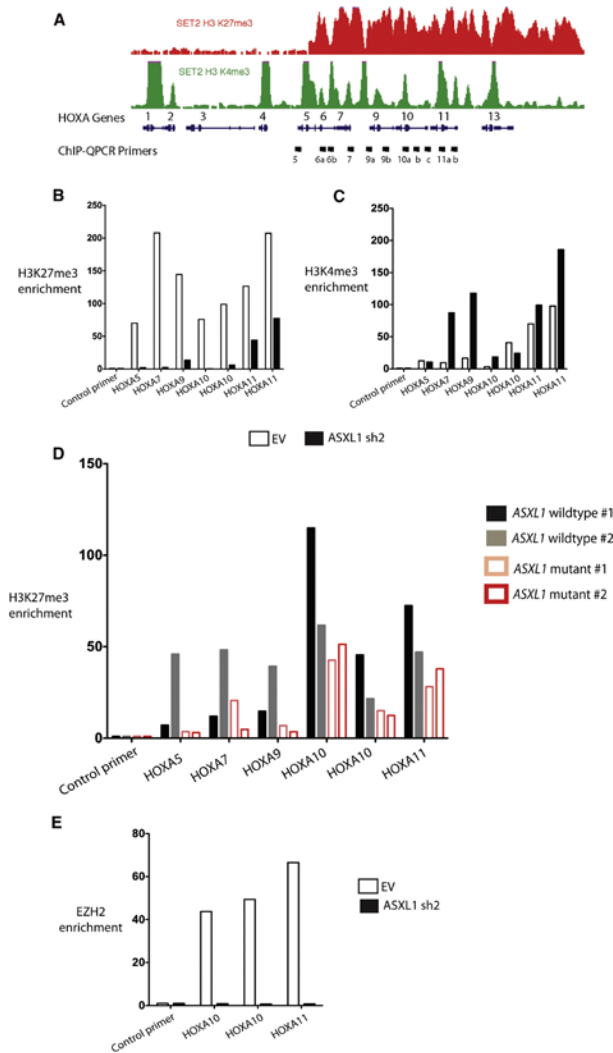
Figure 2.9. ASXL1 Loss Is Associated with Loss of PRC2 Recruitment at the HOXA Locus. (**A**) Chromatin-immunoprecipitation (ChIP) for H3K27me3 and H3K4me3 followed by next-generation sequencing reveals the abundance and localization of H3K27me3 and H3K4me3 at the HoxA locus in SET2 cells. (**B** and **C**) ChIP for H3K27me3 (**B**) and H3K4me3 (**C**) followed by quantitative PCR (qPCR) across the 50 HOXA locus in SET2 cells treated with an empty vector or stable knockdown of ASXL1 reveals a consistent downregulation of H3K27me3 across the 50 HOXA locus following ASXL1 loss and a modest increase in H3K4me3 at the promoters of 50 HOXA genes with ASXL1 loss [primer locations are shown in (**A**)]. (**D**) Similar ChIP for H3K27me3 followed by qPCR across the HOXA locus in primary leukemic blasts from two patients with ASXL1 mutations versus two without ASXL1 mutations reveals H3K27me3 loss across the HOXA locus in ASXL1 mutant cells. (**E**) ChIP for EZH2 followed by qPCR at the 50 end of HOXA locus in SET2 cells reveals loss of EZH2 enrichment with ASXL1 loss in SET2 cells. CHIPqPCR was performed in biologic duplicates and ChIP-qPCR data is displayed as enrichment relative to input. qPCR at the gene body of RRP1, a region devoid of H3K4me3 or H3K27me3, is utilized as a control locus. The error bars represent standard deviation.

61
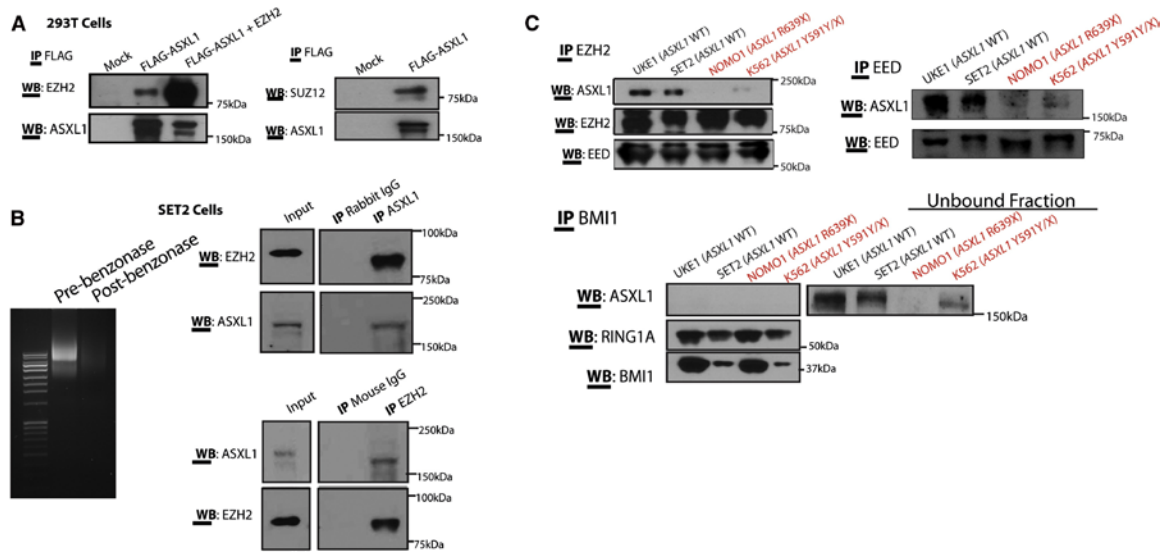
Figure 2.10. ASXL1 Interacts with the PRC2 in Hematopoietic Cells. (**A**) Physical interaction between ASXL1 and EZH2 is demonstrated by transient transfection of HEK293T cells with FLAG-hASXL1 cDNA with or without hEZH2 cDNA followed by immunoprecipitation (IP) of FLAG epitope and western blotting for EZH2 and ASXL1. (**B**) HEK293T cells were transiently transfected with FLAG-hASXL1 cDNA followed by IP of FLAG epitope and western blotting for SUZ12 and ASXL1. Endogenous interaction of ASXL1 with PRC2 members was also demonstrated by IP of endogenous EZH2 and ASXL1 followed by western blotting of the other proteins in whole cell lysates from SET2 cells. (**C**) Lysates from the experiment shown in (**B**) were treated with benzonase to ensure nucleic acid free conditions in the lysates prior to IP as shown by ethidium bromide staining of an agarose gel before and after benzonase treatment. IP of endogenous EZH2 and embryonic ectoderm development (EED) in a panel of ASXL1-wild-type and mutant human leukemia cells reveals a specific interaction between ASXL1 and PRC2 members in ASXL1-wildype human myeloid leukemia cells. In contrast, IP of the PRC1 member BMI1 failed to pull down ASXL1.

hematopoietic cells. We performed IP for EZH2 or ASXL1 followed by western blotting for partner proteins in SET2 and UKE1 cells, which are wild-type for *ASXL1*, *SUZ12*, *EZH2*, and *EED*. These co-immunoprecipitation assays all revealed a physical association between ASXL1 and EZH2 in SET2 (**Figure 2.10B**) and UKE1 cells (**Figure 2.11**). By contrast, immunoprecipitation of endogenous ASXL1 did not reveal evidence of protein-protein interactions between ASXL1 and BMI1 (**Figure 2.11**). Likewise, immunoprecipitation of BMI1 enriched for PRC1 member RING1A, but failed to enrich for ASXL1, suggesting a lack of interaction between ASXL1 and the PRC1 repressive complex (**Figure 2.10C**).

ASXL1 Loss Collaborates with NRasG12D *In Vivo*

We and others previously reported that *ASXL1* mutations are most common in chronic myelomonocytic leukemia and frequently co-occur with *N/K-Ras* mutations in chronic myelomonocytic leukemia (*33*). We therefore investigated the effects of combined *NRasG12D* expression and Asxl1 loss *in vivo*. To do this, we expressed *NRasG12D* in combination with an empty vector expressing GFP alone or one of two different Asxl1 shRNA constructs in whole bone marrow cells and transplanted these cells into lethally irradiated recipient mice. We validated our ability to effectively knock down ASXL1 *in vivo* by performing qRT-PCR in hematopoietic cells from recipient mice (**Figure 2.12A** and **2.13A**). Consistent with our *in vitro* data implicating the HoxA cluster as an ASXL1 target locus, we noted a marked increase in *HoxA9* and *HoxA10* expression in bone marrow nucleated cells from mice expressing *NRasG12D* in combination with Asxl1 shRNA compared to mice expressing *NRasG12D* alone (**Figure 2.12B**).
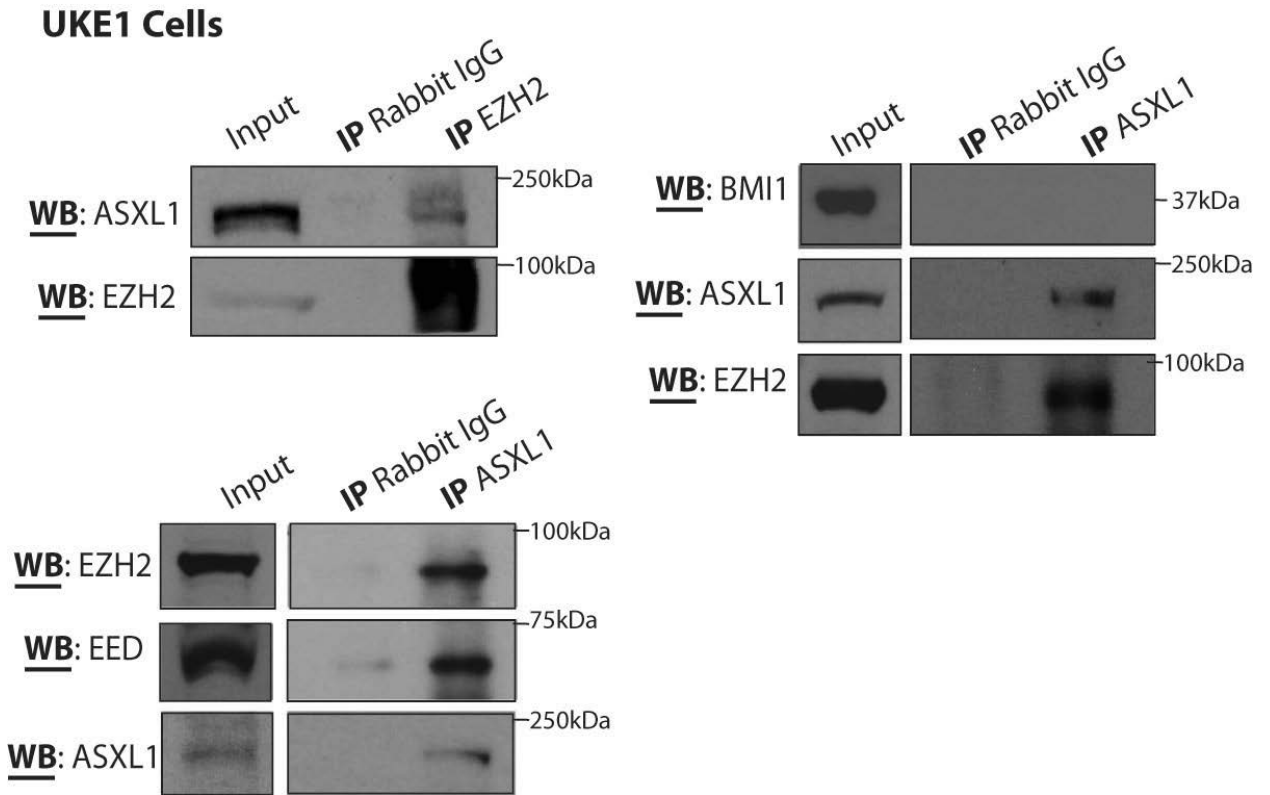
Figure 2.11. ASXL1 physically interacts with the Polycomb Repressive Complex 2 (PRC2), but not the PRC1, in human myeloid leukemia cells. Endogenous interaction of ASXL1 and PRC2 members was demonstrated by immunoprecipitation (IP) of endogenous EZH2 and ASXL1 followed by Western blotting of the other proteins in whole cell lysates from UKE1 cells. IP of ASXL1 did not reveal pulldown of BMI1 in UKE1 cells however.
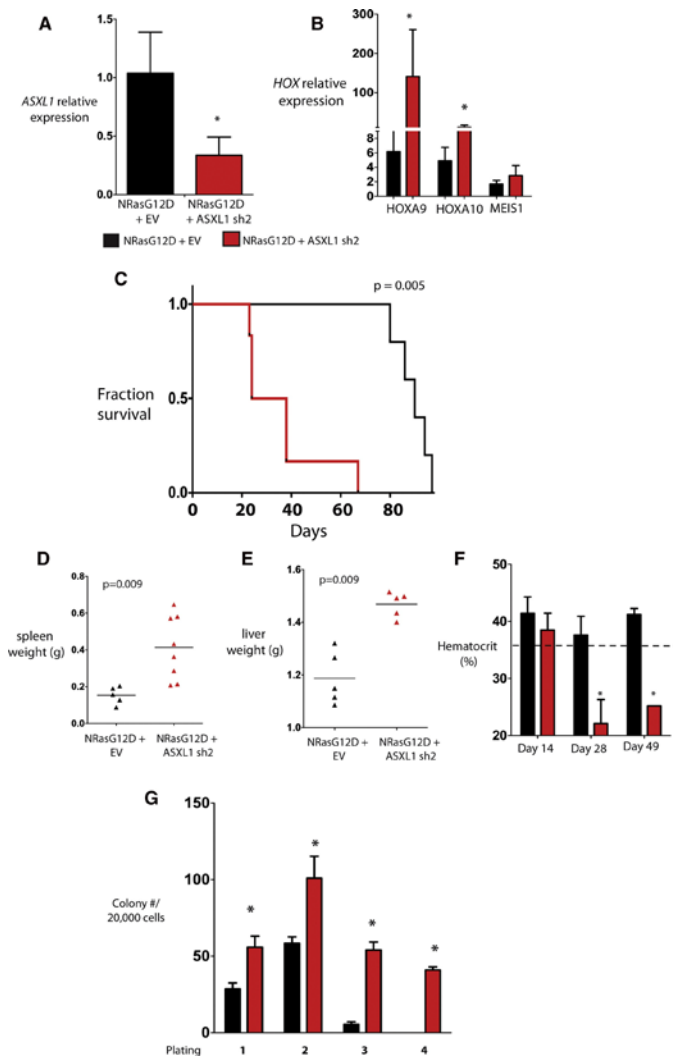
Figure 2.12. Asxl1 Silencing Cooperates with NRasG12D In Vivo. (**A**) Retroviral bone marrow transplantation of NRasG12D with or without an shRNA for Asxl1 resulted in decreased Asxl1 mRNA expression as shown by qRT-PCR results in nucleated peripheral blood cells from transplanted mice at 14 days following transplant. (**B**) qRT-PCR revealed an increased expression of HOXA9 and HOXA10 but not MEIS1 in the bone marrow of mice sacrificed 19 days following transplantation. (**C**) Transplantation of bone marrow cells bearing overexpression of NRasG12D in combination with downregulation of Asxl1 led to a significant hastening of death compared to mice transplanted with NRasG12D/EV. (**D–F**) Mice transplanted with NRasG12D/ASXL1 shRNA experienced increased splenomegaly (**D**) and hepatomegaly (**E**), and progressive anemia (**F**) compared with mice transplanted with NRasG12D + an empty vector (EV). (**G**) Bone marrow cells from mice with combined NRasG12D overexpression/Asxl1 knockdown revealed increased serial replating compared with cells from NRasG12D/EV mice. Error bars represent standard deviation relative to control. Asterisk indicates $p < 0.05$ (two-tailed, Mann Whitney U test).
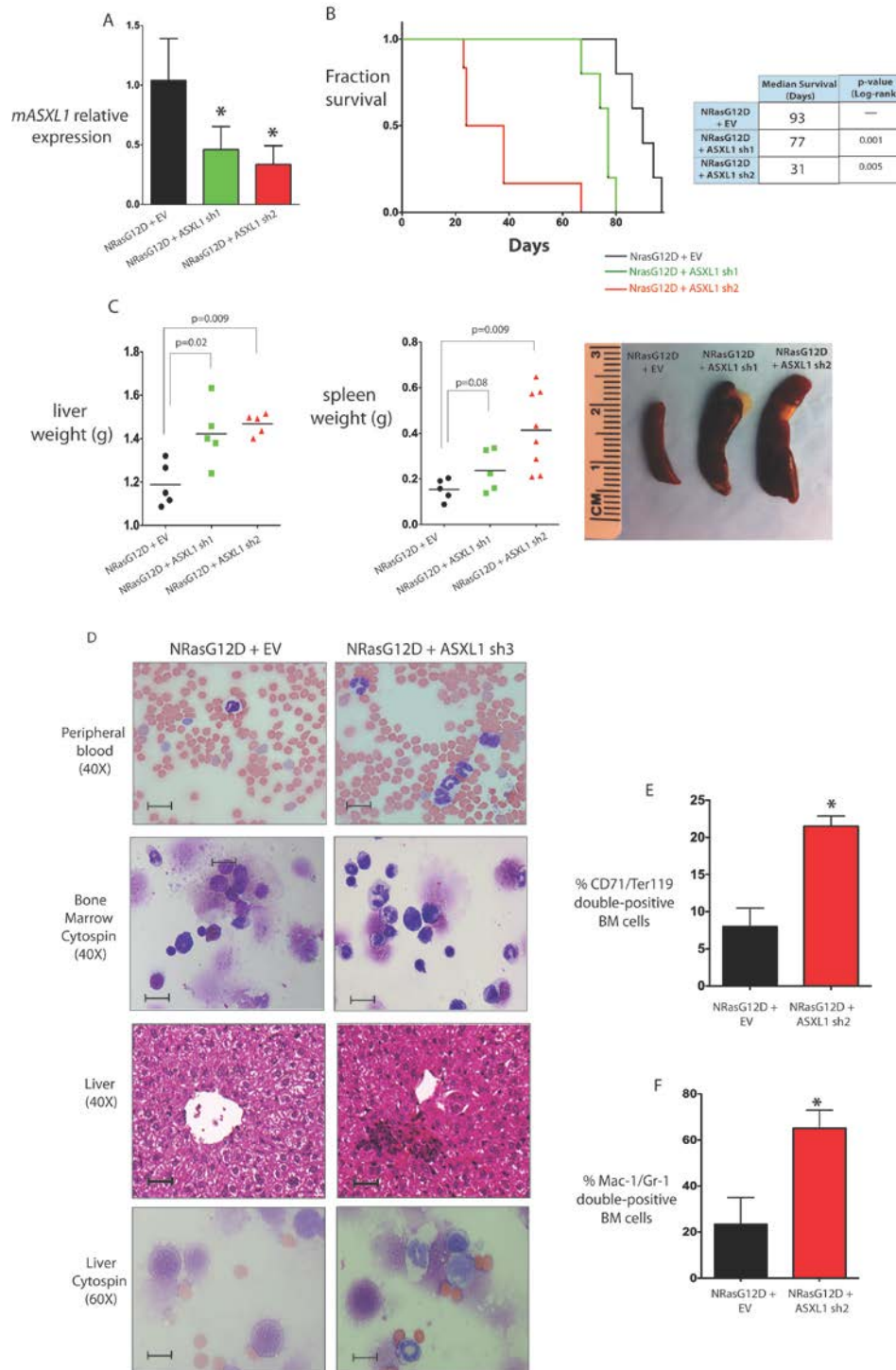
Figure 2.13. Asxl1 silencing in cooperates with NRasG12D to increase disease burden and cause progressive anemia _in vivo_. Retroviral bone marrow transplantation of NRasG12D with 2 different shRNAs for Asxl1 knockdown or an empty vector (EV) results in decreased Asxl1 mRNA expression as shown by qRT-PCR results in nucleated peripheral blood cells from transplanted mice at 14 days following transplant (**A**). Mice transplanted with NRasG12D + Asxl1 shRNA experienced significantly hastened death (**B**) and increased hepatomegaly and splenomegaly (**C**)

compared with mice transplanted with NRasG12D + EV. Histological and morphological analysis of tissues 19 days following transplant with NRasG12D plus EV or Asxl1 shRNA reveals increased monocytes and neutrophils in the blood, bone marrow, and liver of mice with Asxl1 loss in combination of NRasG12D overexpression (**D**). Scale bars represent a size of 100 ☐M in all ph

where they represent a size of 200 ☐M. Flow cyt

from mice sacrificed 19 days following transplant reveals a significant increase in CD71/Ter119 double-positive cells (**E**) and Mac1/Gr1 double-positive cells (**F**) in NRasG12D/Asxl1 shRNA transplanted mice compared with NRasG12D/EV mice. Error bars represent standard deviation relative to control. Asterisk indicates *p*<0.05 (two-tailed, Mann Whitney U test).

Expression of oncogenic *NRasG12D* and an empty shRNA vector control led to a progressive myeloproliferative disorder as previously described (*144*). In contrast, expression of *NRasG12D* in combination with validated mASXL1 knockdown vectors resulted in accelerated myeloproliferation and impaired survival compared with mice transplanted with *NRasG12D*/EV (median survival 0.8 month for ASXL1 shRNA versus 3 months for control shRNA vector: p < 0.005; **Figure 2.12C**) We also noted impaired survival with an independent *mASXL1* shRNA construct (p < 0.01; **Figure 2.13B**). Mice transplanted with *NRasG12D/Asxl1* shRNA had increased splenomegaly and hepatomegaly compared with *NRasG12D*/EV transplanted mice (**Figure 2.12D**,**E** and **Figure 2.13C**). Histological analysis revealed a significant increase in myeloid infiltration of the spleen and livers of mice transplanted with *NRasG12D/Asxl1* shRNA (**Figure 2.13D**).

Mice transplanted with *NRasG12D/Asxl1* shRNA, but not *NRasG12D/EV*, experienced progressive, severe anemia (**Figure 2.12F**). It has previously been identified that expression of oncogenic *K/N-Ras* in multiple models of human/murine hematopoietic systems results in alterations in the erythroid compartment ((*145-147*). We noted an expansion of CD71^{high}/Ter119^{high} erythroblasts in the bone marrow of mice transplanted with *NRasG12D*/Asxl1 shRNA compared with *NRasG12D*/EV mice (**Figure 2.13E**). We also noted increased granulocytic expansion in mice engrafted with *NRasG12D*/*Asxl1* shRNA positive cells, as shown by the presence of increased neutrophils in the peripheral blood (**Figure 2.13D**) and the expansion of Gr1/Mac1 double-positive cells in the bone marrow by flow cytometry (**Figure 2.13F**).

Previous studies have shown that hematopoietic cells from mice expressing oncogenic *Ras* alleles or other mutations that activate kinase signaling pathways do not

exhibit increased self-renewal in colony replating assays (*144, 148*). This is in contrast to the immortalization of hematopoietic cells *in vitro* seen with expression of *MLL-AF9* (*149*) or deletion of *Tet2* ((*150*). Bone marrow cells from mice with combined overexpression of NRasG12D plus Asxl1 knockdown had increased serial replating (to five passages) compared to bone marrow cells from mice engrafted with *NRasG12D/EV* cells (**Figure 2.12G**). These studies demonstrate that Asxl1 loss cooperates with oncogenic *NRasG12D in vivo*.

JAK2V617F and ASXL1 loss collaborate in myeloproliferative neoplasms

A series of studies have shown that JAK2V617F activating mutations co-occur with ASXL1 and co-occurrence of these mutations predicts for poor patient prognosis and poor response to JAK2 inhibitor therapy (*2*). JAK2 is a non-receptor tyrosine kinase that is frequently mutated in myeloproliferative neoplasms leading to activation of downstream STAT signaling. JAK2 has been shown to regulate chromatin by phosphorylating the histone H3 at tyrosine 41 (*48*). To model the co-mutation of JAK2V617F and Asxl1 loss, we crossed a Jak2V617F KI mouse (*151*) with a conditional Asxl1 KO mouse (*47*). We found that deletion of one or two copies of Asxl1 in mice expressing the Jak2V617F allele resulted in decreased survival (**Figure 2.14A**). Interestingly, heterozygous deletion of Asxl1 in Jak2V617F KI cells conferred a stem cell advantage while homozygous deletion does not. These data suggest that deletion of one or two copies of ASXL1 may result in different mechanisms of disease transformation. We next examined H3Y41 levels in JAK2V617F mutant leukemia cell lines with and without ASXL1 shRNA knockdown. Knockdown of ASXL1 resulted in increased H3Y41 phosphorylation (**Figure 2.15A**). Treatment of JAK2V617F cell lines with a JAK2 inhibitor resulted in decreased expression of the downstream target gene LMO2. However, knockdown of ASXL1 reversed this effect (**Figure 2.15B**). Future work is
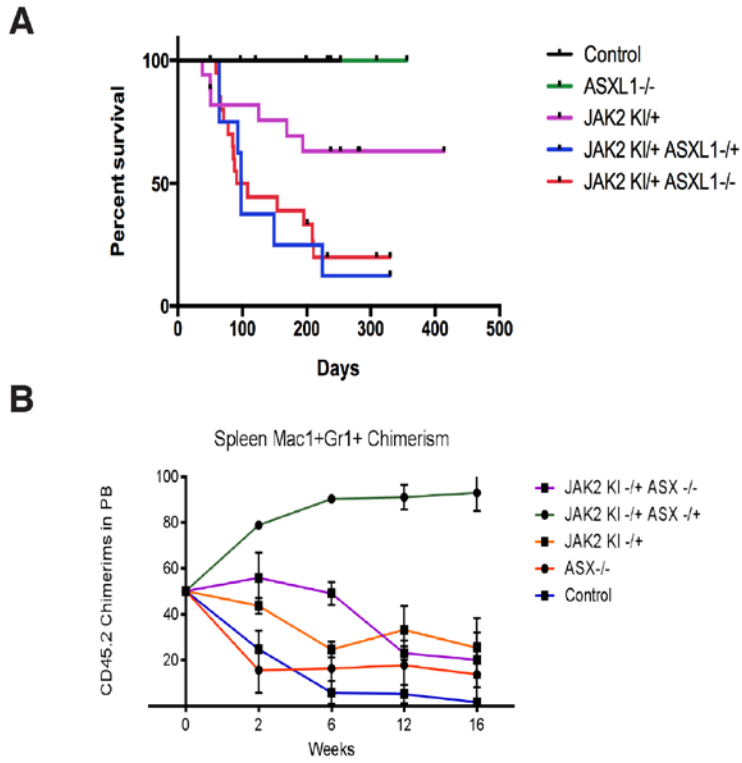
Figure 2.14 JAK2V617F and ASXL1 collaborate in disease transformation. (**A**) Survival curve of indicated gentoypes after induction of excision at six weeks of age (**B**) *In vivo* chimerism studies with indicated genotypes.
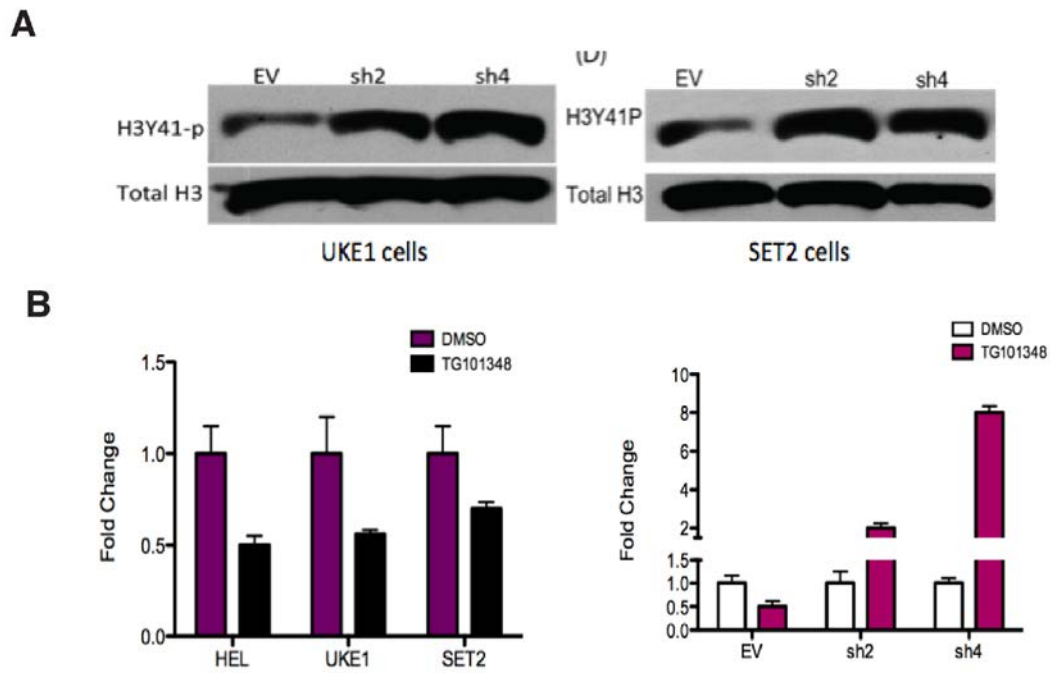
Figure 2.15. ASXL1 knockdown upregulated H3Y41 phosphorylation. (A) Knockdown of ASXL1 in two cell lines resulted in increased H3Y41 phosporylation. (**B**) Quantitative qPCR of LMO2 in ASXL1 KD cells.

required to determine the mechanism by which JAK2V617F and ASXL1 collaborate to modulate gene expression and chromatin.

DISCUSSION

The data presented here identify that ASXL1 loss in hematopoietic cells results in reduced H3K27me3 occupancy through inhibition of PRC2 recruitment to specific oncogenic target loci (**Figure 2.16**). Recent studies have demonstrated that genetic alterations in the PRC2 complex occur in a spectrum of human malignancies (*152-154*). Activating mutations and overexpression of *EZH2* occur most commonly in epithelial malignancies and in lymphoid malignancies (*8, 105*). However, there are increasing genetic data implicating mutations that impair PRC2 function in the pathogenesis of myeloid malignancies. These include the loss-of-function mutations in *EZH2* (*33, 108, 109*) and less common somatic loss-of-function mutations in *SUZ12*, *EED*, and *JARID2* (*155*) in patients with myeloproliferative neoplasms, myelodysplastic syndrome, and chronic myelomonocytic leukemia. The data from genetically-engineered mice also support this concept with Ezh2 overexpression models, revealing evidence of promotion of malignant transformation (*113*), and recent studies demonstrate a role for Ezh2 loss in leukemogenesis (*117*). Thus, it appears that alterations in normal PRC2 activity and/or H3K27me3 abundance in either direction may promote malignant transformation. Our data implicate *ASXL1* mutations as an additional genetic alteration that leads to impaired PRC2 function in patients with myeloid malignancies. In many cases, patients present with concomitant heterozygous mutations in multiple PRC2 members or in *EZH2* and *ASXL1*; these data suggest that haploinsufficiency for multiple genes that regulate PRC2 function can cooperate in hematopoietic transformation through additive alterations in PRC2 function.

72
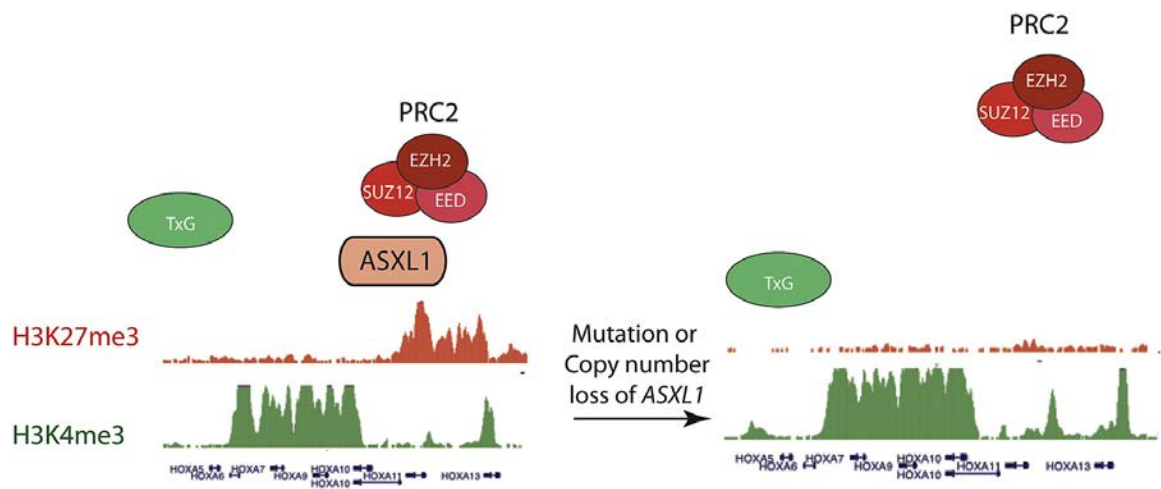
Figure 2.16. Schematic of the mechanism by which ASXL1 loss results in upregulation of HOXA target genes.

Many studies have investigated how mammalian PcG proteins are recruited to chromatin in order to repress gene transcription and specify cell fate in different tissue contexts. Recent *in silico* analysis suggested that ASXL proteins found in animals contain a number of domains that likely serve in the recruitment of chromatin modulators and transcriptional effectors to DNA (*21*). Data from ChIP and co-immunoprecipitation experiments presented here suggest a specific role for ASXL1 in epigenetic regulation of gene expression by facilitating PRC2-mediated transcriptional repression of known leukemic oncogenes. Thus, ASXL1 may serve as a scaffold for recruitment of the PRC2 complex to specific loci in hematopoietic cells, as has been demonstrated for JARID2 in embryonic stem cells (*5, 86, 156, 157*).

Recent data suggested that ASXL1 might interact with BAP1 to form a H2AK119 deubiquitanase (*22*). However, our data suggest that ASXL1 loss leads to BAP1-independent alterations in chromatin state and gene expression in hematopoietic cells. These data are consonant with recent genetic studies, which have shown that germline loss of BAP1 increases susceptibility to uveal melanoma and mesothelioma (*55, 58*). In contrast, germline loss of ASXL1 is seen in the developmental disorder Bohring-Opitz Syndrome (*32*), but has not, to date, been observed as a germline solid tumor susceptibility locus. Whether alterations in H2AK119 deubiquitanase function due to alterations in BAP1 and/or ASXL1 can contribute to leukemogenesis or to the pathogenesis of other malignancies remains to be determined.

Integration of gene expression and chromatin state data following ASXL1 loss identified specific loci with a known role in leukemogenesis that are altered in the setting of *ASXL1* mutations. These include the posterior *HOXA* cluster, including *HOXA9,* which has a known role in hematopoietic transformation. We demonstrate that ASXL1 normally serves to tightly regulate *HOXA* gene expression in hematopoietic cells, and that loss of

74

ASXL1 leads to disordered *HOXA* gene expression *in vitro* and *in vivo*. Overexpression of *5′ HOXA* genes is a well-described oncogenic event in hematopoietic malignancies (*158*) and previous studies have shown that *HOXA9* overexpression leads to transformation *in vitro* and *in vivo* when co-expressed with *MEIS1* (*159*). Interestingly, *ASXL1* loss was not associated with an increase in *MEIS1* expression, suggesting that transformation by *ASXL1* mutations requires the co-occurrence of oncogenic disease alleles which dysregulate additional target loci. These data and our *in vivo* studies suggest that *ASXL1* loss, in combination with co-occurring oncogenes, can lead to hematopoietic transformation and increased self-renewal. Further studies in mice expressing ASXL1 shRNA or with conditional deletion of *Asxl1* alone and in concert with leukemogeneic disease alleles will provide additional insight into the role of ASXL1 loss in hematopoietic stem/progenitor function and in leukemogenesis.

Given that somatic mutations in chromatin modifying enzymes (*160*), DNA methyltransferases (*161*), and other genes implicated in epigenetic regulation occur commonly in human cancers, it will be important to use epigenomic platforms to elucidate how these disease alleles contribute to oncogenesis in different contexts. The data here demonstrate how integrated epigenetic and functional studies can be used to elucidate the function of somatic mutations in epigenetic modifiers. In addition, it is likely that many known oncogenes and tumor suppressors contribute, at least in part, to transformation through direct or indirect alterations in the epigenetic state (*48*). Subsequent epigenomic studies of human malignances will likely uncover novel routes to malignant transformation in different malignances, and therapeutic strategies that reverse epigenetic alterations may be of specific benefit in patients with mutations in epigenetic modifiers.

CHAPTER III

Loss of BAP1 function leads to EZH2-dependent transformation

SUMMARY

BAP1 and ASXL1 interact to form a polycomb deubiquitinase complex that can remove monoubiquitin from histone H2A lysine 119 (H2AK119Ub). However, *BAP1* and *ASXL1* are mutated in distinct cancer types, consistent with independent roles in regulating epigenetic state and in malignant transformation. Here we demonstrate that *Bap1* loss results in increased trimethylated histone H3 lysine 27 (H3K27me3), elevated *Ezh2* expression, and enhanced repression of Polycomb Repressive Complex 2 (PRC2) targets. These findings are in contrast to the reduction in H3K27me3 seen with *Asxl1* loss. Conditional deletion of *Bap1* and *Ezh2 in vivo* abrogates the myeloid progenitor expansion induced by *Bap1* loss alone. Loss of Bap1 results in a marked decrease in H4K20 monomethylation (H4K20me1). Consistent with a role for H4K20me1 in EZH2 transcriptional regulation, expression of SETD8, the H4K20me1 methyltransferase, reduces EZH2 expression and abrogates the proliferation of *BAP1*-mutant cells. Further, mesothelioma cells that lack BAP1 are sensitive to EZH2 pharmacologic inhibition, suggesting a novel therapeutic approach for *BAP1*-mutant malignancies.

INTRODUCTION

Genomic studies of cancer have identified somatic alterations in epigenetic modifying proteins across a wide spectrum of human malignancies. These include mutations in genes that encode proteins regulating DNA methylation and histone post-translational modifications. The identification of activating *EZH2* mutations in lymphoid malignancies

(*8, 162, 163*) and neomorphic mutations in *IDH1/2* (*164, 165*) has led to the [2]

development of epigenetic therapies that specifically target malignant cells with aberrant

epigenetic states. Despite these important advances, most mutations in epigenetic

regulators result in loss-of-function effects, such that they function as tumor suppressors

and do not present themselves as tractable direct therapeutic targets. These include

inactivating mutations in *TET2* and *DNMT3A* in hematologic malignancies (*161, 166,

167*) and loss-of-function mutations in histone methyltransferases and in chromatin

remodeling proteins in a wide range of human cancers (*168*). As such, there is a need to

better understand how these mutations contribute to malignant transformation, and to

identify therapeutic liabilities in cancer cells with inactivating mutations in epigenetic

regulators. Among the most common epigenetic regulatory complexes targeted by

somatic mutations in human cancers is the BAP1-ASXL1 protein complex. In Drosophila,

Asx and Calypso form the PR-DUB (Polycomb-Repressive Deubiquitinase) complex,

which removes the repressive H2AK119-Ub mark placed by polycomb repressive

complex 1 (PRC1) (*22*). In mammalian cells, the Asx homolog ASXL1 (Addition of sex

combs-like 1) interacts with the Calypso homolog BAP1 (BRCA-1 associated protein 1)

(*76, 169*). *In vitro* studies have demonstrated that the BAP1/ASXL1 complex can remove

H2AK119-Ub from histone H2A (*22*). However, the role of the PR-DUB complex in

regulating gene expression in mammalian cells and in malignant transformation has not

been elucidated.

Genetic and functional data suggest that ASXL1 and BAP1 have distinct roles in

regulating epigenetic state independent from the PR-DUB complex. Mutations in *ASXL1*

and *BAP1* contribute to distinct types of malignancies. Somatic inactivating mutations in

ASXL1 are most common in myeloid malignancies (*33, 34, 36*). By contrast, somatic

[b] The work described in this chapter is under review at Nature Medicine.

BAP1 mutations are frequently observed in mesothelioma (23% of patients) and renal cell carcinoma (15% of patients) (*61, 63, 65*), and are specifically associated with metastasis in uveal melanoma (84% of metastatic tumors) (*61*). We recently identified that ASXL1 interacts with members of the Polycomb Repressive Complex 2 (PRC2), a complex that contains EZH2, the catalytic member that places the repressive H3K27me3 mark on chromatin. Depletion of *ASXL1* leads to a marked reduction in H3K27me3 levels and in increased expression of *HOXA9* and of other PRC2 target genes (*169*). By contrast, the ASXL1- independent mechanisms by which BAP1 regulates chromatin state have not been delineated. Recent studies have shown that *BAP1* loss can lead to transformation. Specifically, somatic loss of *BAP1* leads to myeloproliferation, and transplantation studies demonstrated this phenotype is due to cell autonomous effects in the hematopoietic compartment. *In vivo* proteomic studies demonstrated that Bap1 interacts with Asxl1 as well as known PR-DUB target substrates Hcf-1 and Ogt (*76*). However, HCF-1 and OGT have not been shown to contribute to BAP1-mediated transformation, and the BAP1-ASXL1 complex has not been shown to have a functional role in *BAP1*-deficient transformation *in vivo*. We therefore sought to identify the mechanisms by which BAP1 loss leads to transformation *in vivo*, and to identify therapeutic vulnerabilities in BAP1-mutant cells that can be translated to the clinical setting.

MATERIALS AND METHODS

Animals

All animals were housed at Memorial Sloan Kettering Cancer Center. All animal procedures were completed in accordance with the Guidelines for the Care and Use of Laboratory Animals and were approved by the Institutional Animal Care and Use

Committees at Memorial Sloan Kettering Cancer Center. The number of mice chosen in each experiment was chosen to give 90% statistical power with a 5% error level given the differences in standard deviation that was observed in the pilot study.

Generation of *Bap1*-deficient and *Bap1/Ezh2*-deficient mice

Embryonic stem cells targeting exons 6-12 of *Bap1* were obtained from the European Conditional Mouse Consortium. A *Frt*-flanked premature stop cassette containing a lacZ and neomycin cassette was inserted upstream (*170*). ES cell clones were expanded and injected into primary blastocysts. Generated mice were crossed to the germline *Flp*-deleter (The Jackson Laboratory) to excise the *Frt*-flanked cassette. These mice were subsequently crossed to the IFN-α-inducible *Mx1-cre* transgenic mice (The Jackson Laboratory) to assess the effects of inducible loss of *Bap1* in the hematopoietic system. *Bap1 fl/fl*, *Bap1 fl/+*, and *Bap1+/+* littermate mice were genotyped by PCR with the primers BAP1-up (actgcagcaatgtggatctg), BAP1-down (gaaaaggtctgacccagatca) using the following parameters: 95°C for 10min, followed by 40 cycles of 94°C for 10s, 65°C for 40s, and 72°C for 1min, and then 72°C for 5min. The WT allele was detected at 300 bp while the floxed allele was detected at 500 bp PCR. Excision after IFN-α-induction was confirmed by a PCR with primers to detect the floxed and excised band: BAP1-F (actgcagcaatgtggatctg), BAP1-F2 (gcgcaacgcaattaatgata), and BAP1-R (cagtgtccagaatggctcaa), using the same PCR parameters listed above.

Mx1-Cre-Bap1 f/f mice were crossed to *Ezh2 f/f* mice (*116*). *Mx-cre Bap1f/f* conditional and *Bap1f/f* control mice received four intraperitoneal injections of polyI:polyC of 200 µL of a 1 mg/mL solution. Two weeks after excision, peripheral blood was collected via cheek bleeding using heparinized microhematocrit capillary tubes (Thermo Fisher Scientific). Excision was confirmed and peripheral blood counts were obtained using a

HemaVet according to standard manufacturer's instruction. Formalin-fixed paraffin-embedded tissue sections were stained with hematoxylin and eosin (H&E). Deletion of *Bap1* was confirmed by genomic excision PCR and Western blot analysis. Tails were submitted to the Transnetyx genotyping service (Cordova, TN) for qPCR-based genotyping for floxed and excised *Ezh2* alleles. Excision was confirmed by Western blot. Animals were not excluded from genetic experiments.

Xenografts and *in vivo* EPZ011989 administration

Groups of 10 week old NOD-SCID mice were injected subcutaneously in the flank with $6–10\times10^6$ mesothelioma cell lines (MSTO-211H, Meso10, H226 and H2452) in a 1:1 mixture of matrigel and media. When tumors reached a size of approximately 60-80mm^3, we began treatment with either vehicle (0.5% NaCMC+0.1% Tween-80 in water) or EPZ011989. Either EPZ011989 or vehicle were given orally BID at a concentration of 500 mg/kg for the duration of the experiment. Tumor volumes were assessed in three dimensions using a caliper. Tumors or lung tissue were extracted following treatment and utilized for Western blotting to assess target inhibition. We pre-established criteria to exclude mice in xenograft experiments if tumors did not form after implantation (75% smaller than the mean of the implanted animals from the same group. Animals were not excluded from drug trials. For all xenograft drug studies, tumor size was followed for 10 days and mice were randomized at this point for tumor size. The genetic *Bap1* KO EPZ011989 trial was conducted with randomization utilizing CBC analysis 3 weeks after polyI:polyC and confirming that WBC count averages were equivalent in both vehicle and treated groups. Five animals per group were treated orally with either vehicle (described above) or 500 mg/kg EPZ011989 BID for 16 days. Researchers were not blinded in these experiments.

80

Histological analyses

Mice were sacrificed and autopsied, and then dissected tissue samples were fixed for 24 hours in 4% paraformaldehyde, dehydrated, and embedded in paraffin. Paraffin blocks were sectioned at 4 µm and stained with H&E. Images were acquired using an Axio Observer A1 microscope (Carl Zeiss).

Cell culture

293T cells were cultured in Dulbecco's modified Eagle's medium (DMEM) supplemented with 10% fetal bovine serum (FBS) and nonessential amino acids. Human leukemia cell lines (SET2) and human mesothelioma cell lines (Met5a, MSTO-211H, Meso10, H2373, H226, H2452) were cultured in RPMI-1640 medium supplemented with 10% FBS. MSTO-211H was obtained from ATCC while Meso10 was a generous gift from David Scheinberg and the remaining mesothelioma lines were generous gifts from Prasad Adusumilli.

RNA isolation, SMARTer amplification, Proton Transcriptome sequencing and analysis

Bone marrow cells were FACS sorted for GMPs (Lin⁻c-Kit⁺Sca1⁻CD34⁺Fcγ⁺) using the FACS Aria. Total RNA from 200-500K cells was extracted using TRIzol RNA Isolation Reagents (cat# 15596-026, Life Technologies). Quality of RNA was ensured before amplification by analyzing 20–50 pg of each sample using the RNA 6000 pico kit and a bioAnalyzer (Agilent). 10 ng of high quality (RIN>8) total RNA was subsequently amplified using the SMARTer® Universal Low Input RNA Kit for Sequencing (Clonetech Laboratory, cat# 634940) according to instructions provided by the manufacturer. Amplified material underwent whole transcriptome Library preparation according to the Ion Total RNA-Seq Kit v2 protocol (Life Technologies), with 16 cycles of PCR. Samples

were barcoded and template-positive Ion PI™ Ion Sphere™ Particles (ISPs) were prepared using the ion one touch system II and Ion PI™ Template OT2 200kit v2 Kit (Life Technologies). Enriched particles were sequenced on a Proton sequencing system using 200 bp version 2 chemistry. An average of 70 to 80 million reads per sample were generated and 76 to 82% of the reads mapped to mRNA bases.

RAW output BAMs were converted back to FASTQ using PICARD Sam2Fastq. The reads are first mapped to the mouse genome using rnaStar. The genome used was MM9 with junctions from ENSEMBL (Mus_musculus.NCBIM37.67) and a read overhang of 49. Then any unmapped reads were mapped to MM9 using BWA MEM (version 0.7.5a). The two mapped BAMs were then merged and sorted and gene level counts were computed using htseq-count (options -s y -m intersection-strict) and the same gene models (Mus_musculus.NCBIM37.67). Raw data was uploaded to the GEO database with the following accession number: GSE61360.

Analyses of TCGA data in AML and mesothelioma

Average gene expression from TCGA AML patients was expressed as mathematical mean and standard error of normalized read counts as provided by DESeq2 (*171*). For TCGA mesothelioma patients, these same values were calculated from normalized read counts as provided by TCGA as level 3 data. To compare EZH2 expression of mesothelioma tumors to normal lung tissue (*172*), GSE51024 was analyzed using Geo2R, which makes use of the Limma Bioconductor R package. Normalized expression values for EZH2 were extracted from this analysis, and used to generate the boxplots provided. Log$_2$ Fold Change, nominal p-value, and Benjamini-Hochberg FDR were calculated by Geo2R/Limma.

Histone extraction, histone ELISAs, histone Western blots, and histone LC/MS

Histones were extracted by standard extraction techniques or overnight using the Active Motif Histone Extraction Minikit (40026). Histone ELISAs were conducted using the trimethyl K27 Elisa Kit (Active Motif, 53106) normalized to a H3K27me3 standard curve and total H3 protein. Histone Western blots were conducted with 3-5 µg of histones. For Histone LC/MS, 12 million control and *Bap1* KO cells were lysed, nuclei were isolated and histones were extracted using 0.4N H_2SO_4 and chemically derivatized using propionic anhydride, as previously described (*173*). Histones were then digested with trypsin and separated by nano-liquid chromatography (75 µm i.d., 15 cm long, packed with MagicC18aq media, d_p 3 µ) coupled to a TSQ Quantum Ultra mass spectrometer. Data were analyzed with Skyline (*174*) and relative quantification was performed by peak area.

Chromatin preparation and immunoprecipitation, ChIP Library preparation and sequencing, and analysis of ChIP-Seq data

Bone marrow cells were enriched for c-Kit^{+} cells (or sorted for GMPs) using the EasySep Mouse Hematopoietic cell Enrichment Kit (Stem Cell Technologies, 19756). 5×10^6 cells were fixed in a 1% methanol-free formaldehyde solution and then resuspended in SDS lysis buffer. Lysates were sonicated in an E220 focused-ultrasonicator (Covaris) to a desired fragment size distribution of 100-500 base pairs. IP reactions were performed using anti-trimethyl H3K27 (abcam, 6002), anti-monomethyl H4K20 (Abcam, 9051), and IgG (Santa Cruz, 2027) each on approximately 400,000 cells as previously described (*175*). ChIP assays were processed on an SX-8G IP-STAR Compact Automated System (Diagenode) using a Direct ChIP protocol as described elsewhere (*176*). Eluted chromatin fragments were then de-crosslinked and the DNA fragments purified using Agencourt AMPure XP beads (Beckman Coulter).

Barcoded libraries were prepared from the ChIP-enriched and input DNA using a NEBNext ChIP-Seq Library Prep Master Mix Set for Illumina (New England Biolabs) and TruSeq Adaptors (Illumina) according to manufacturer's instructions on an SX-8G IP-STAR Compact Automated System (Diagenode). Phusion High-Fidelity DNA Polymerase (New England Biolabs) and TruSeq PCR Primers (Illumina) were used to amplify the libraries, which were then purified to remove adaptor dimers using AMPure XP beads and multiplexed on the HiSeq 2000 (Illumina).

Reads were quality and adapter-trimmed using 'trim_galore' before aligning to mouse assembly mm9 with bowtie2 using the default parameters. Aligned reads with the same start position and orientation were collapsed to a single read before subsequent analysis. Density profiles were created by extending each read to the average library fragment size and then computing density using the BEDTools suite. Enriched regions were discovered using MACS 1.4 with default parameters, and scored against matched input libraries. All genome browser tracks and read density tables were normalized to sequencing depth. For comparison of ChIP-seq samples in control and KO conditions, the signals of three replicates per condition were tested using either the Mann-Whitney U test or the t-test. Cluster analysis was performed on normalized count data in Matlab with the kmeans clustering package. Motif analysis was performed in Homer using default parameters for the findMotifsGenome program.

Western blot and immunoprecipitation

Cells were lysed for Western blot and immunoprecipitation experiments in the following buffer: 150 mM NaCl, 20 mM Tris (pH 7.4), 5 mM EDTA, 1% Triton, protease arrest (EMD) and phosphatase inhibitors (Calbiochem). To perform immunoprecipitations in the

presence of benzonase, cells were lysed in the BC-300 buffer: 20 mM Tris (pH 7.4), 10% glycerol, 300 mM KCl, 0.1% NP-40. The cleared lysate was treated with $MgCl_2$ to 2.5 mM and benzonase was added at 1250 U/mL. The lysate was incubated for 1 hour with rotation and the reaction was terminated by adding 5 mM EDTA. DNA digestion was confirmed by running lysate on an ethidium bromide gel before setting up the immunoprecipitation experiment. Antibodies used included: BAP1 (C-4; Santa Cruz sc-28383), EZH2 (Active Motif, 39933, Active Motif, 39901, or Millipore, 07-689), SUZ12 (Abcam, Ab12073), ASXL1 (N-13; Santa Cruz sc-85283), L3MBTL2 (Active Motif, 39569), Myc-Tag (Cell Signaling, 2276), SETD8 (ab3798), Tubulin (Sigma, T9026), H3K27me3 (Abcam, 6002 or Millipore, 07-449), H3 (Abcam, Ab1791), and H4K20me1 (Abcam, Ab9051).

Flow cytometry analyses and antibodies

Surface marker staining of live bone marrow was conducted by first lysing cells with ammonium chloride-potassium bicarbonate lysis buffer and washing cells with phosphate-buffered saline (PBS). Cells were stained with antibodies in PBS for 20 minutes on ice. For hematopoietic stem and progenitor staining, cells were stained with a lineage cocktail including CD4 (RM4-5), CD3 (17A2), B220 (RA3-6B2), NK1.1 (PK136), Gr-1 (RB6-8C5), Cd11b (M1/70), and Ter119, allowing for mature lineage exclusion from the analysis. Cells were also stained with antibodies against c-Kit (2B8), Sca-1 (D7), FcγRII/III (2.4G2), and CD34 (RAM34). To assess the composition of the mature mononuclear cells we used Mac1, Gr-1, B220, and CD4/CD3. Cell cycle analysis was conducted by staining cells with the hematopoietic stem and progenitor mix described above. Cells were fixed using the FIX and PERM kit (Invitrogen cat# GAS-003). Cells were stained with Ki67 after fixation and then stained with DAPI before

85

analysis on the LSR Fortessa. Sorting was conducted by staining as described in text and above and utilization of a FACSAria sorter.

Plasmids

The cDNA full-length clone of human FLAG-L3MBTL2 was obtained from Addgene (Plasmid 28232). The Myc-His tagged ubiquitin construct was a generous gift from Xuejun Jiang. The cDNA human full-length clone of HA-FLAG BAP1 was obtained from Addgene (Plasmid 22539). The 3X FLAG-tagged BAP1 construct was a generous gift from Marc Ladanyi. Deubiquitinase mutant constructs (C91A, C91S) were generated using Agilent site-directed mutagenesis kits and confirmed by full-length DNA sequencing. Short-hairpin RNAs were obtained from the RNAi Consortium (TRC) in a pLKO.1 puromycin vector. Sequences for the short-hairpins were as follows: human BAP1 (TRC Oligo IDs: TRCN0000078702 and TRCN0000078698), mouse BAP1 (TRCN0000030719 and TRCN0000030720), human L3MBTL2 (TRCN0000021724 and TRCN0000021726) and a control pLKO.1-puromycin vector encoding an shRNA for luciferase (shLUC). The EZH2 overexpression construct was a generous gift from the Omar Abdel-Wahab lab. The SETD8 overexpression construct was a generous gift from Minkui Luo.

Ubiquitin assays

HEK293T cells were seeded in a 10-cm dish and 24 hours later were transduced with 4 μg of a Myc-His-Ubi expression construct and control, 1 μg L3MBTL2 and/or 1-10 μg BAP1-GFP overexpression constructs. Forty-eight hours after the transfection, cells were lysed in a Guanidine HCl based lysis buffer: 6 M guanidine, 0.1 M NaH_2PO_4, 10 mM Tris, pH 8.0, and 10 mM BME. His-Ubi proteins were purified by incubation by 20 μL of Ni-NTA agarose (Qiagen) for 4 hours at room temperature. Beads were washed sequentially with 1 mL of 4 wash buffers: buffer A 6 M guanidine, 0.1 M NaH_2PO_4, 10

mM Tris, pH 8.0, 10 mM BME, and 0.2% Triton-X, buffer B 8 M urea, 0.1 M NaH_2PO_4, 10 mM Tris, pH 8.0, 10 mM BME, and 0.2% Triton-X, buffer C 0.1 M NaH_2PO_4, 10 mM Tris, pH 6.3, 10 mM BME, and 0.2% Triton-X, and buffer D 0.1 M NaH_2PO_4, 10 mM Tris, pH 6.3, 10 mM BME, and 0.1% Triton-X. All buffers were supplemented with 15 mM imidazole. His-tagged proteins were purified from the beads by boiling with 2x SDS Laemmli buffer supplemented with imidazole. Proteins were then analyzed by Western blot.

In vitro colony forming assays

Cells were sorted for Lin⁻c-Kit⁺Sca1⁺ cells using the FACSAria. 100 cells were plated in duplicate in methylcellulose (MethoCult GF M3434, Stem Cell Technologies). Colonies were counted 14 days after plating and colonies were collected by washing with PBS. Cells were then lysed for RNA and histone extraction.

Transient Transfection

293T cells were transfected with indicated constructs with X-treme gene transfection reagent (Roche). Protein and/or histones were extracted 48-72 hours after transfection.

Invasion Assays

Mesothelioma cells (MSTO-211H, H2373, H226 and H2452) were seeded in T75 flasks (100,000 cells). 12 hours later the plated cells were treated with GSK126 (0-2 µM) (Chemitek) and then left to proliferate for 7 days. 250,000 treated cells were then placed on the top of a Matrigel invasion chamber (BD Biosciences, cat no. 354480) in serum free media while the lower chamber contained media with serum. 22 hours later the cells on the bottom of the membrane were stained with crystal violet and quantitated with ImageJ.

Luciferase Assays

293T cells were transiently transfected with the pGL3 EZH2 promoter reporter construct (generous gift from Naomi Goldfinger) and a Switchgear Renilla control construct in addition to EV, BAP1, and L3MBTL2 constructs. Cells were assessed for luciferase activity using the Dual Luciferase Reporter Assay System (Promega). Cells were seeded in 24 well plates and were cotransfected with 200 ng pGL3-EZH2-Luciferase, 200 ng of the Renilla luciferase control construct, and 500 ng of experimental constructs. Cells were incubated 48 hours after the transfection, lysed for 15 minutes at room temperature and luciferase activity was assessed on a luminometer. The Firefly luciferase readings were normalized to the Renilla transfection control.

Cell Titer Glo Viability Assays

Adherent mesothelioma cell lines were plated in 96 well dishes at about 100 cells per well to allow space for cells to proliferate. Cells were plated and given one day to adhere (an initial day one reading was taken at this time). ATP luminescence readings were taking at times specified in the manuscript. For assays in which we assessed response to EPZ001989, drug was added on day one and then replenished every four days.

Apoptosis Assays

For apoptosis analysis, $1x10^6$ cells were stained using the Annexin V-FITC apoptosis detection kit (BD) according to the manufacturer's recommendations. DAP1 was used as a counterstain in these experiments and heat-shock controls were used as positive controls.

3D Growth Assays

To perform 3D assays in these cell lines, we utilized the technique using poly-HEMA as published for mesothelioma cell lines (*177*). We prepared plates and spheroids as described with cells that had been pre-treated for 4 days with 500 nM EPZ011989. 5 days post-treatment we assessed viability with Cell Titer Glo assays.

Statistical Analyses

The Student t-test was used to analyze statistical significance unless described in the text. Normality tests were used to test the assumption of a normal distribution. Prizm GraphPad Software was used for statistical calculations. Error was calculated using SEM, $*p<0.05$, $**p<0.005$.

Replicates

c-Kit enrichment ChIP-Seq experiments were conducted with four biological replicates, with two replicates combined for sequencing. GMP ChIP-Seq experiments were conducted with three replicates for each group. c-Kit and GMP RNA-Seq was conducted with three biological replicates from each group. Histone mass spec experiments were conducted with three biological and three technical replicates. Genetic phenotyping experiments were replicated three times independently. Flow cytometric experiments were replicated independently two-three times. Pilot studies were conducted with drug studies and results were replicated in a larger study to achieve enough statistical power. *In vitro* experiments were replicated two-three times, with viability experiments being completed in triplicate.

RESULTS

Conditional deletion of *Bap1* in the hematopoietic compartment leads to myeloid

89

progenitor proliferation

Genomic studies identified somatic mutations in the tumor suppressors *ASXL1* and *BAP1* in different malignancies. Inactivating mutations in *ASXL1* are most common in myeloid malignancies (*33, 34, 36*), whereas recurrent *BAP1* mutations are commonly observed in mesothelioma (*63*), renal cell carcinoma (*65*), and metastatic uveal melanoma (*61*). We sequenced 32 paired tumor and normal samples with *de novo* MDS. In this cohort, we identified a frameshift mutation in BAP1 that resulted in premature truncation in the UCH catalytic domain that was not present in the matched normal sample (**Figure 3.1**). This patient was wild-type for all other known MDS mutations and had a single del(20)(q11.2q13.3) cytogenetic abnormality. We also found that BAP1 expression was decreased overall in MDS patient samples (**Figure 3.2**). However, *BAP1* mutations in hematopoietic malignancies have been found to be uncommon, unlike *ASXL1* mutations.

To assess whether tissue-specific expression explained these differential mutational patterns, we analyzed the expression of *BAP1* and *ASXL1*, in addition to the *ASXL1* family members *ASXL2* and *ASXL3*, in mesothelioma and AML TCGA datasets. We found that *BAP1* and *ASXL1-2* in were expressed in both datasets, but not *ASXL3*. We also assessed the expression of *BAP1* and *ASXL1-3* in murine sorted hematopoietic stem and progenitor (HSPCs) in addition to more mature hematopoietic lineages, and also noted expression of *BAP1* and *ASXL1-2*, but not *ASXL3*. Therefore, these distinct mutational profiles cannot be explained by differential tissue-specific *BAP1* and *ASXL1* expression (**Figure 3.3A-C**). We sought to identify mechanisms by which *BAP1* loss leads to transformation, independent of ASXL1*,* and to identify therapeutic vulnerabilities in *BAP1*-mutant cancer cells.

Tumor   **Normal**

F

R

c.248delC
p.Ala82*fs*
Results in STOP 3 amino acids later at amino acid 85
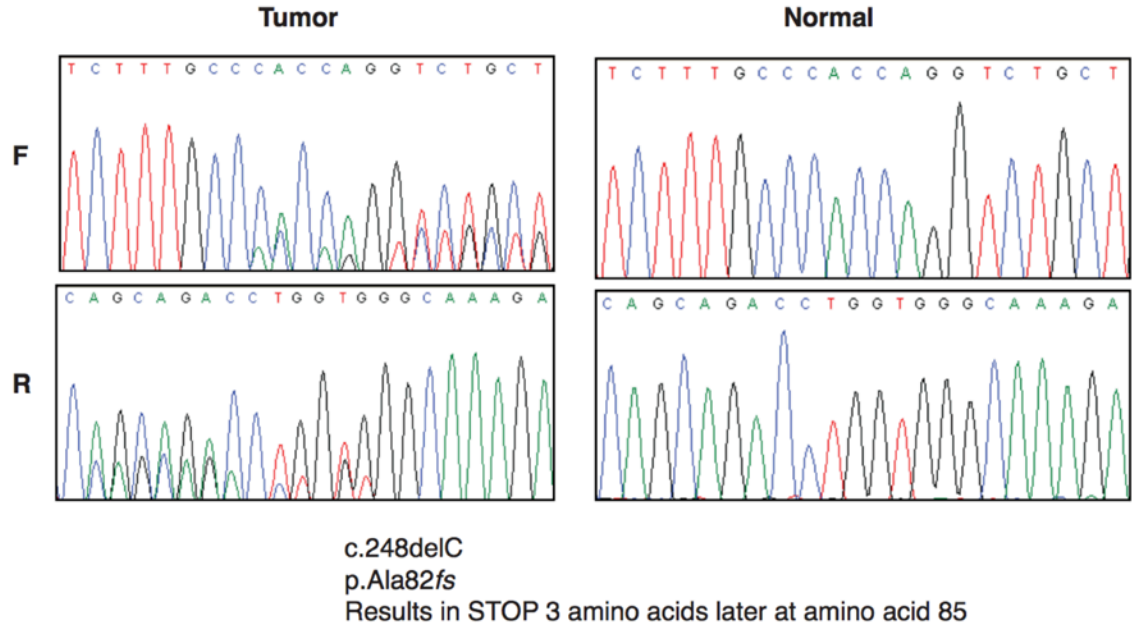
Figure 3.1. Identification of a frameshift mutation in a *de novo* MDS patient. Sanger sequencing tracks depicting the mutation only in the tumor sample and not in matched normal tissue. Reprinted by permission from Macmillan Publishers Ltd: NATURE REVIEWS CANCER 12(9), copyright 2012.
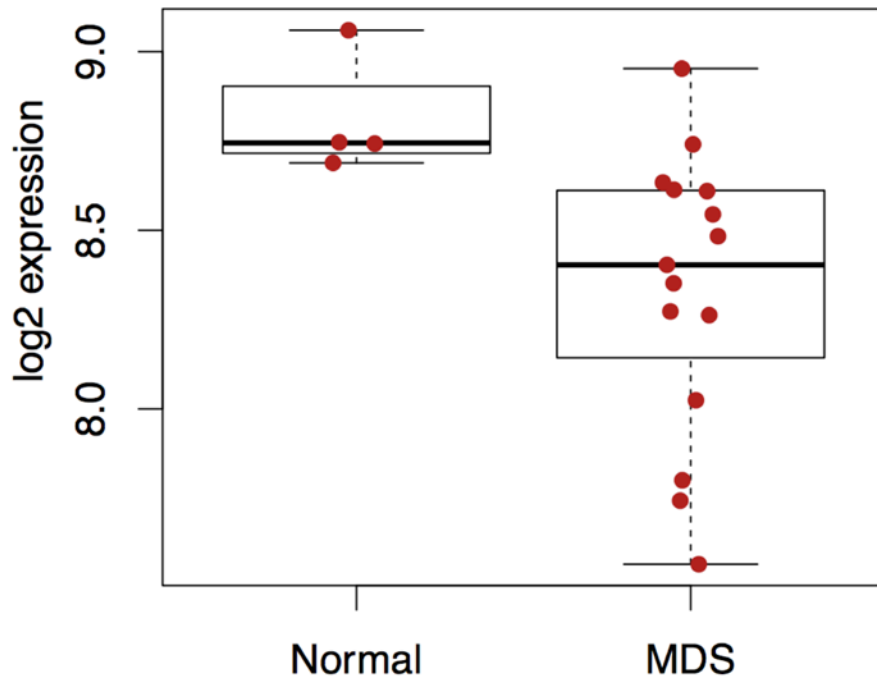
Figure 3.2. BAP1 expression is decreased in MDS patients samples, consistent with the tumor suppressive function of BAP1. Reprinted by permission from Macmillan Publishers Ltd: NATURE REVIEWS CANCER 12(9), copyright 2012.
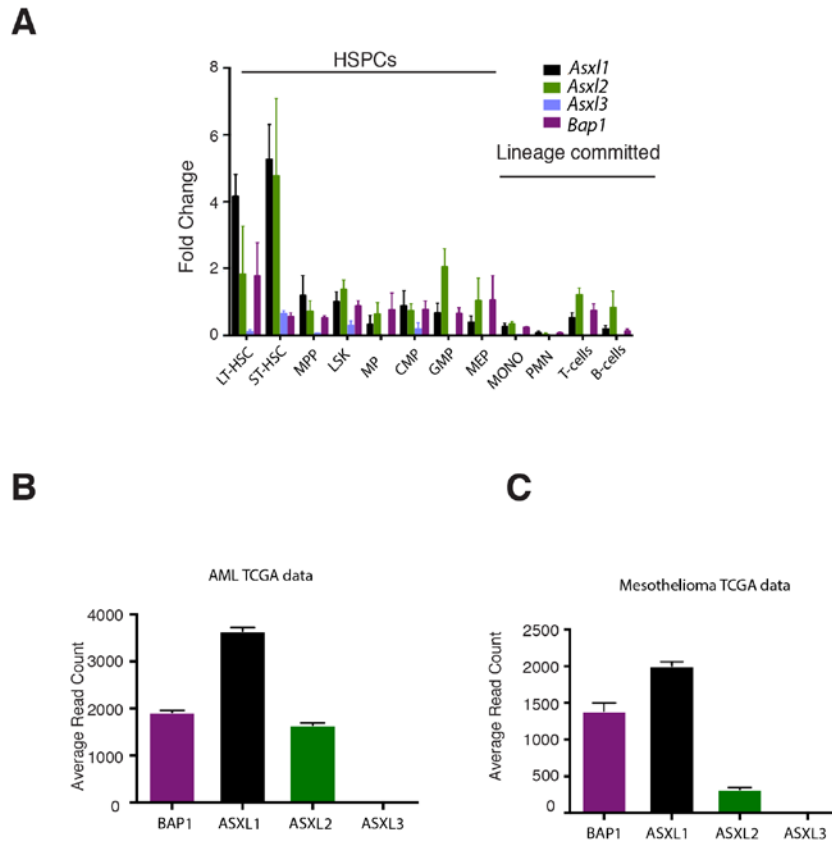
Figure 3.3. BAP1, ASXL1 and ASXL2 but not ASXL3 are expressed in AML and mesothelioma samples, and in murine hematopoietic cells. (**A**) Average gene expression of BAP1, ASXL1, ASXL2, and ASXL3 in TCGA AML (acute myeloid leukemia) and (**B**) mesothelioma patients as expressed as a mathematical mean with standard error of normalized read counts. (**C**) *Bap1* expression by qRT-PCR in purified populations of hematopoietic cells in C57/B6H mice. LT-HSC, long term hematopoietic stem cells (HSCs), (Lin⁻Sca-1⁺c-Kit⁺CD150⁺CD48⁻); ST-HSC, short term HSCs (Lin⁻Sca-1⁺c-Kit⁺CD150⁺CD48⁺); MPP, mulitpotent progenitor, (Lin⁻Sca-1⁺c-Kit⁺CD150⁻CD48⁺); LSK, Lin⁻Sca-1⁺c-Kit⁺; MP, myeloid progentiors (Lin⁻Sca-1⁻c-Kit⁺), GMP, Granulocyte Macrophage Progenitors (Lin⁻Sca-1⁻c-Kit⁺ CD34⁺FcY⁺); CMP, Common Myeloid Progenitors (Lin⁻Sca-1⁻c-Kit⁺ CD34⁺FcY^lo); MEP, Macrophage Erythroid Progenitors (Lin⁻Sca-1⁻c-Kit⁺ CD34⁻FcY⁻); MONO, monocytes (Mac1⁺Gr1); PMN, (polymorphonuclear neutrophil, Mac1⁺Gr1⁺); T cells, CD3⁺; and B cells, B220⁺.

Recent work using a Rosa-CreERT transgene to inducibly delete *Bap1* from somatic tissues demonstrated that conditional loss of *Bap1* led to a myeloproliferative disease phenotype *in vivo* (*76*). We investigated the impact of conditional *Bap1* deletion on gene expression and chromatin state in hematopoietic cells. We generated mice expressing a conditional *Bap1* allele with loxP sites surrounding exons 6-12 utilizing targeted ES cells obtained from the EUCOMM consortium (**Figure 3.4A**). Recombination was confirmed using PCR and Southern blotting (**Figure 3.4B**). Homozygous floxed Bap1 mice (*Bap1* f/f) were then crossed to the IFNα (interferon alpha)-inducible *Mx1*-Cre transgenic mice, allowing for disruption of the ubiquitin hydrolase domain and complete loss of Bap1 protein expression following Cre-mediated deletion (**Figure 3.4B,C**). *Bap1* was excised in adult animals at six weeks of age by injection of polyI:polyC to trigger IFNα (*Bap1-/-* referred to as *Bap1* KO mice hereafter; littermate *Bap1 f/f* controls referred to as CON). Similar to the phenotype observed with systemic, inducible *Bap1* loss, conditional deletion of *Bap1* in the hematopoietic compartment led to a rapid, fully penetrant myeloproliferative disease characterized by splenomegaly (**Figure 3.5A**), leukocytosis (**Figure 3.5B**), and anemia (**Figure 3.5C**). The CBC indication of high white blood cell counts and low hematocrit levels was validated with flow cytometry for $Mac1^+Gr1^+$ (**Figure 3.5D**) and $CD71^+Ter119^+$ (**Figure 3.5E**). Deletion of Bap1 led to a marked expansion of myeloid progenitors ($Lin^-c\text{-}Kit^+Sca1^-$) (**Figure 3.5F**) in the bone marrow, most notably in the granulocyte macrophage progenitor population (GMPs) (**Figure 3.6A,B**). Of note, the expansion of myeloid progenitors was due to increased proliferation and cell cycle progression, as Bap1-deficient myeloid progenitors were characterized by a marked increase in the proportion of Ki67 positive cells and by an increase in the proportion of myeloid progenitors in G1/G2 (**Figure 3.6C**).

Loss of *Bap1* leads to opposite transcriptional effects compared to loss of *Asxl1*

95
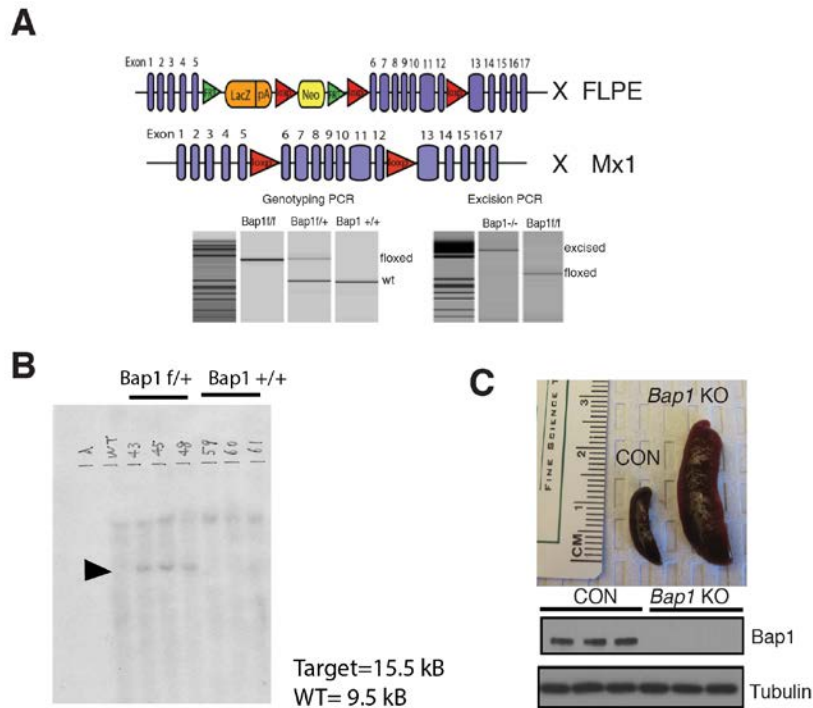
Figure 3.4. Generation of a *Bap1* conditional knockout mouse. (**A**) *Bap1* targeting scheme in murine embryonic stem cells obtained from the EUCOMM consortium. After chimera generation, mice were crossed with transgenic FLPE mice to excise the premature stop cassette. Mice were then crossed to Mx1-*Cre* transgenic mice. Genotyping schemes confirming genotype and excision 4 weeks post-polyIpolyC (pIpC) treatment. (**B**) Southern blot confirming recombination at 5'. (**C**) Representative spleen images four weeks after conditional deletion of *Bap1* and verification of *Bap1* deletion by Western blot of control (littermate *Bap1f/f* mice, CON) and *Bap1* knockout (*Mx1-Cre Bap1f/f* mice, *Bap1* KO) bone marrow.

96
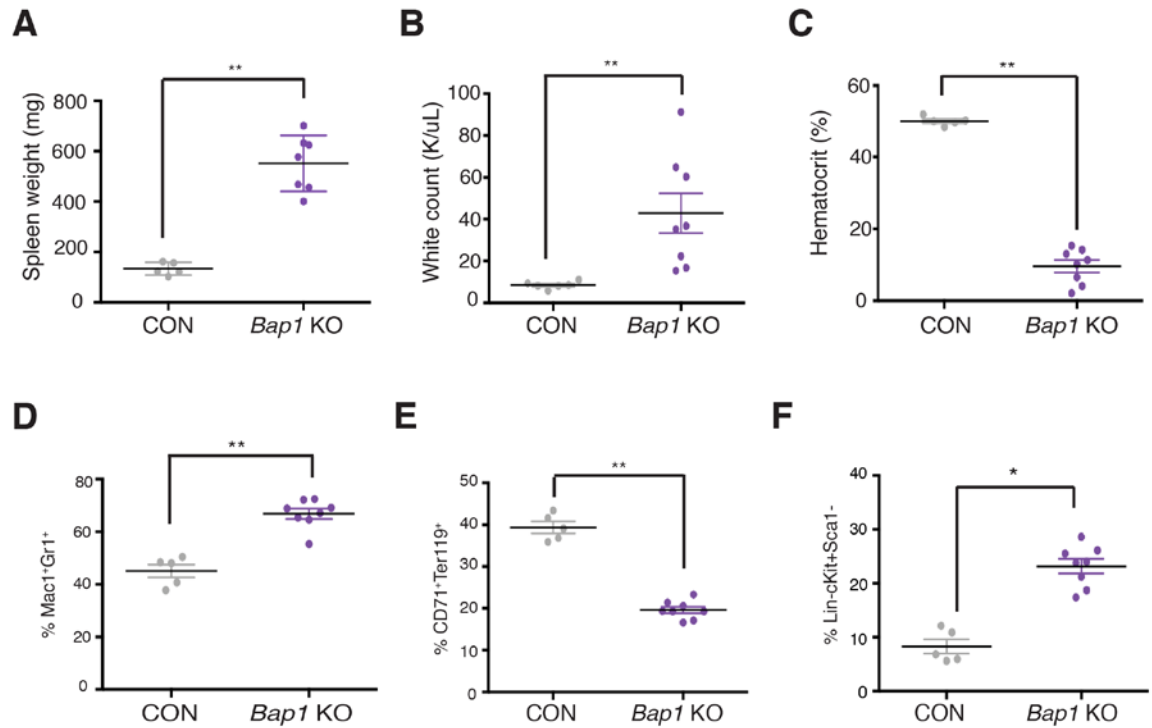
Figure 3.5. Deletion of *Bap1* in hematopoietic cells results in a myeloproliferative phenotype. (**A**) Spleen size in CON and *Bap1* KO animals (**B**) Enumeration of white blood cells in peripheral blood in control and *Bap1* KO mice after treatment with (pIpC) to induce excision and (**C**) flow cytometric enumeration of myeloid cells (Mac1$^+$Gr1$^+$). (**D**) Hematocrit percentages in peripheral blood and (**E**) flow cytometric enumeration of red blood cell precursors (CD71$^+$Ter119$^+$) in control and *Bap1* KO mouse bone marrow after pIpC-induced excision. (**F**) Relative frequencies of control and *Bap1* KO bone marrow myeloid progenitor populations (Lin$^-$c-Kit$^+$Sca1$^-$). Cells were gated on live lineage-negative populations.
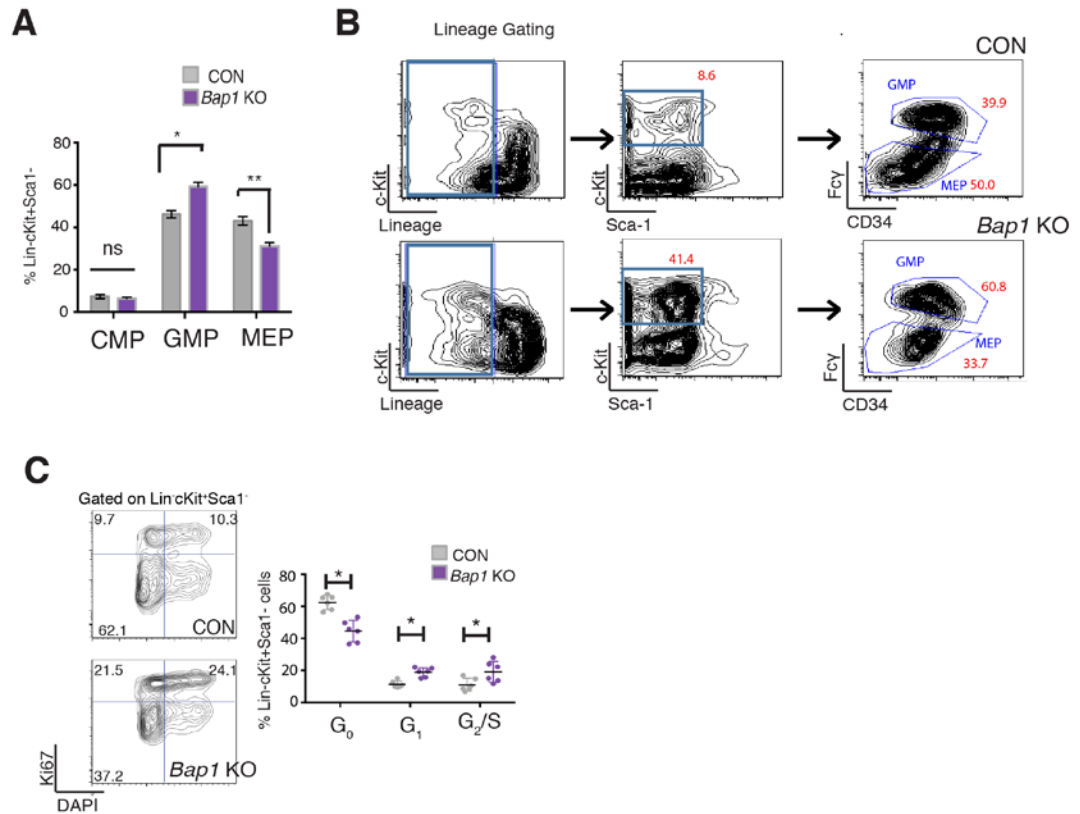
Figure 3.6. Myeloid progenitors are expanded and increasingly cycling in *Bap1* KO cells. (**A**) Relative quantification of bone marrow myeloid progenitor cell populations (GMP, CMP, MEP) in control and *Bap1* KO mice (**B**) Flow plots from example control and bone marrow animals to demonstrate progenitor and GMP expansion (**C**) Flow cytometric enumeration of cycling progenitor cells (Ki67/DAPI stain); for all experiments: n=5 CON mice and n=8 *Bap1* KO mice.

We next sought to investigate which transcriptional programs were altered in *Bap1*-deficient purified myeloid populations. We performed mRNA sequencing (RNA-Seq) of *Bap1* KO and littermate control GMPs (n=3 per group). RNA sequencing analysis revealed the majority of differentially expressed genes in *Bap1*-deficient GMPs had reduced expression (*p*-adj<0.001) (**Figure 3.7A**).

Although we observed significant global overlap between the set of differentially expressed genes in *Bap1* and *Asxl1* KO progenitors, in many cases we observed a paradoxical inverse effect on gene expression (**Figure 3.7B**). We next performed gene set enrichment analysis (GSEA) to identify target gene sets enriched in *Bap1* KO myeloid progenitors. We compared gene sets enriched in Bap1 KO myeloid progenitors to those in *Asxl1* KO myeloid progenitors to determine if these gene sets were coordinately regulated by *Bap1* and *Asxl1*. We noted a significant number of gene sets that were enriched both in *Bap1*-deficient cells and in Asxl1-deficient cells, but many of these gene sets were inversely correlated (**Figure 3.7C**). *ASXL1* silencing leads to increased expression of *HoxA* cluster genes consistent with reduced PRC2 activity (*169*). We observed increased expression of *HoxA* target gene sets in *Asxl1* KO cells, and reduced expression of *HoxA* target genes in Bap1 deficient cells (Takeda Targets of HOXA9 and HESS targets of HOXA9 and MEIS1) (**Figure 3.8A**) (*143, 178*). We confirmed the inverse impact of Bap1 loss on HoxA gene expression by real time quantitative PCR (**Figure 3.8B**). These data suggested that loss of *Asxl1* and *Bap1* can have opposite effects on gene regulation.

We have previously shown ASXL1 directly interacts with the PRC2 complex, and that loss of *ASXL1* leads to global and site-specific reductions in H3K27me3. Given the divergent effects of *Asxl1* loss and *Bap1* loss on gene expression, we investigated the

99

A

CON
Bap1 KO

B

Differentially expressed

p<0.001

3532   714   1047

Bap1 KO   *Asxl1* KO

Direction of expression

p=ns

3838   247   1511

Bap1 KO   *Asxl1* KO

C

BAP1 Genesets   ASXL1 Genesets

2529   143   907

66
inversely correlated

77
correlated

Asxl1 vs. Bap1 GSEA analyses (p-values)

	BAP1 KO	ASXL1 KO
Cellular Defense Response	0.0004	0.2443
Chemokine Activity	0.0150	0.1323
Chemokine Receptor Activity	0.0086	0.1307
Defense Response	0.0060	0.1629
Hess Targets of HOXA9 and MEIS1 DN	0.0004	0.1647
Inflammatory Reponse	0.1123	0.1347
KEGG Cytokine Cyokine Receptor Interaction	0.0169	0.2163
Reactome Chemokine Receptors bind Chemokines	0.0014	0.700
Takeda Targets of NUP98 HOXA9 Fusion 3D DN	0.0033	0.2330
Zheng IL22 Signaling Up	0.2112	0.1274

Figure 3.7. Loss of *Bap1* or *Asxl1* have opposite effects on gene transcription. (A) RNA-Seq data of differentially expressed genes in control versus *Bap1* KO mice granulocyte-macrophage progenitors (GMPs; Lin⁻c-Kit⁺Sca1⁻ CD34⁺ Fcγ⁺); cells analyzed with DESeq2 (cutoff *p*-value *p<0.05*). Heatmap indicates genes increasing (red) and decreasing (blue) in expression. (**B**) Venn diagrams comparing myeloid progenitor gene expression in *Bap1* and *Asxl1* KO mice, *p<0.05*; comparisons include gene overlap and genes changing in the same direction. (**C**) Number of positively and negatively enriched genesets from the *Bap1* KO and *Asxl1* KO GSEA analysis hitting an FDR<0.25 (top). Venn diagram depicting gene sets that are oppositely enriched in *Bap1* KO and *Asxl1* KO myeloid progenitors by RNA-Seq (bottom).

100
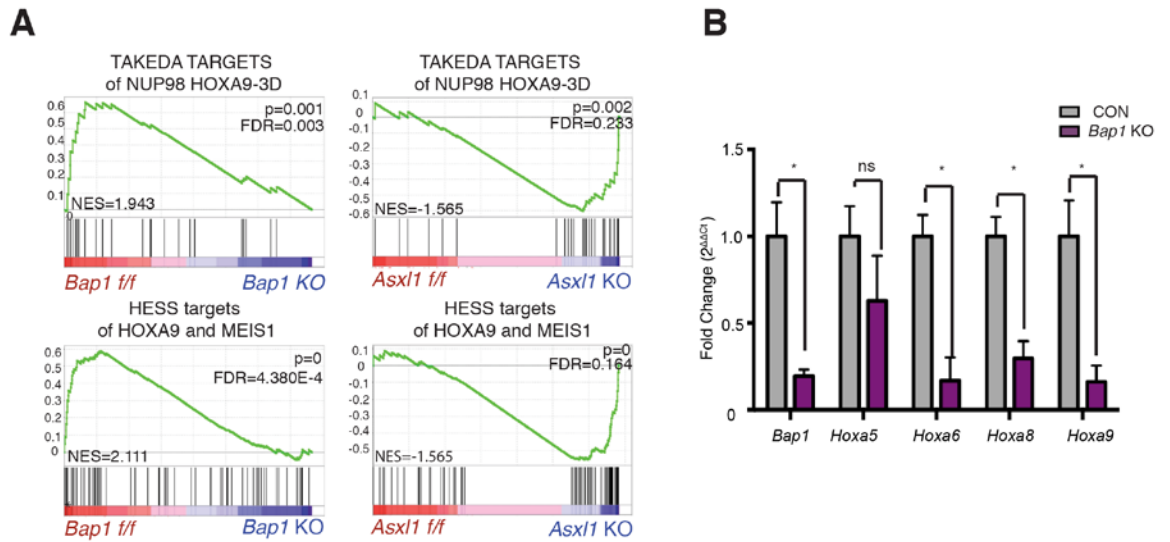
Figure 3.8. Hoxa gene expression is inversely altered by loss Bap1 or *Asxl1*. (A) GSEA of oppositely enriched and statistically significant *HoxA* cluster gene sets in *Bap1* KO and *Asxl1* KO progenitor cells. *p*-values and FDR values are indicated. (**B**) Quantitative real time qPCR (qRT-PCR) of the *HoxA* cluster in sorted granulocyte-macrophage progenitors (GMPs; Lin⁻c-Kit⁺Sca1⁻ CD34⁺ Fcγ⁺); from *Bap1* KO and control mice (n=3).

impact of Bap1 loss on PRC2 target gene expression. GSEA confirmed that *Bap1* loss led to marked enrichment of Suz12 and Ezh2 siRNA gene signatures identified in human embryonic fibroblasts, consistent with increased repression of PRC2 target genes with Bap1 deletion (PRC2_SUZ12_Helin p<0.018; PRC2_EZH2_Helin *p*<0.004) (**Figure 3.9A**) (*179*). We also noted an overlap between genes that were transcriptionally silenced with Bap1 loss and genes with increased expression in Eed (a core component of the PRC2 complex)-deficient hematopoietic cells (*p*<0.024) (**Figure 3.9B**) (*100*). These data demonstrate that PRC2 target genes characterized by increased transcriptional repression in the setting of *Bap1* loss.

Bap1 loss leads to increases in global H3K27me3

ASXL1 directly interacts with the PRC2 complex and *ASXL1* depletion reduces global and site specific H3K27me3 (*169*). Given the divergent effects of *As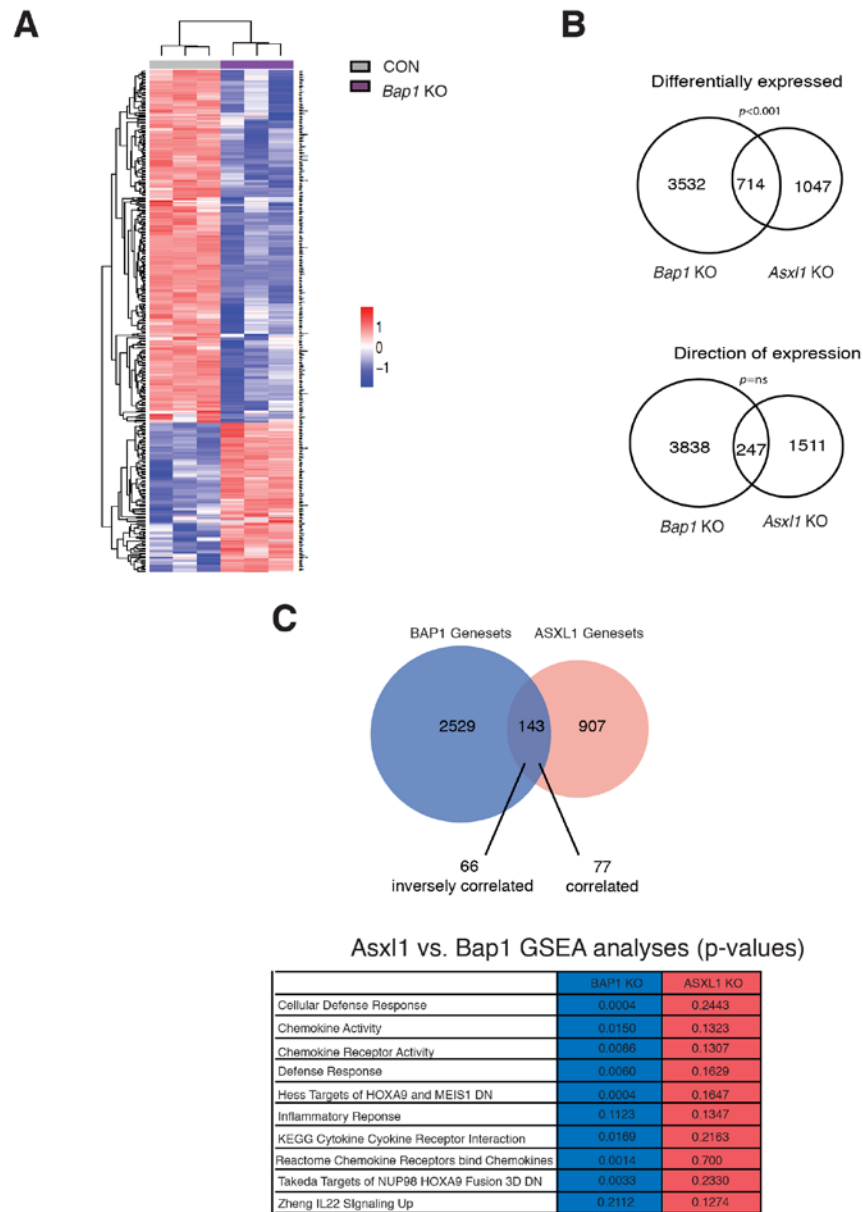xl1* and *Bap1* loss on gene expression, we investigated the impact of *Bap1* deletion on H3K27me3. H3K27me3 levels were increased in *Bap1* KO cells as assessed by Western blot (**Figure 3.10A**) and histone ELISA (**Figure 3.10B**). To confirm that our findings were not due to differences in cell type composition or due to antibody specificity, we performed mass spectrometric analysis on histones extracted from c-Kit enriched control and Bap1 KO bone marrow cells. This revealed a significant increase in H3K27me2 and H3K27me3 in Bap1-deficient cells compared to control, with a concomitant decrease in unmodified and monomethylated H3K27 (**Figure 3.10C**). H3K27me3 chromatin immunoprecipitation sequencing (ChIP-Seq) in c-Kit enriched CON and *Bap1* KO cells revealed a global increase in *Bap1* KO mice (**Figure 3.11A**). We utilized a broad domain peak caller to identify domains of H3K27me3 enrichment (*114*). H3K27me3 broad domains were characterized as either called only in the control sample (CON only), only in the *Bap1* KO samples (*Bap1* only), or in both groups (common loci). We found an

102
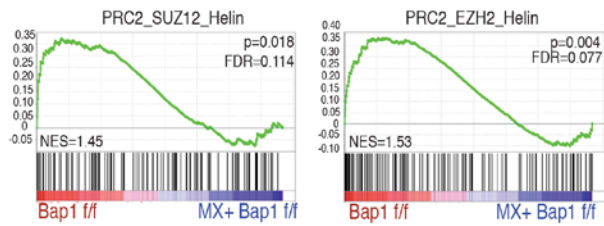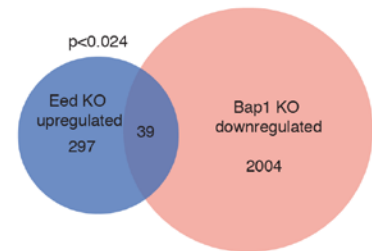
Figure 3.9. PRC2 gene signatures are enriched in GSEA analyses comparing CON with *Bap1* KO. (**A**) PRC2 loss-of-function genesets are anti-correlated with *Bap1* loss-of-function gene expression profiles. (**B**) A statistically significant number of genes that are upregulated with loss of *Eed* overlap with genes that are downregulated with loss of *Bap1*.
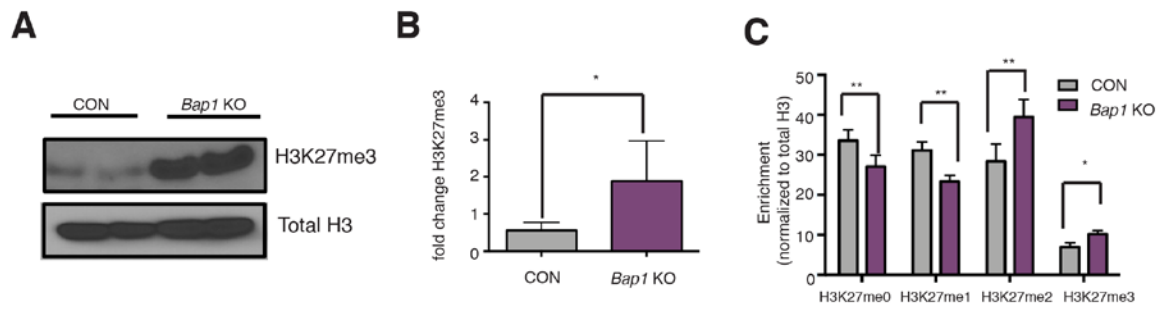
Figure 3.10. H3K27me3 is globally increased in *Bap1* KO mice. (**A**) Western blot of H3K27me3 and total H3 in purified histones from *Bap1* KO and control bone marrow. (**B**) ELISA of H3K27me3 normalized to total H3 in histones purified from bone marrow cells from *Bap1* KO and control mice. (**C**) Mass spectrometric analysis of purified histones from c-Kit[+] enriched bone marrow cells from *Bap1* KO and controls normalized to total histone H3.
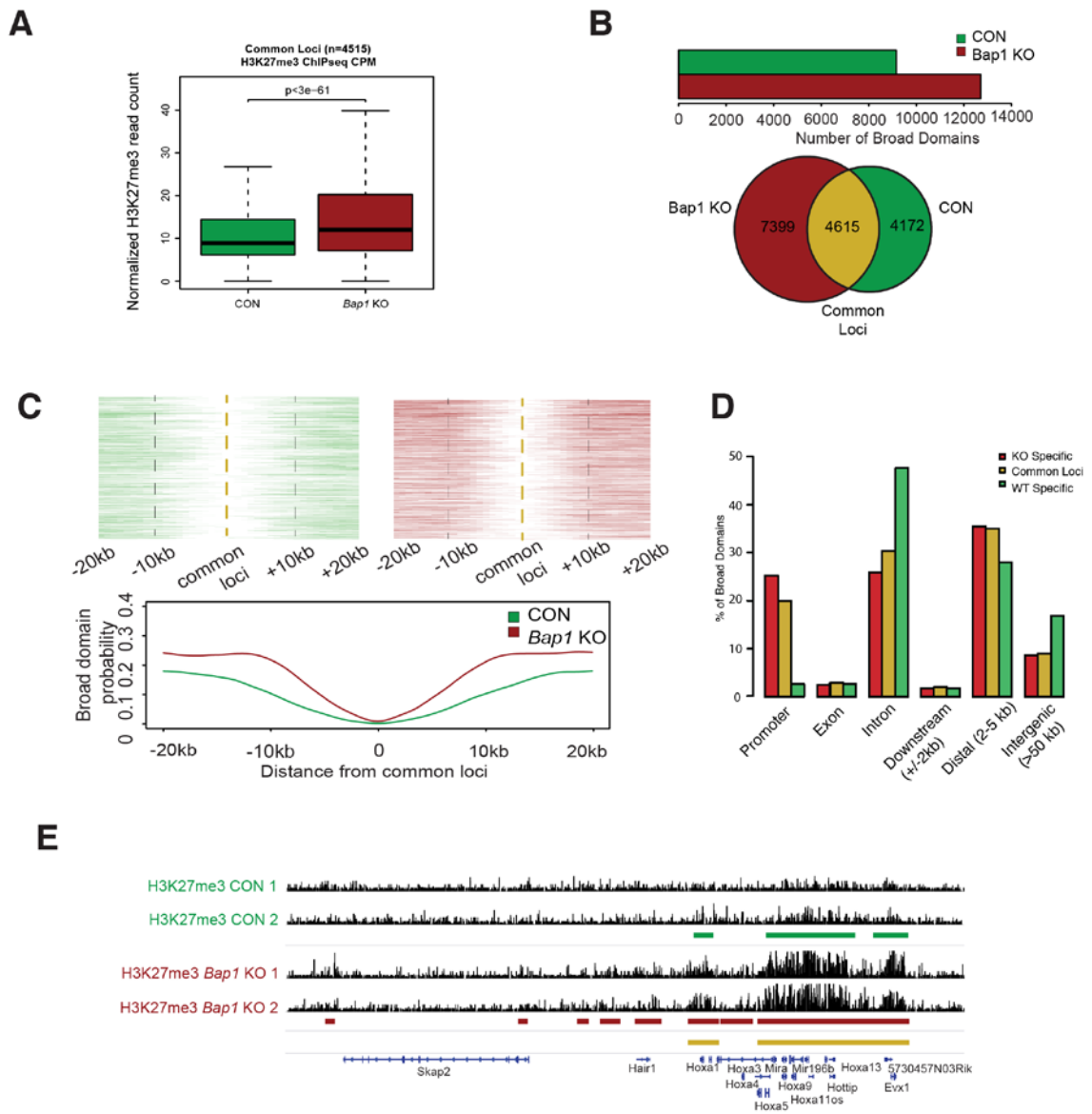
Figure 3.11. ChIP-Seq analyses revealed increased H3K27me3 broad domains at Polycomb targets in *Bap1* KO mice. (**A**) Box plot showing normalized H3K27me3 reads in c-Kit enriched bone marrow cells (n=2) (**B**) Number of H3K27me3 broad domains that are called in the CON and *Bap1 KO* samples. Venn diagram showing unique and overlapping broad domain. (**C**) Plotting broad domain density as a function of distance from an H3K27me3 domain that was called in both CON and *Bap1* KO samples. (**D**) Percentage of H3K27me3-broad domains called in relation to gene transcriptional start site (promoter, exon, intron, downstream (+/-2 kb), distal (2-5 kb), and intergeneic (>50 kb)). (**E**) Local plot of H3K27me3 ChIP-seq at the HOXA locus.

increased number of broad domains in the *Bap1* KO only groups and larger domains in common loci marked with H3K27me3 (**Figure 3.11A,B**). Interestingly, we also found increased H3K27me3 broad domain "spreading" into nearby loci (**Figure 3.11C**). This H3K27me3 increase and spreading is well illustrated within the *HoxA* locus in *Bap1* KO cells (**Figure 3.11E**). The sites marked with H3K27me3 in *Bap1* KO cells, primarily occurred in gene promoter regions (**Figure 3.11D**) and genes with H3K27me3-occupied promoters were enriched for enhanced repression (FDR<0.001) (**Figure 3.12A**). We wanted to confirm that the differences in H3K27me3 were not due to differences in cell type with the c-Kit enriched population. Therefore, we completed ChIP-Seq in sorted GMP cells and found that H3K27me3 was also strikingly increased in the *Bap1 KO* cells compared to control (**Figure 3.12B**). Genes dysregulated by *Bap1* KO-associated H3K27me3 and gene repression were implicated in EZH2-dependent regulation, lineage commitment/differentiation and proliferation (**Figure 3.12C**). When comparing to RNA-Seq profiles of normal HSPCs (*180*), we found that genes that were downregulated in expression and marked by increased H3K27me3 after *Bap1* loss were associated with important genes in progenitor populations (**Figure 3.13**).

We next sought to determine if perturbations of BAP1 *in vitro* would lead to similar changes in H3K27me3. *BAP1* silencing in the human leukemic SET2 cell line with two independent shRNAs led to increased H3K27me3 as assessed by Western blot (**Figure 3.14A**). We next re-expressed human full-length BAP1 in murine *Bap1*-deficient cells *in vitro* to assess the impact of BAP1 reintroduction on H3K27me3. *Bap1*-deficient cells were characterized by a marked increase in H3K27me3, which was abrogated by re-expression of BAP1 (**Figure 3.14B**). Changes in H3K27me3 expression were dependent on the deubiquitinase domain as re-introduction of BAP1 but not the deubiquitinase mutant BAP1 C91A resulted in a rescue of increased H3K27me3 levels (**Figure 3.14C**).
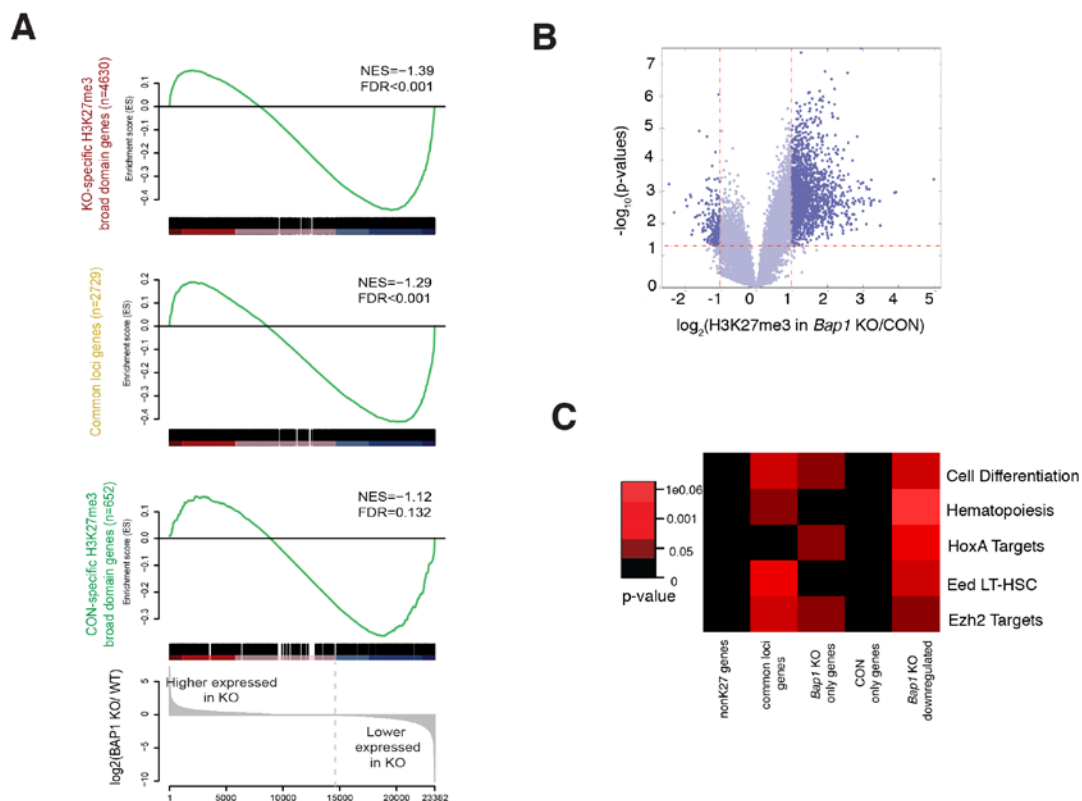
Figure 3.12. Decreased gene expression corresponds to genes that are marked by H3K27me3 in *Bap1* KO cells. (**A**) GSEA demonstrating gene expression correlations to downregulated genes. (**B**) Peak calls from H3K27me3 ChIP-Seq in sorted GMP cells displayed in a volcano plot as displayed by ratio (KO/CON) vs. p-value. (**C**) Significance of specified gene signatures to H3K27me3 bound genes and RNA-Seq. Statistics were calculated with Student t-test.
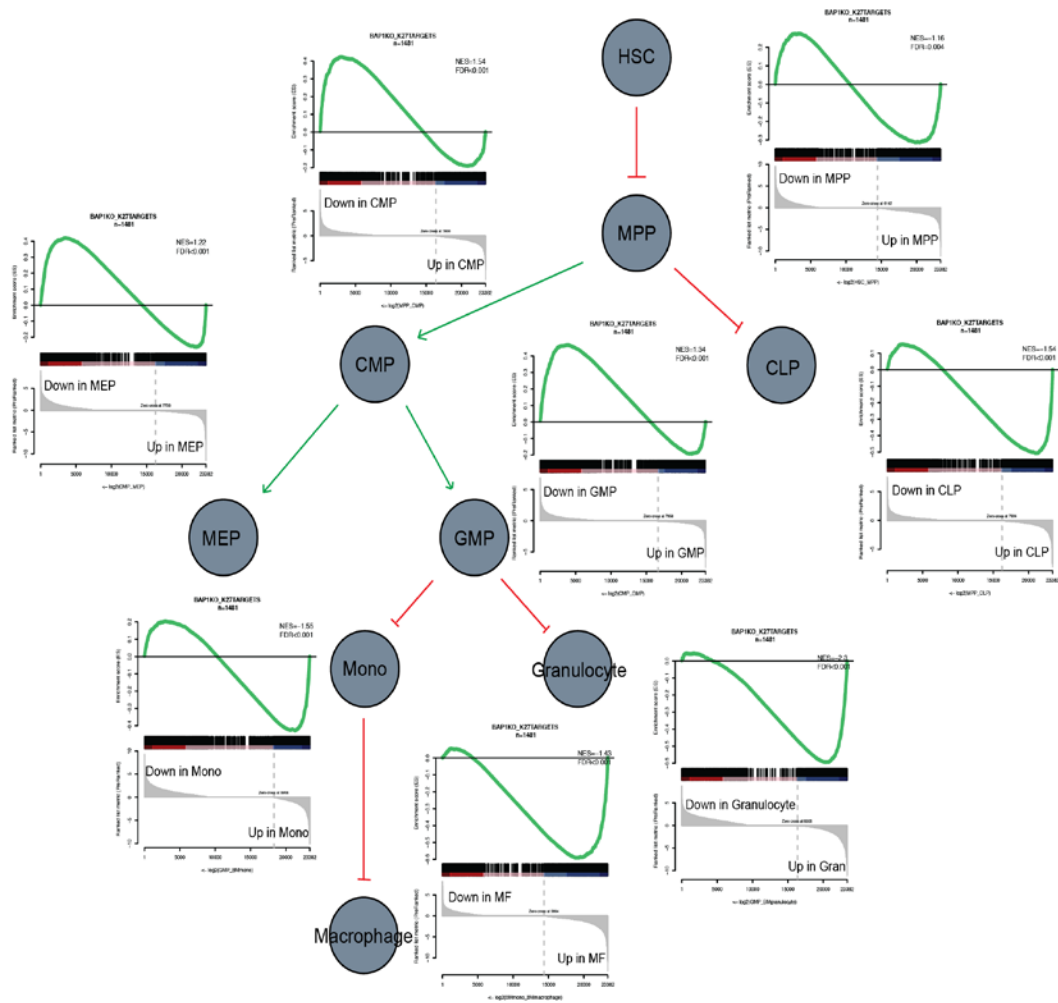
Figure 3.13. H3K27me3 target genes in *Bap1* KO mice correspond to genes that are differentially expressed in normal progenitor cells. Published RNA-Seq from sorted bone marrow populations (*180*) was analyzed and compared to genes that were differentially downregulated and marked with H3K27me3 following *Bap1* loss were analyzed using GSEA. Genes that were downregulated and marked by H3K27me3 were only correlated with the hematopoietic progenitor populations, suggesting that these may be the relevant target populations. These data are explanatory of the progenitor expansion that we see in the *Bap1* KO mouse model.
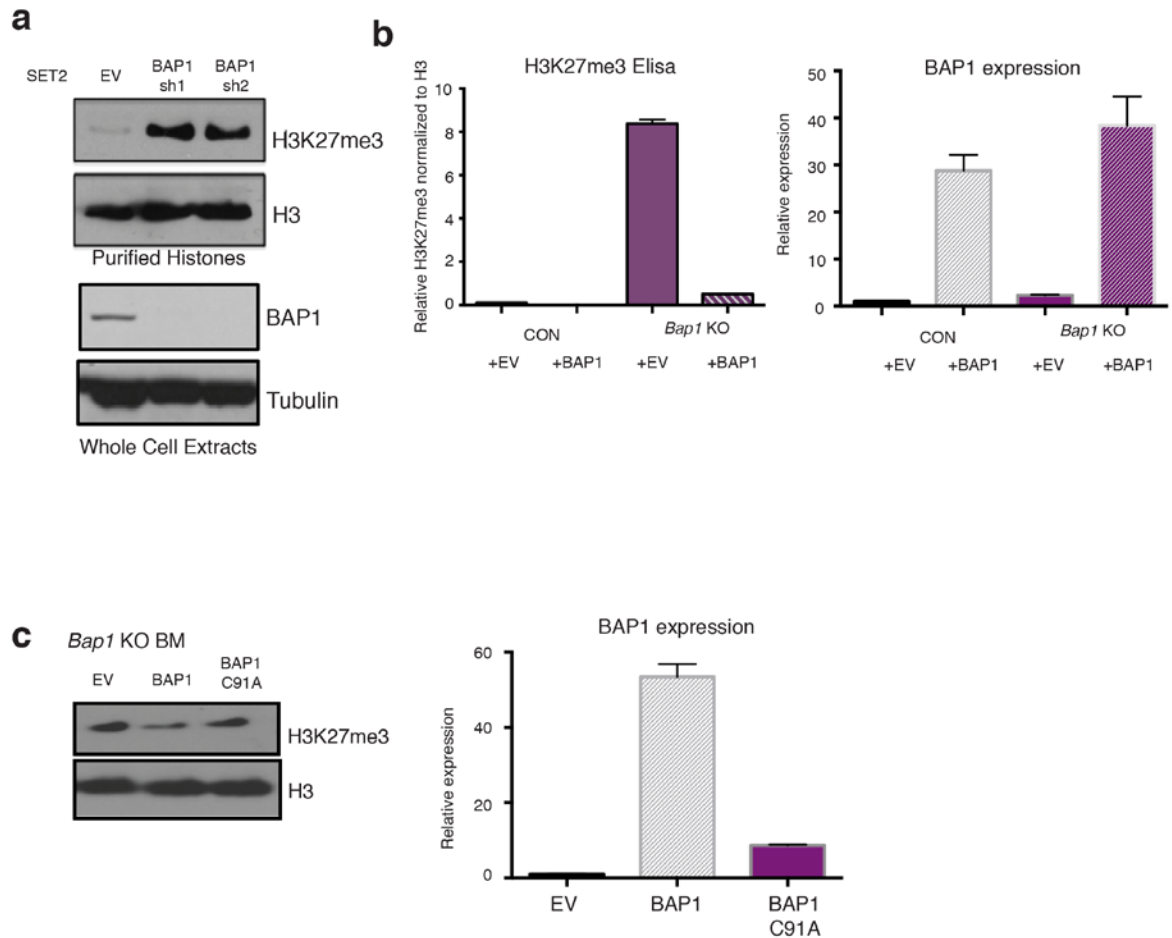
Figure 3.14. *In vitro* BAP1 perturbations lead to changes in H3K27me3. (**A**) Western blot of SET2 cells transduced with two independent BAP1 shRNAs revealing H3K27me3 levels in purified histones and BAP1 knockdown from whole cell extract. (**B**) Methylcellulose assay with control and *Bap1* KO bone marrow cells. BAP1 cDNA constructs were reintroduced into control and Bap1 deleted cells. Histone ELISA assays were performed for H3K27me3. Quantitative qPCR to assess expression of BAP1 construct. (**C**) Reintroduction of BAP1 and deubiquitinase mutant BAP1 C91A in *Bap1*-deficient murine cells. Histone Western blots were performed for H3K27me3 and total H3. Quantitative qPCR shows levels of construct expression.

However, we were unable to express the BAP1 C91A to the same levels as BAP1, which we believe are due to the stem cell defect in *Bap1* KO HSPCs. Likely reintroduction of BAP1 results in a rescue of stem cell fitness. Taken together, these data demonstrate that BAP1 loss leads to increased H3K27me3 and that these changes in chromatin state contribute to altered gene expression in BAP1 deficient cells.

Generation of a *Bap1/Asxl1* double knockout mouse

Based on the fact that mutations in *Bap1* and *Asxl1* occur in different disease types, yet are both expressed, and that there are opposing effects on transcription and chromatin, we next asked whether the severe murine *Bap1* KO phenotype was independent of or dominant to the *Asxl1* KO phenotype. We crossed the Mx1-Cre *Bap1* KO mouse to the previously published *Asxl1* KO mouse (*47*). Successful generation of the Mx1-Cre *Bap1/Asxl1* double knockout mouse was confirmed with established PCR protocols. *Bap1* and *Asxl1* were excised in adult animals, in addition to appropriate single allele controls, at six weeks of age by injection of polyI:polyC (**Figure 3.15A**). Four weeks after polyI:polyC, the *Bap1/Asxl1* double knockout mice had counts indistinguishable from the *Bap1* KO mice. Flow cytometric analysis confirmed that myeloid skewing as evidenced by increased myeloid progenitors cells (**Figure 3.15B**) and expanded mature myeloid populations (**Figure 3.15C**). These data suggest that the Bap1 KO phenotype is dominant to the Asxl1 KO phenotypes. More detailed analyses of chromatin and transcriptional effects are warranted to confirm this observation.

Genetic deletion or pharmacologic inhibition of *Ezh2* rescues the *Bap1* KO proliferative phenotype

Given the alterations in H3K27me3 and PRC2 target gene expression in *Bap1*-deficient

110
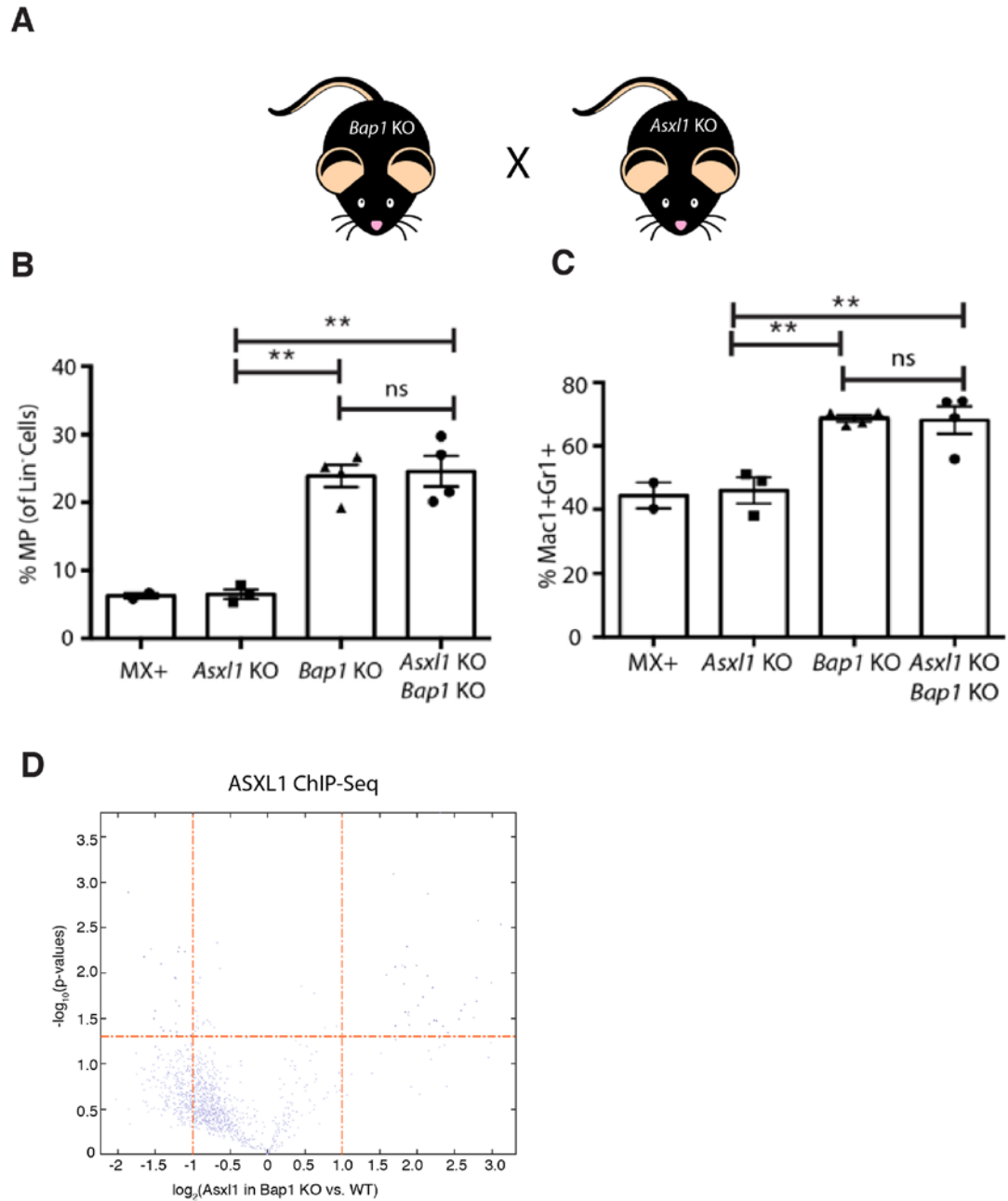
Figure 3.15. Generation of a *Bap1/Asxl1* double knockout mouse model. (**A**) The two conditional alleles, *Bap1* and *Asxl1*, that were crossed into the Mx1-Cre transgenic model. (**B**) Flow cytometric enumeration of myeloid progenitor cells for all indicated genotypes. (**C**) Flow cytometric analyses for mature myeloid cells for indicated genotypes.
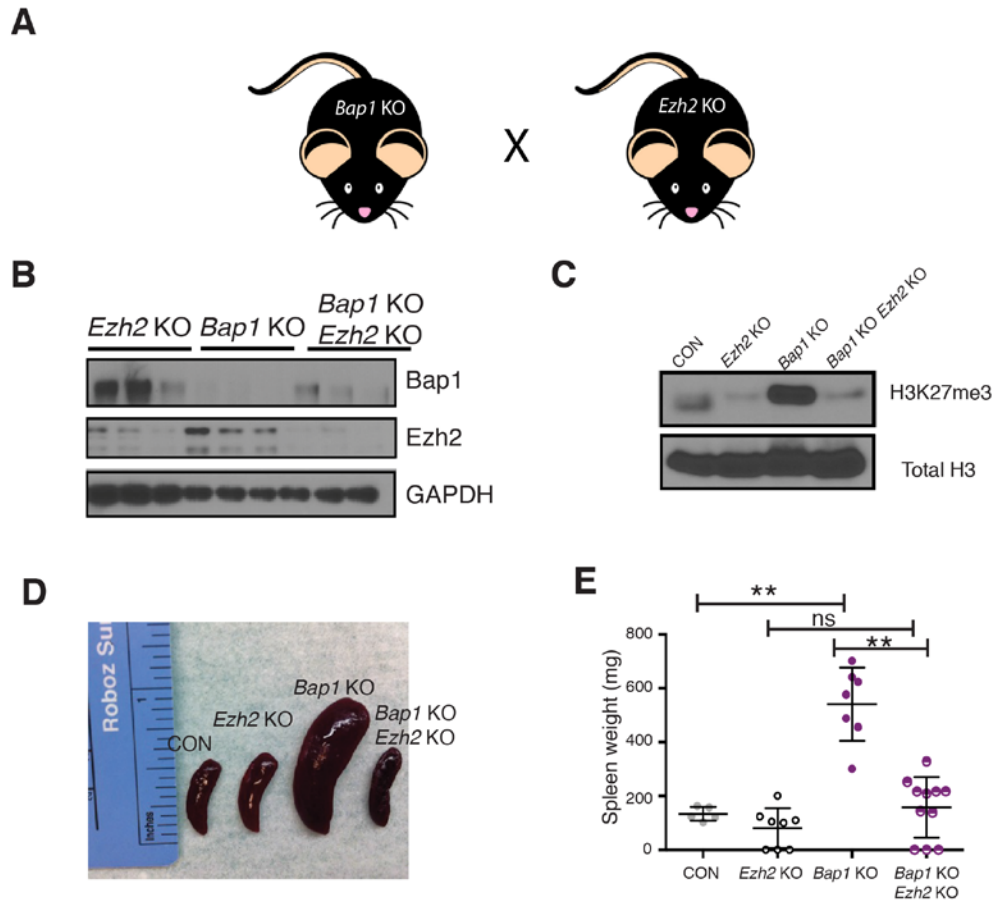
Figure 3.16. Ezh2 deletion rescues the splenomegaly in Bap1 KO mice. (**A**) Strategy for generation of conditional *Bap1/Ezh2* double knockout mice. (**B**) Western blot of Bap1, Ezh2, and Gapdh expression in mice from indicated genotypes. (**C**) Western blot of H3K27me3 levels in histones purified from bone marrow of *Bap1* KO, *Ezh2* KO, *Bap1/Ezh2* KO and control mice. (**D**) Representative images of spleens and (**E**) enumeration of spleen weight from the indicated genotypes of mice, 3 weeks post pIpC.

cells, we next investigated whether *Bap1*-deficient transformation could be rescued by abrogation of PRC2-mediated gene repression. We crossed *Bap1* floxed mice to mice bearing an *Ezh2* floxed allele (*116*) and assessed the impact of *Ezh2* deletion on the myeloproliferative disease induced by Bap1 loss. Excision was induced in Mx1-Cre *Bap1/Ezh2* compound knockout mice, as well as in single allele controls (**Figure 3.16A**). All mice were assessed for evidence of disease 4 weeks after excision. *Ezh2* and *Bap1* deletion were confirmed by Western blot (**Figure 3.16B**). A marked reduction in H3K27me3 in *Bap1/Ezh2* compound knockout mice was observed compared to *Bap1* KO mice alone (**Figure 3.16C**) consistent with abrogation of Ezh2-mediated H3K27me3. *Ezh2* loss reversed the splenomegaly observed with *Bap1* loss (*Bap1* KO avg. 541.6 mg, *Bap1/Ezh2* KO avg. 157.0 mg, p<0.005) (**Figure 3.16D,E**) and rescued the leukocytosis (*Bap1* KO avg. 51 x 109 WBCs, *Bap1/Ezh2* KO avg. 8 x 109 K/uL WBCs, p<0.005) (**Figure 3.17A**) and anemia (*Bap1* KO avg. 28.2%, *Bap1/Ezh2* KO avg. 46.0%, p<0.005) (**Figure 3.17B**) observed with loss of *Bap1 in vivo*. Histopathologic analysis confirmed that concomitant *Ezh2/Bap1* loss attenuated the *Bap1*-dependent expansion of bone marrow myeloid cells, with reversal of the myeloid expansion observed with *Bap1* deletion *in vivo* (**Figure 3.17C**). Flow cytometric analysis confirmed that *Ezh2* deletion in *Bap1*-deficient cells abrogated Bap1-dependent myeloid progenitor expansion (Lin-c-Kit+Sca1-) (*Bap1* KO avg. 23.0%, *Bap1/Ezh2* KO avg. 12.3%, p<0.05) (**Figure 3.17D**) and attenuated the expansion of mature myeloid (Mac1+Gr1+) cells (**Figure 3.17E**). Cell cycle analysis demonstrated reduced proliferation of *Bap1/Ezh2* deficient myeloid progenitors, with a cell cycle distribution similar to control cells (**Figure 3.17F**). Moreover, the reduction in erythroid progenitors (CD71+Ter119+) observed with *Bap1* loss was restored to normal levels by *Ezh2* deletion (**Figure 3.17G**). These data demonstrate that PRC2, and specifically Ezh2, is required for *Bap1*-deficient myeloid transformation *in vivo*. Furthermore, assessment of the impact of *Ezh2*
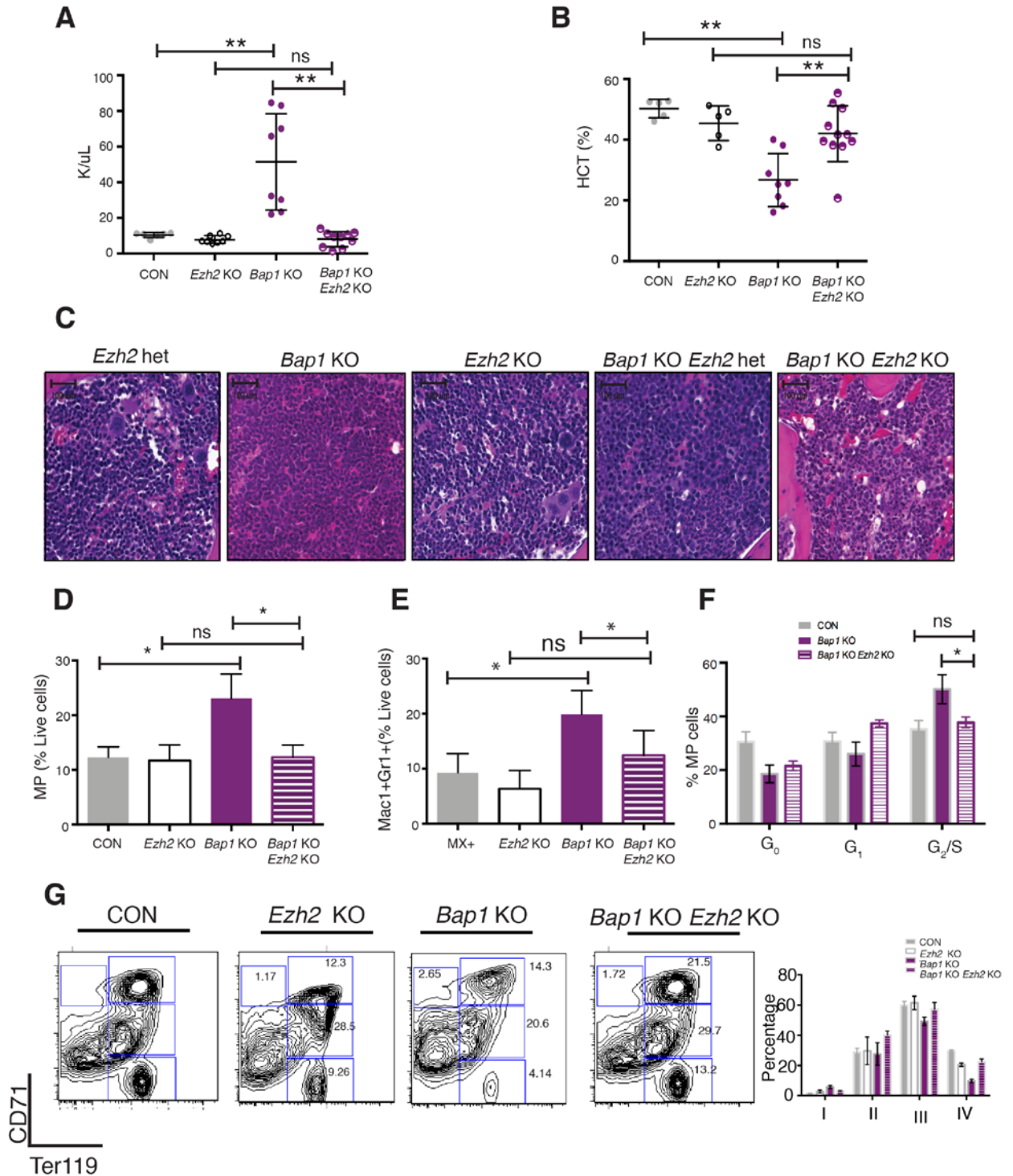
Figure 3.17. Loss of Bap1 leads to leukocytosis and anemia. (**A**) Peripheral white blood cell counts and (**B**) hematocrit percentages as quantified by CBCs. (**C**) Bone marrow pathology for various *Bap1/Ezh2* genotypes. (**D**) Flow cytometric enumeration of myeloid progenitors (Lin$^-$ c-Kit$^+$ Sca1$^-$) and (**E**) Mature myeloid cells (Mac1$^+$Gr1$^+$) (**F**) Cell cycle analyses in myeloid progenitors using Ki67 and DAPI stain (n=3/group) (**G**) Flow

114

cytometric staining for erythroid cells in indicated genotypes (CD71, Ter119) and quantification. (I-IV) are indicative of stages of erythroid differentiation with I being the most immature and IV being the most mature. Quantitation of these phenotypes on the right of the representative flow plots.

haploinsufficiency on *Bap1*-deficient myeloproliferation revealed a partial rescue of splenomegaly and blood counts (**Figure 3.18**), consistent with a dose-dependent requirement for *Ezh2* in *Bap1*-deficient transformation.

We next asked whether the rescue phenotype we observed was due to the catalytic activity of Ezh2. Initially, we attempted to treat the *Bap1* KO mice with the Ezh2 inhibitor GSK126 which is administered via intraperitoneal (IP) injection. *Bap1* KO mice have severe thrombocytopenia and therefore have a decreased affinity for coagulation, which does not allow for recovery from daily IP injection. We collaborated with Epizyme to obtain an EZH2 inhibitor tool compound (EZP011989) that can be administered via oral gauvage. We induced excision in a cohort of *Bap1* KO mice and randomized animals based on blood counts. Vehicle or EZP011989 was given to animals BID at 500 mg/kg for 16 days. Consistent with the genetic data, treatment of *Bap1* KO mice with the small molecule inhibitor EPZ011989 (*125*) decreased H3K27me3, splenomegaly, and white blood cell counts (**Figure 3.19A-C**). These data demonstrate that PRC2, and specifically *Ezh2* activity, is required for *Bap1*-deficient myeloid transformation.

Ezh2 is upregulated in *Bap1* KO mice

Given the increase in H3K27me3 in *Bap1*-deficient cells and the requirement for Ezh2 in *Bap1*-deficient proliferation *in vivo*, we next sought to delineate the mechanism by which *Bap1* deletion leads to dysregulation of the PRC2 complex. We previously demonstrated that ASXL1 directly interacts with the PRC2 complex, and that ASXL1 loss led to reduced PRC2 recruitment to target loci (*169*). Although we could detect interactions between ASXL1 and BAP1 and between ASXL1 and EZH2, we did not detect any interaction between BAP1 and EZH2 (**Figure 3.20A**). These data suggested that *Bap1*
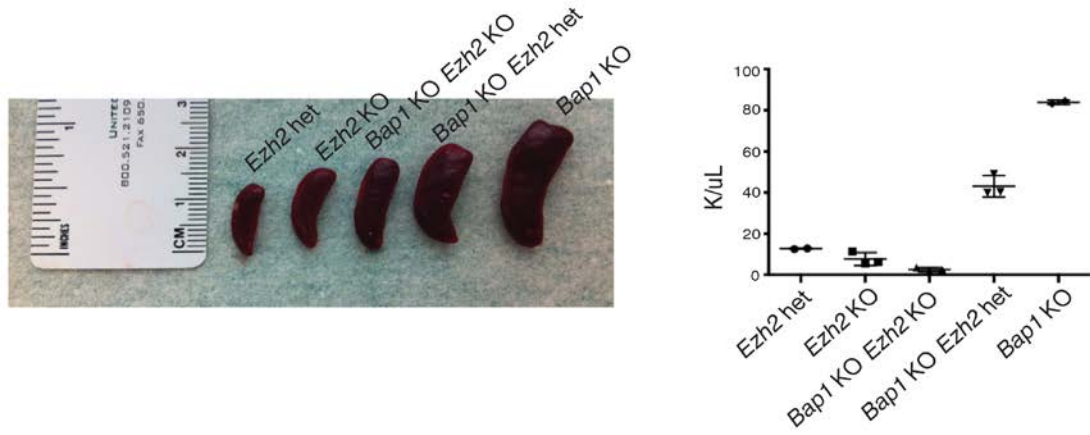
Figure 3.18. Ezh2 haploinsufficiency results in a partial rescue phenotype. Spleen sizes and white blood cell counts for indicated genotypes, 4 weeks post-pIpC.
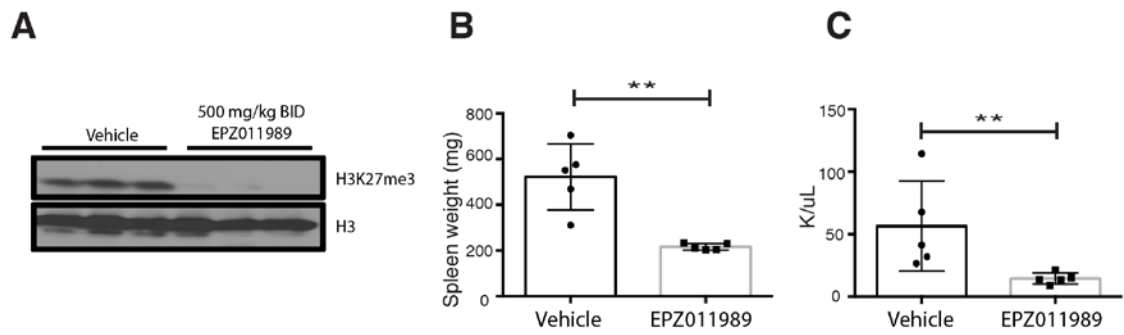
Figure 3.19. *Bap1* KO mice treated with EPZ0011989 had reduced splenomegaly and white counts. (**A**) Western blot for H3K27me3 levels in mice (n=5/group) treated with EPZ011989 twice a day at 500 mg/kg for 16 days. (**B**) Spleen weights and (**C**) white blood cell counts after treatment. Unless otherwise indicated, n=5/CON, n=5/*Ezh2* KO, n=8/*Bap1* KO, and n=11/ *Bap1/Ezh2* KO, Statistics were calculated with Student t-test; *p<0.05, **p<0.005; ± SEM values reported.
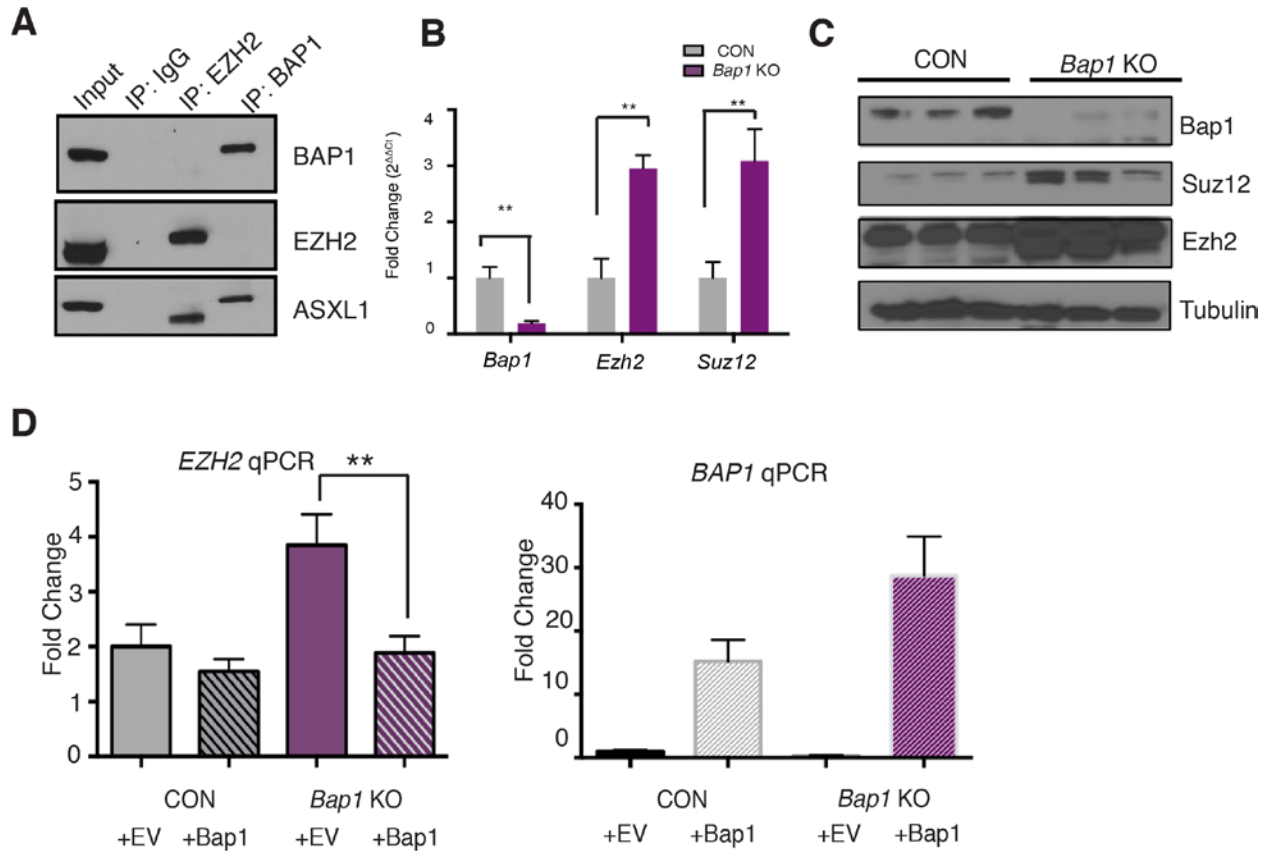
Figure 3.20. BAP1 depletion leads to an increase in PRC2 component expression.
(**A**) Co-immunoprecipitation of endogenous EZH2 and BAP1 in SET2 cells followed by Western blot analysis (performed in presence of benzonase to inhibit interactions dependent on DNA). (**B**) *Bap1, Ezh2* and *Suz12* expression by qRT-PCR from sorted granulocyte-macrophage progenitor (GMP; Lin⁻c-Kit⁺Sca1⁻CD34⁺Fcγ⁺). (**C**) Western blot analysis of Bap1 and Ezh2 in bone marrow cells from *Bap1* KO and control mice. (**D**) EZH2 transcription as assessed by qPCR in control and Bap1 KO cells. Cells were either transduced with empty vector or a BAP1 overexpression construct.

loss affected PRC2 function through a mechanism distinct from direct physical interaction with the PRC2 complex. We next investigated whether expression of PRC2 members was increased in *Bap1*-deficient cells. Real-time PCR analysis demonstrated that mRNA expression of *Ezh2* and *Suz12* levels were increased approximately two- to three-fold in *Bap1*-deficient GMPs and mature myeloid cells (**Figure 3.20B**). Consistent with the mRNA data, we observed a significant increase in EZH2 and SUZ12 protein expression in Bap1 KO bone marrow cells (**Figure 3.20C**). Moreover, re-expression of BAP1 in Bap1 KO bone marrow cells restored Ezh2 mRNA expression to normal levels (**Figure 3.20D**). These data suggest that Bap1 regulates *Ezh2/Suz12* transcription and that *Bap1* loss leads to overexpression of both PRC2 core components.

BAP1 loss leads to increased H4K20me1 and decreased dependency on SETD8

We next investigated the mechanism by which BAP1 regulates PRC2 complex expression and H3K27me3. We hypothesized that BAP1 loss might directly alter other chromatin marks, which would then lead to changes in chromatin state at key target loci, including *EZH2*. Histone mass spectrometry in c-Kit enriched cells revealed a marked decrease in H4K20me1 in *Bap1* KO cells (**Figure 3.21A**) compared to other measured histone marks (**Figure 3.21B**). Expression of BAP1, but not ASXL1 or BMI1, increased H4K20me1 at the *EZH2* locus (**Figure 3.22**). We therefore hypothesized that loss of the H4K20me1 mark may have an important role in BAP1-dependent gene expression. SETD8 is the only known methyltransferase that places H4K20me1 (*181*). Expression of SETD8 in *BAP1*-mutant mesothelioma cells (H226, H2452) increased apoptosis and reduced proliferation, whereas wild-type (MSTO-211H and Meso10) cells were unaffected (**Figure 3.23A,B**). SETD8 overexpression in mesothelioma cells decreased EZH2 mRNA and protein expression (**Figure 3.23C,D**). *BAP1* wild-type cell lines were
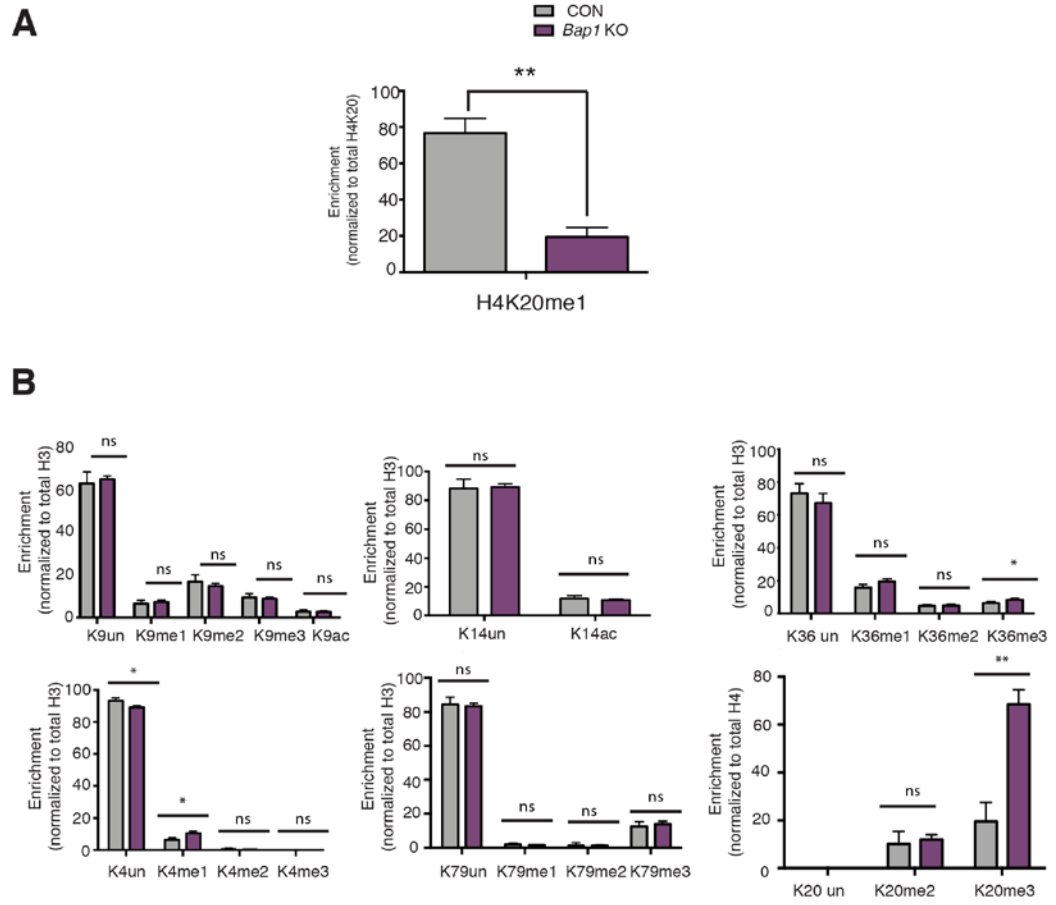
Figure 3.21. H4K20me1 is decreased in _Bap1_ KO mice. (**A**) Histone mass spectrometry in control and Bap1 KO animals c-kit enriched bone marrow cells, n=2 for H4K20me1 and (**B**) all other analyzed marks.
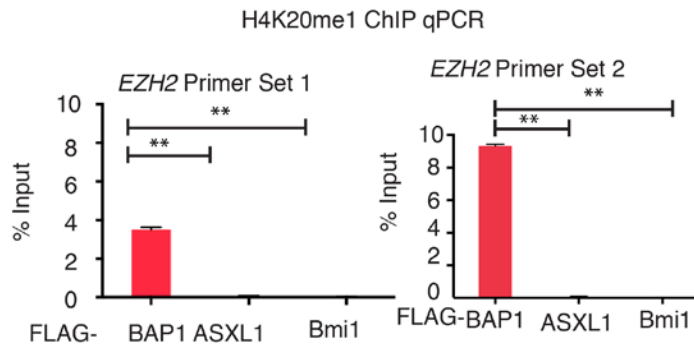
Figure 3.22. H4K20me1 is increased at the EZH2 locus with BAP1 overexpression.
H4K20me1 ChIP-qPCR experiments in 293T cells that overexpress FLAG-tagged BAP1,
ASXL1 and Bmi1.
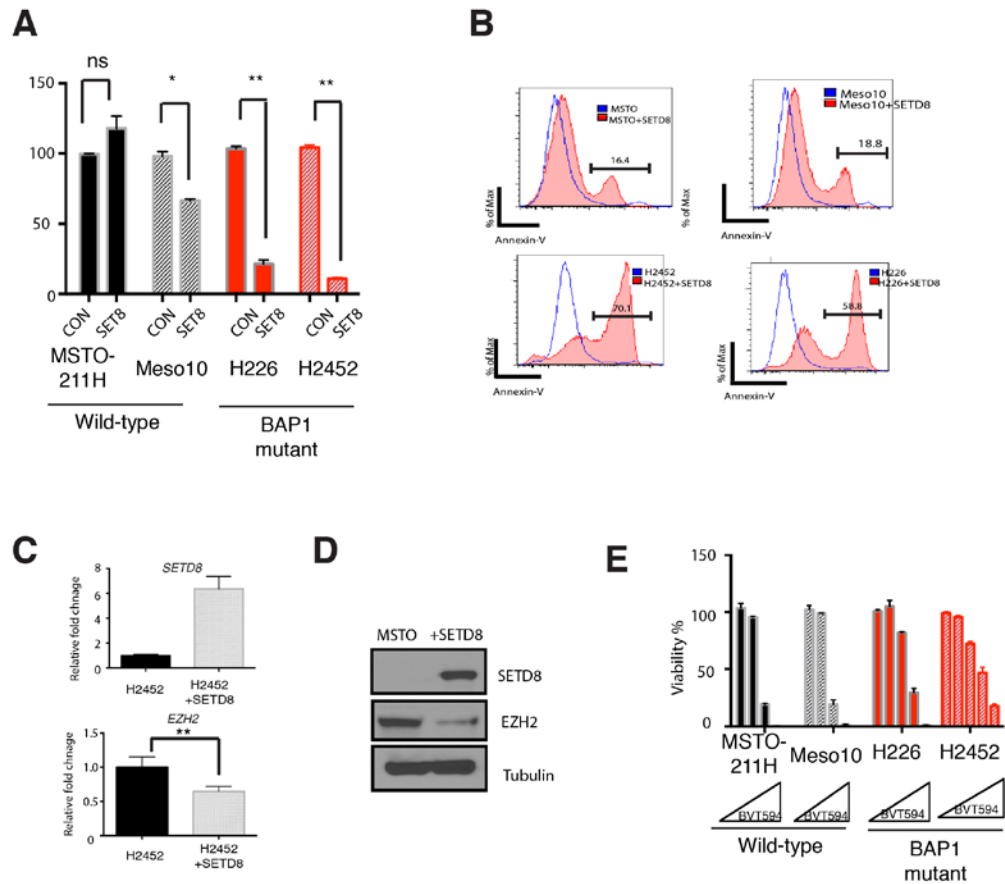
Figure 3.23. Overexpression and inhibition of SETD8 have differential effects on viability in BAP1 wild-type and mutant mesothelioma cell lines.
(**A**) Cell viability as assessed by Cell Titer Glo viability assay and (**B**) Annexin V assays for SETD8 overexpression experiments in *BAP1* wild-type (MSTO-211H, Meso10) and mutant cell lines H226, deletion; H2452 catalytic mutation). (**C**) Quantitative qPCR for *SETD8* and *EZH2* in BAP1 mutant cells with SETD8 overexpression. (**D**) Western blot analysis for SETD8 and EZH2 in a BAP1 wild-type cell line. (**E**) Cell Titer Glo assay in cells treated with DMSO or 5, 10, 20 μM BVT594.

more sensitive to a SETD8 inhibitor (*182*) (BVT594) than *BAP1*-mutant cell lines (**Figure 3.23E**).

L3MBTL2 is a deubiquitination target of BAP1

We hypothesized that BAP1 deubiquitinates a chromatin modulator that regulates H4K20me1. We analyzed Asxl1, Bap1, Hcf-1, and Ogt1 ChIP-Seq data from prior studies and identified a cluster of genes with significant Bap1 occupancy, but not Asxl1 binding (Cluster 1) (**Figure 3.24A**) (*47, 76*) were enriched for an E-box motif (**Figure 3.24B**). Previous studies have shown the atypical polycomb proteins L3MBTL1 and L3MBTL2 bind E-box motifs, and can bind and maintain H4K20me1 (*129, 130, 183, 184*). *L3mbtl1*-deficient mice have no overt phenotype (*185*), whereas *L3mbtl2*-deficient mice are embryonic lethal similar in timing to *Bap1* loss (*76, 129*). We therefore investigated whether *Bap1* loss led to alterations in L3mbtl2 expression. L3mbtl2 protein but not RNA expression was reduced in *Bap1* KO hematopoietic cells (**Figure 3.25A**) and in *BAP1*-mutant mesothelioma cells compared to *BAP1* wild-type mesothelioma cells (**Figure 3.25B**).

We assessed L3MBTL2 ubiquitination with a Myc-His ubiquitin overexpression system. We found that L3MBTL2 ubiquitination was reduced in cells overexpressing BAP1 (**Figure 3.25C**). MG132 proteasome inhibitor treatment increased L3MBTL2 stability in *BAP1*-mutant cells (**Figure 3.25D**) reaffirming that L3MBTL2 protein was regulated via the proteasome pathway. L3MBTL2 expression decreased EZH2 protein levels with and without BAP1 co-expression (**Figure 3.26A**) and expression of BAP1 or L3MBTL2 overexpression reduced EZH2 promoter activity in luciferase assays (**Figure 3.26B**). Conversely, shRNA mediated L3MBTL2 silencing increased expression of EZH2 (**Figure 3.26C**). We also observed enrichment for L3MBTL2 and BAP1 at the *EZH2* locus in cells
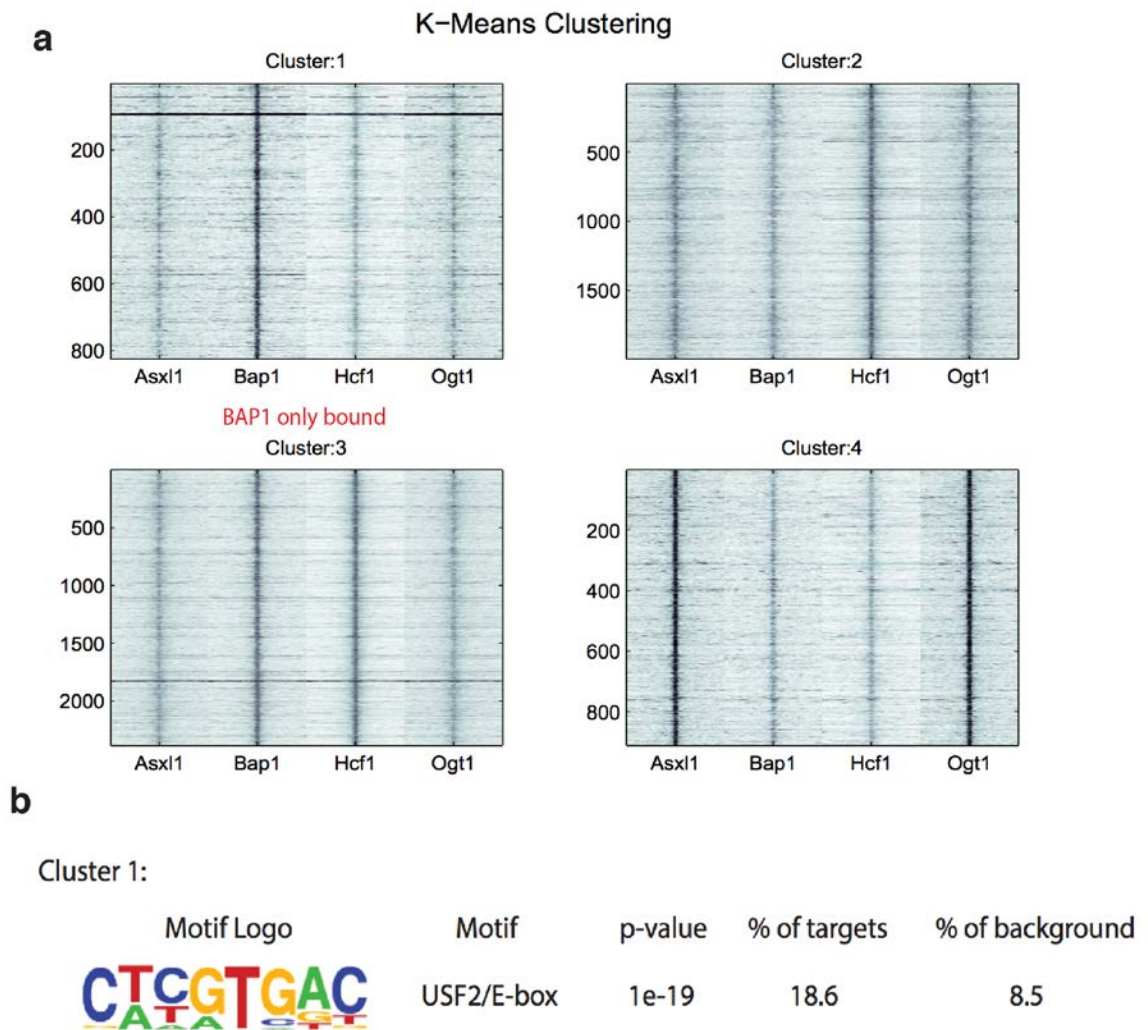
Figure 3.24. Analysis of BAP1, ASXL1, HCF-1, and OGT binding. (**A**) K-means clustering analyses for BAP1, ASXL1, HCF-1, and OGT ChIP-Seq. (**B**) Homer de novo motif analyses in BAP1-bound clusters.
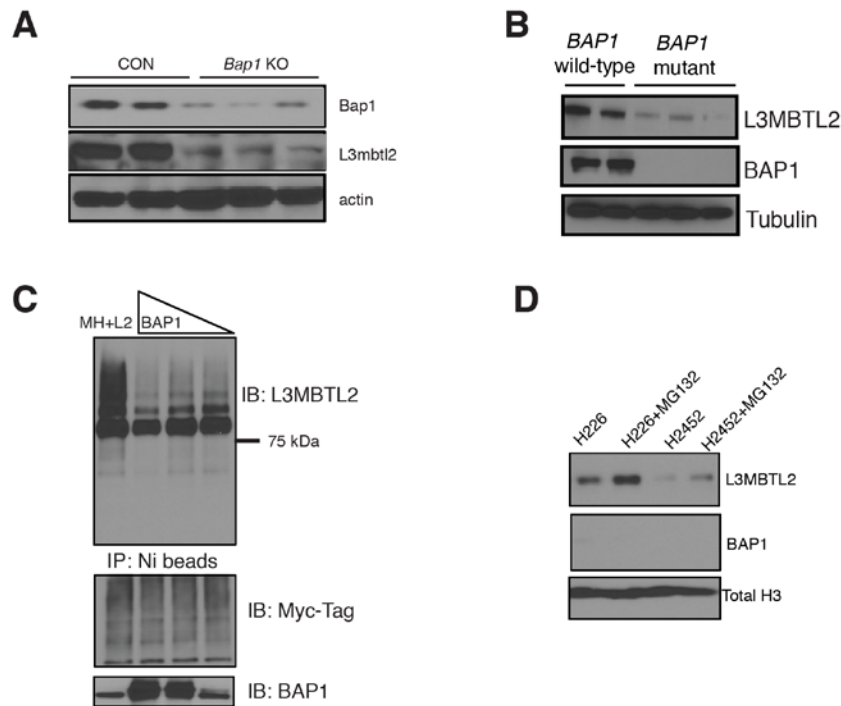
Figure 3.25. L3MBTL2 protein expression is downregulated with BAP1 loss. (A) Expression of Bap1 and L3mblt2 in control and Bap1 KO bone marrow cells **(B)** L3MBTL2 and BAP1 expression in *BAP1* wild-type (Met5a, JMN) and mutant mesothelioma cell lines (H226, H2452, H28) **(C)** 293T cells overexpressing Myc-His tagged ubiquitin and L3MBTL2 cDNA and varying levels of BAP1 (0, 5 μg, 2.5 μg, 1 μg). Co-immunoprecipitation experiments were conducted with Ni-beads and a series of stringent washes. **(D)** Western blot of H226 and H2452 cells treated with 25 uM MG132. Insoluble fractions were extracted using 2% SDS containing lysis buffer.
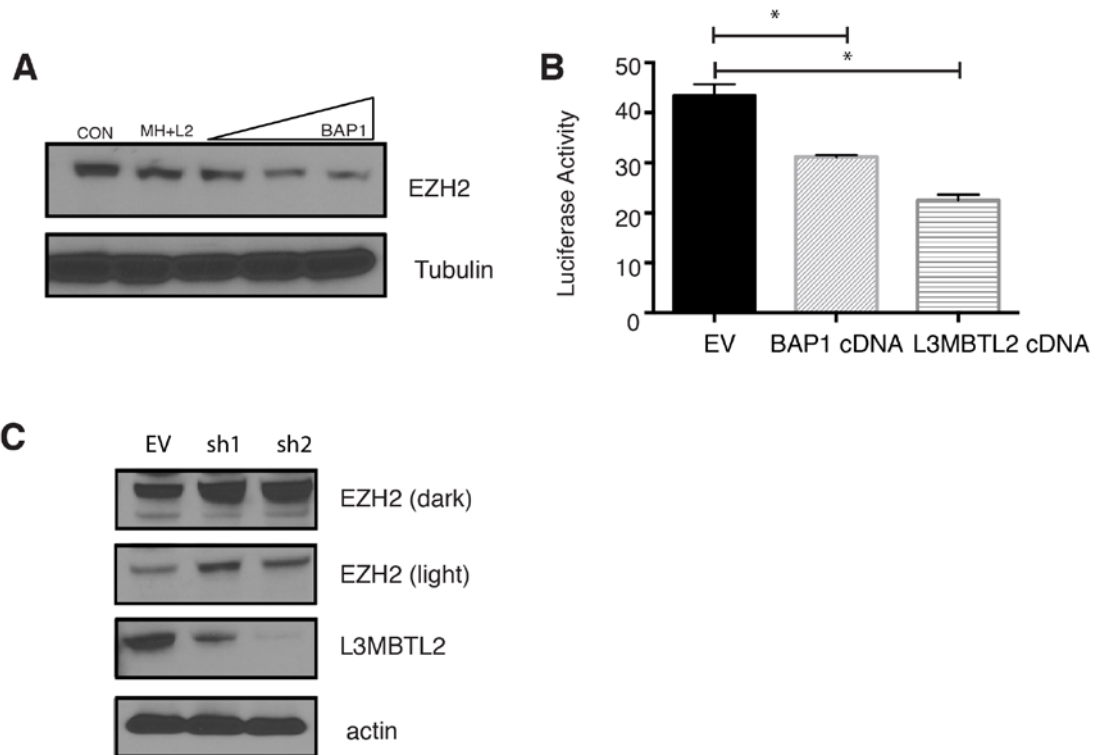
Figure 3.26. L3MBTL2 regulates EZH2 expression. (A) Expression of EZH2 in cell lines overexpressing L3MBTL2 from ubiquitination assay **(B)** EZH2 promoter activity assay with a construct containing 1.9 kB of the EZH2 promoter and a Renilla control vector transiently transfected into 293T cells with either empty vector, a BAP1 or L3MBTL2 expression vector. Firefly luciferase activity was normalized to Renilla activity in each of these conditions. **(C)** Two independent hairpins were used to knockdown L3MBTL2 protein in SET2 cells. Western blot analyses were conducted on L3MBTL2, EZH2, and actin including short and long exposures.

expressing L3MBTL2 and BAP1 (**Figure 3.27A,B)** in endogenous and FLAG-overexpression settings. We also show that L3MBTL2 and BAP1 physically interact with each other in immunoprecipitation experiments (**Figure 3.27C**). These data show that BAP1 and L3MBTL2 co-occupy specific loci including EZH2 and regulate their transcription. *BAP1* loss leads to reduced L3MBTL2 stability and increased *EZH2* transcriptional output (**Figure 3.28**).

BAP1-mutant cell lines are increasingly sensitive to EZH2 knockdown or inhibition

Analysis of TCGA data revealed that EZH2 mRNA expression was increased in mesothelioma compared to normal controls (**Figure 3.29**). We sought to assess whether EZH2 inhibition might inhibit the survival of *BAP1*-mutant mesothelioma cell lines. Two EZH2 short hairpins were identified that effectively reduce EZH2 RNA and protein levels. *EZH2* silencing in *BAP1*-mutant cell lines resulted in changes in cell morphology and apoptosis, whereas wild-type cell lines continued to proliferate (**Figure 3.30A,B**). We then implanted one wild-type and one mutant cell line with and without EZH2 knockdown into the flank of NOD-SCID mice. EZH2 silencing abrogated *in vivo* tumor formation of *BAP1*-mutant but not wild-type cell lines (**Figure 3.30C**). Overexpression of EZH2 in *BAP1* wild-type cell lines increased proliferation in xenograft studies (**Figure 3.31A**) and sensitivity to EZH2 inhibition *in vitro* (**Figure 3.31B,C**).

EZP011989 is the clinical tool compound from Epizyme that was recently published (*125*). *BAP1*-mutant cell lines were more sensitive to EZH2 inhibition (EPZ011989) *in vitro* both in 2D (**Figure 3.32A**) and 3D culture (**Figure 3.32B**). We next assessed the impact of EZH2 inhibition *in vivo*. We implanted two BAP1 wild-type (Meso10 and MSTO-211H) and mutant (H226 and H2452) cell lines into the flank of NOD-SCID mice. Tumors were given time to grow to about 60-80 mm^3 and mice were treated with 500
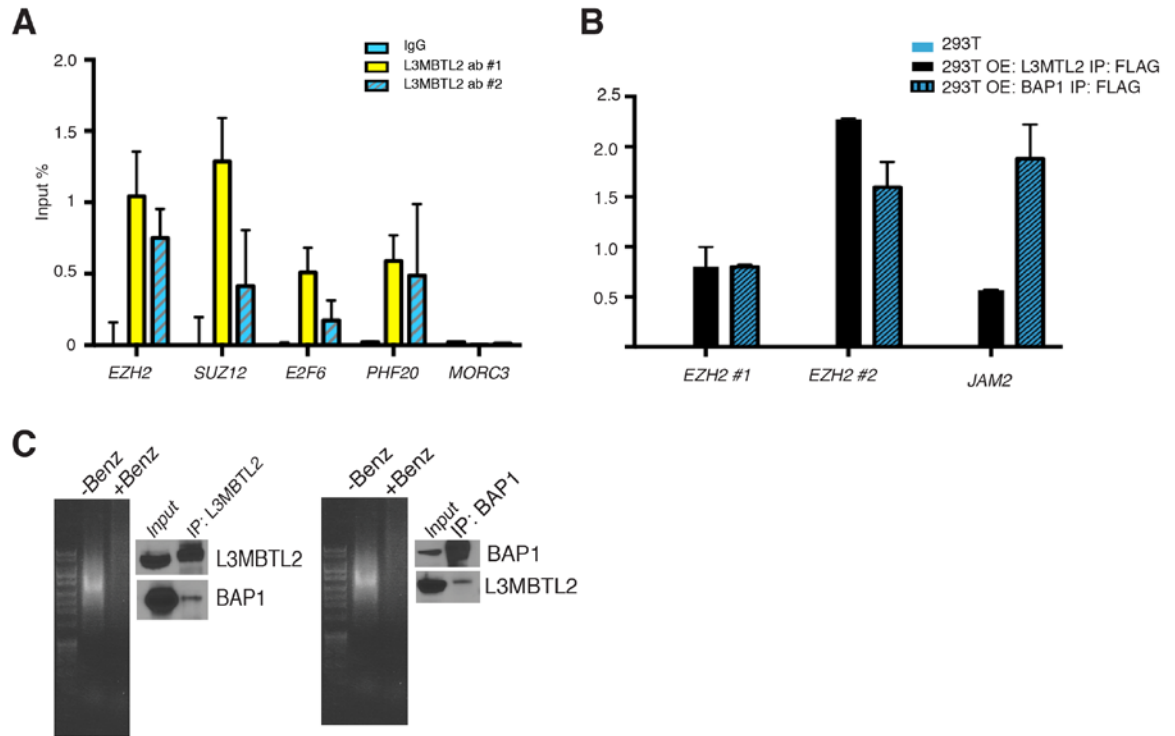
Figure 3.27. L3MBTL2 and BAP1 interact and regulate expression at the EZH2 promoter. (A) ChIP for *L3MBTL2* followed by qPCR at the *EZH2*, *SUZ12*, *E2F6* (positive control), *PHF20* (positive control), and *MORC3* (negative control) loci in 293T cells. **(B)** Anti-FLAG ChIP followed by qPCR at the *EZH2* locus in 293T cells overexpressing FLAG-L3MBTL2 or FLAG-BAP1. JAM2 is a positive control. Compared to 293T cells without FLAG overexpression **(C)** Western blot for L3MBTL2 and BAP1 following respective IPs in 293T cells. Agarose DNA gel included to show DNA digestion.
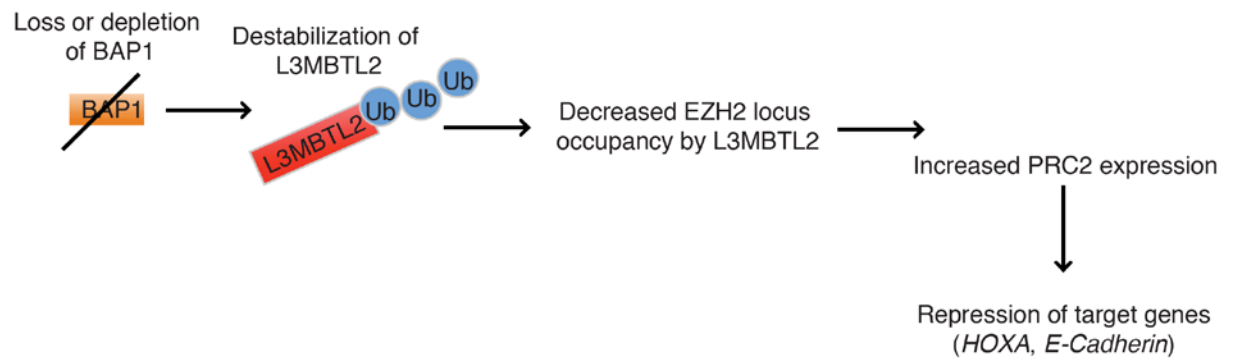
Figure 3.28 Schematic depicting BAP1 and L3MBTL2 dependent regulation of EZH2
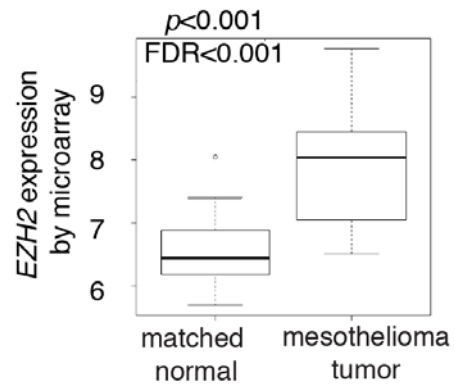
Figure 3.29. EZH2 expression is increased in mesothelioma tumor samples. Microarray data from TCGA normal and mesothelioma tumors.
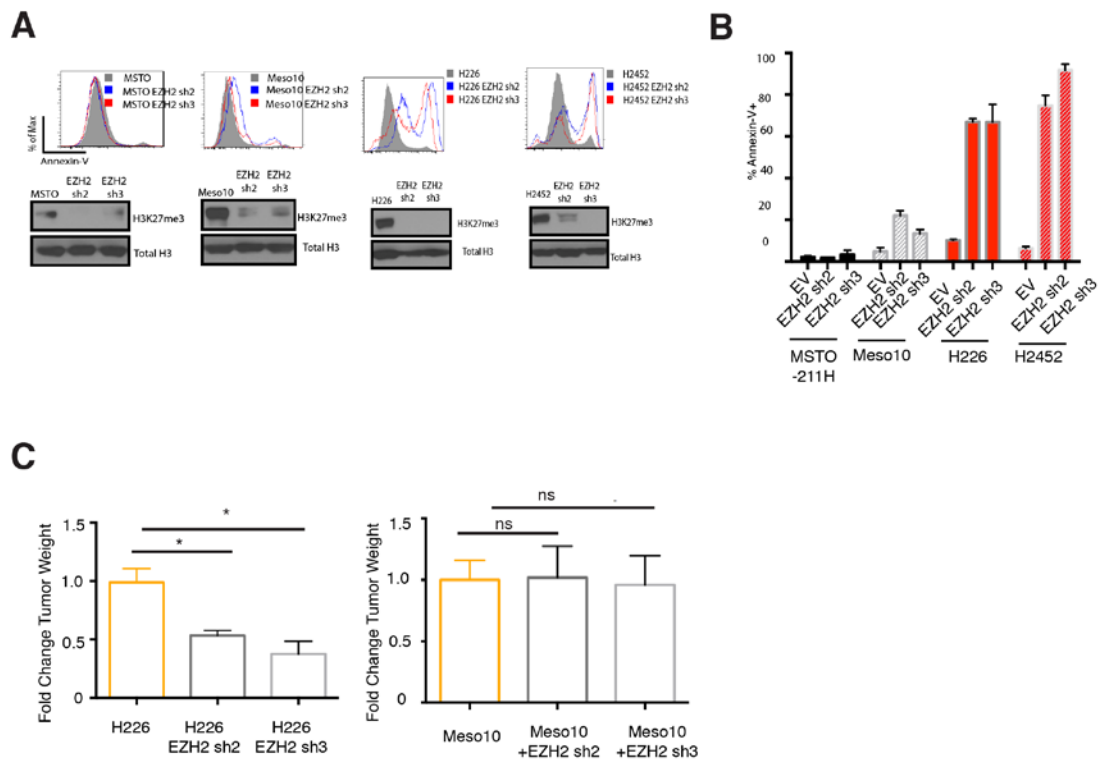
Figure 3.30. *BAP1*-**mutant mesothelioma cell lines and xenograft models are sensitive to EZH2 knockdown.** (**A**) Annexin V assays in *BAP1* wild-type and mutant cell lines expressing either empty vector or hairpins targeting EZH2. (**B**) Quantitation of Annexin V experiments in mesothelioma cell lines (**C**) Tumor size of Meso10 and H226 cell lines expressing EZH2 hairpins implanted into NOD-SCID mice, n=6/group.
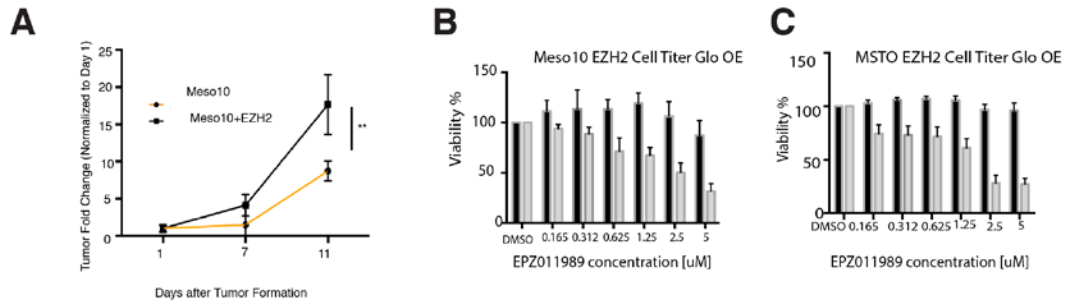
Figure 3.31. EZH2 overexpression leads increased proliferation. (**A**) Meso10 overexpressing cell lines increasingly proliferated when being injected into the flank of NOD-SCID mice. (**B-C**) EZH2 was overexpressed in MSTO-211H and Meso10 cell lines. The cell lines became increasingly sensitive to EZP011989 with EZH2 overexpression.
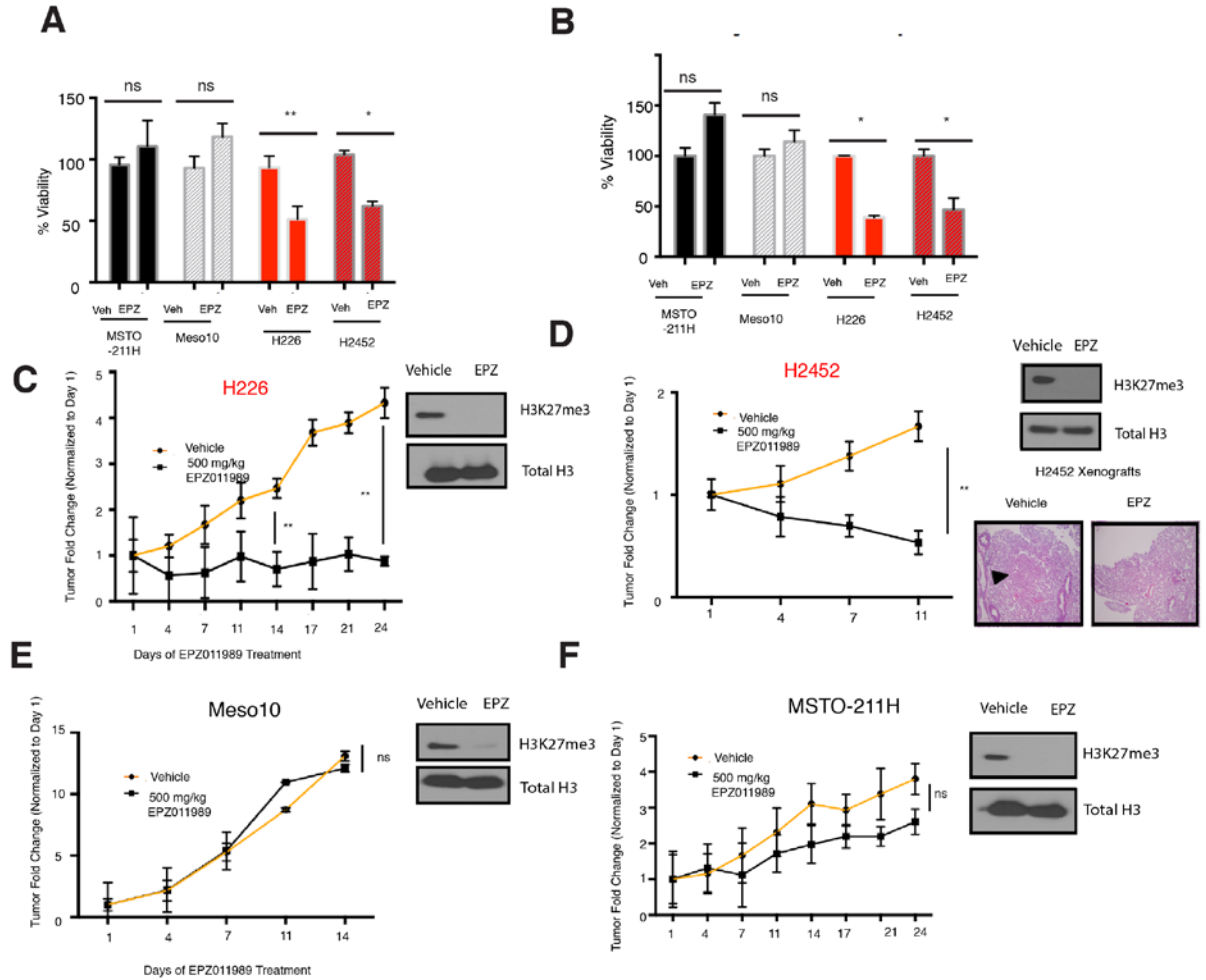
Figure 3.32. *BAP1*-**mutant mesothelioma cell lines and xenograft models are sensitive to EZH2 inhibition.** (**A**) 2D Cell Titer Glo viability assays after 2 week treatment with EPZ011989 at 1.25 μM. (**B**) 3D Cell Titer Glo viability assays after 3 weeks EPZ011989 treatment at 1.25 μM. (**C,D**) Tumor size formation from *BAP1* mutant (H226 and H2452) or (**E,F**) wild-type cells (MSTO-211H and Meso10) implanted into NOD-SCID mice and treated with either vehicle or 500 mg/kg BID EPZ011989. Tumors were measured 3X weekly. Target inhibition was assessed by histone western blots in extracted tumors (shown in respective figures). Lung pathology of H2452 cells with vehicle and EPZ011989 treatment. Arrow indicates bulk metastasized tumor.

134

mg/kg EPZ011989 two times a day. EZH2 inhibition significantly reduced *BAP1*-mutant tumor size compared to vehicle treated mice (**Figure 3.32C,D**), whereas wild-type tumors were less/not responsive to EZH2 inhibition (**Figure 3.32E,F**) despite similar effects on H3K27me3. One cell line, H2452, metastasized to the lung about two weeks post-implantation. Analysis of the lung indicated solid nodules that were not present in control lung tissue. After metastasis, we continued to treat mice with EPZ011989. EZH2 inhibition abrogated pulmonary metastasis in a *BAP1*-mutant mesothelioma cell line with metastatic potential (**Figure 3.32D**) consistent with a role for BAP1/EZH2 in metastasis (*61*). EZH2 inhibition reduced invasion and increased E-Cadherin expression *in vitro* (**Figure 3.33A-C**). These data indicate that EZH2 represents a potential therapeutic target in *BAP1*-mutant cancer cells.

H2AK119Ub is increased in *Bap1* KO mice

We next wanted to address whether H2AK119Ub levels were changing in the *Bap1* KO mice and whether changed in H2AK119Ub changed with loss or inhibition of Ezh2. We first assessed H2AK119Ub in c-Kit enriched bone marrow cells. Bone marrow cells with deleted *Bap1* had increased H2AK119Ub and decreased H3K27me3 (**Figure 3.34A**). These data suggest that the BAP1/ASXL1 complex is functional in *Bap1 KO* cells. However, this data is not consistent with results from the previously published whole body *Bap1* KO mouse. The differences could be due to antibody specificity; there are reports that the H2AK119Ub reagents are non-specific. We then wondered if deletion of EZH2 altered H2AK119Ub levels. Western blot assessment revealed that H2AK119Ub was unchanged in *Bap1* KO and *Bap1/Ezh2* KO mice, suggesting that PRC1 changes are not required for the *Ezh2* rescue (**Figure 3.34B**). Further, we saw no changes in H2AK119Ub when we treated mice with EPZ011989 (**Figure 3.34C**). We then completed ASXL1 ChIP-Sequencing in both control and *Bap1* KO cells. We assessed
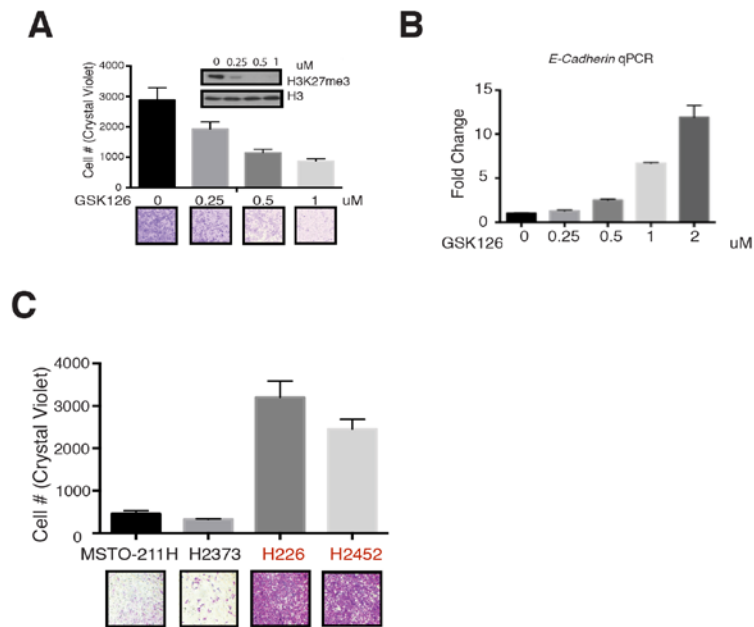
Figure 3.33. BAP1-mutant cells are increasingly invasive and the invasion can be inhibited by inhibition of EZH2. (**A**) *BAP1*-mutant cells became less invasive when treated with the EZH2 inhibitor GSK126. (**B**) E-Cadherin expression increased in the cell line H226 following treatment with GSK126. (**C**) Invasion of BAP1 wild-type and BAP1 mutant cell lines.
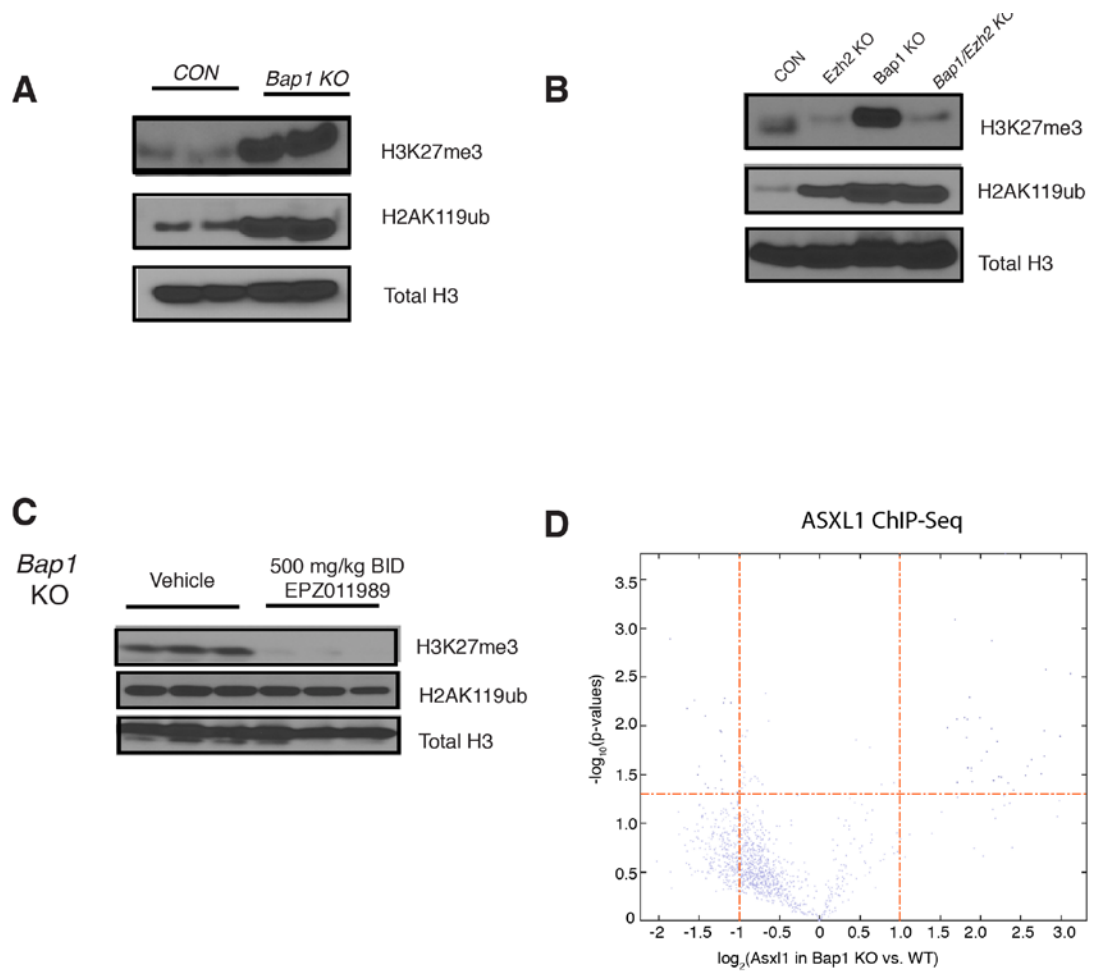
Figure 3.34. H2AK119Ub is increased in *Bap1* KO cells but is not altered with EZH2 knockdown or inhibition. (**A**) H2AK119ub levels as assessed by western blot in *Bap1 KO* mice (**B**) H2AK119ub in control and *Bap1*/*Ezh2* double KO(**C**) in *Bap1* KO mice treated with EZP011989 (**D**) ASXL1 ChIP-Seq in control and *Bap1 KO* mice.

ASXL1 binding globally via MACS peak calling. We found that ASXL1 binding was slightly altered, however, there was not a statistically significant difference in binding globally. Further, ASXL1 binding did not change binding at the EZH2 locus. Additional work will be required to understand whether the BAP1/ASXL1 and BAP1-independent functions work in concert to mediate gene expression.

Loss of BAP1 leads to a stem cell defect

For the experiments discussed previously in this chapter, we focused primarily on the GMP cells. Deletion of *Ezh2* rescues the progenitor *Bap1* KO myeloproliferation phenotype, however, it does not restore functionality to stem cells. The *Bap1* KO LSK (Lin-Sca-1+Kit+) population has a stem cell defect as evidenced by ineffective replating in methylocellulose assays (**Figure 3.35A**) and the inability to compete with wild-type stem cells in CD45.1/CD45.2 congenic marker competition assays (**Figure 3.35B**). Flow cytometric analysis of the hematopoietic stem cell compartment revealed that *Bap1* loss results in the expansion of the long term HSCs (CD150+) and multipotent progenitors (CD150-CD48-) and depletion of the short term HSCs (CD48+) (**Figure 3.35C**). We crossed *Tet2* KO mice with the *Bap1* KO mice to determine if we could reverse the stem cell disadvantage. However, the *Bap1/Tet2* double KO mice still had defective stem cells. Therefore, unlike with loss of *Asxl1*, the increased self-renewal of *Tet2* KO cells could not restore stem cell functionality (*77*). We are currently undertaking shRNA and CRISPR-Cas screening approaches to identify genes that may be critical in mediating this stem cell defect.

DISCUSSION

Previous studies have demonstrated BAP1 and ASXL1 form a complex that can remove H2AK119-Ub; however, genetic data implicate BAP1 and ASXL1 in distinct human
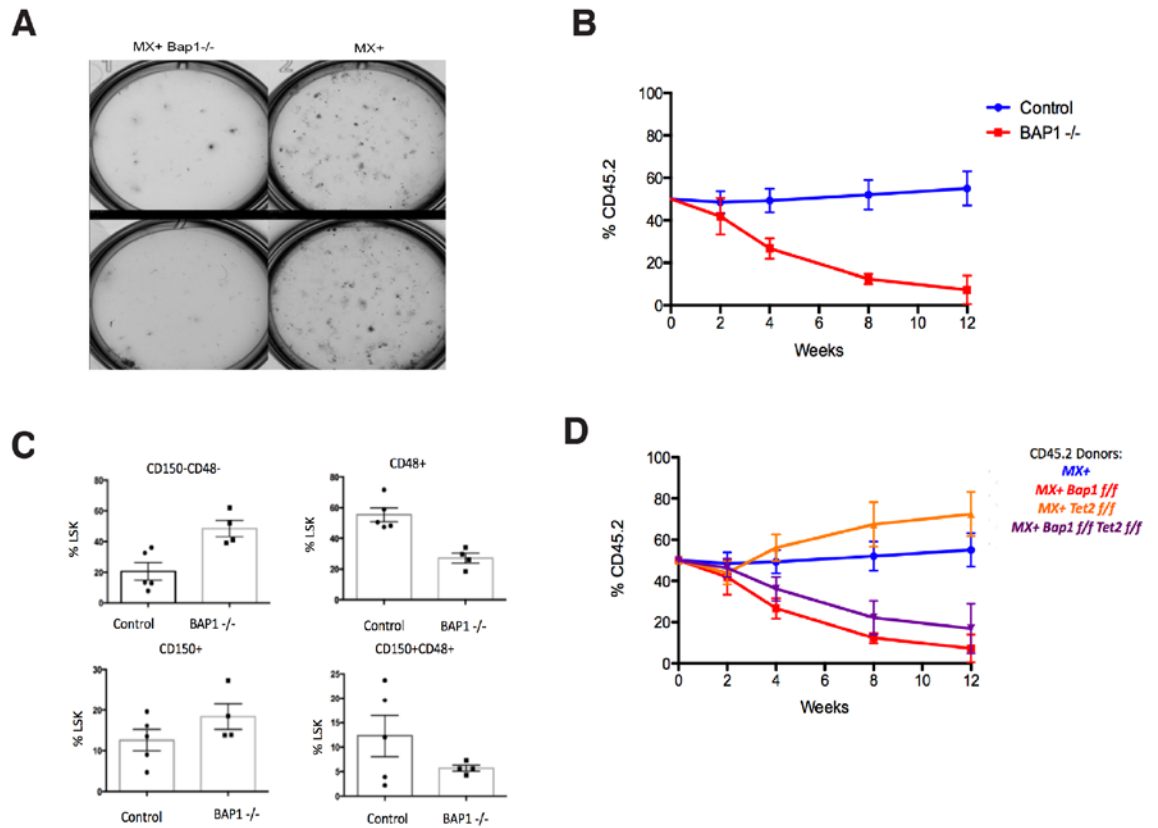
Figure 3.35. BAP1 loss results in a defect in hematopoietic stem cells. (**A**) Methylcellulose replating assays with control and **Bap1** KO cells (**B**) Competition assays with CD45.2 congenic mice (control or *Bap1* KO) mixed at a 1:1 ratio with CD45.1 marrow (**C**) Flow cytometric enumeration of the hematopoietic stem cell compartments (**D**) Competition assays with specified genotypes.

malignancies consistent with an ASXL1-independent role for BAP1 in gene regulation and in malignant transformation. ASXL1 loss results in a significant decrease in global H3K27me3 and increased expression of PRC2 targets (*169*), which is mediated through direct interaction between ASXL1 and PRC2. By contrast, we found that *Bap1* loss *in vitro* and *in vivo* results in increased H3K27me3 and transcriptional silencing of PRC2 targets. The increase in H3K27me3 observed with *Bap1* loss was due to increased expression of PRC2 members. Importantly, *Bap1*-deficient transformation *in vivo* was abrogated by *Ezh2* deletion, demonstrating the importance of EZH2 activity to *Bap1*-deficient proliferation and suggesting that *Bap1* has an important role in regulating PRC2 occupancy.

A recent study has shown that enzymatic activity of BAP1 is critical for its normal tumor suppressive activity (*54*) and mutations in the BAP1 deubiquitinase domain have been identified in primary tumors (*61, 63, 65*). However, the specific BAP1 substrates that contribute to BAP1-deficient transformation have not been identified. Previous biochemical studies have shown that HCF-1 and OGT interact with and are deubiquitinated by BAP1; however, these proteins have not been linked to BAP1-mutant malignant transformation (*51, 73, 75, 76*). Consistent with upstream regulation of PRC2 transcription by BAP1, we found that BAP1 binds and deubiquitinates L3MBTL2. L3MBTL2 has previously been identified as a novel member of a repressive PRC1 complex (*129*), and a recent study suggested posttranscriptional regulation of L3MBTL2 contributes to transcriptional regulation and chromatin compaction (*186*). In the setting of BAP1 loss or somatic mutations, we observed a marked reduction in L3MBTL2 expression and in H4K20me1. L3MBTL2 and BAP1 bind to the EZH2 locus; suggesting BAP1 and L3MBTL2 collaborate in a complex to reduce the expression of PRC2 complex members and of other downstream effectors. Our data suggest that L3MBTL2

140

may be a critical regulator of PRC2 transcription, as well as other targets, and that BAP1-mediated deubiquitination of L3MBTL2 has an important role in gene regulation *in vitro* and *in vivo*.

In uveal melanoma, BAP1 mutations are observed almost exclusively in patients with Class 2 transcriptional signatures, which have been shown to be associated with a high rate of distant metastasis and poor overall survival (*61*). Moreover, mesothelioma and renal cell carcinoma have a high rate of local and metastatic spread that leads to poor overall prognosis even in the setting of local disease control. The PRC2 complex is known to regulate genes linked to epithelial-mesenchymal transition (EMT), including E-Cadherin (*112, 187*). These data suggest that BAP1 loss leads to altered expression of genes which regulate invasion and metastasis, and that these transcriptional effects are due, at least in part, to alterations in PRC2 activity. We have shown that BAP1 invasion and metastasis can be inhibited by inhibition of EZH2 in mesothelioma cell lines. These data suggest a potential therapeutic intervention with patients with BAP1-mutant metastatic disease.

As genomic studies of human tumors continue to identify novel cancer genes, there is an increasing appreciation of the role of mutations in epigenetic regulation of transformation in a wide spectrum of malignancies. In some cases, these mutations lead to increased function of epigenetic enzymes, which has informed the development of mutant-specific therapies. For example, the identification of activating mutations in EZH2 in lymphoid malignancies has resulted in the development of small molecule EZH2 inhibitors. However, recent studies in SWI/SNF mutant rhabdoid tumors suggest that PRC2 inhibition may have therapeutic efficacy in tumors driven by mutations in epigenetic regulators outside of the PRC2 complex (*188, 189*). Our genetic studies demonstrated a

role for EZH2 enzymatic activity in BAP1-deficient transformation. Consistent with the genetic data, EZH2 inhibition attenuated the proliferation of BAP1-mutant mesothelioma cells, reduced their invasive potential, and restored the expression of E-cadherin consistent with reduced EMT. EZH2 inhibitors have recently entered clinical trials and our data provide a potential indication for a mutation-specific dependency in PRC2 that should be further explored in subsequent preclinical and clinical studies. Taken together, our data suggest that detailed studies of mutations in epigenetic regulation can be used to inform the development of therapies that reverse mutant-specific effects on epigenetic state and gene regulation in different malignant contexts.

REFERENCES

1. L. D. Wang, A. J. Wagers, Dynamic niches in the origination and differentiation of haematopoietic stem cells. *Nature reviews. Molecular cell biology* **12**, 643-655 (2011).

2. A. M. Vannucchi, T. L. Lasho, P. Guglielmelli, F. Biamonte, A. Pardanani, A. Pereira, C. Finke, J. Score, N. Gangat, C. Mannarelli, R. P. Ketterling, G. Rotunno, R. A. Knudson, M. C. Susini, R. R. Laborde, A. Spolverini, A. Pancrazzi, L. Pieri, R. Manfredini, E. Tagliafico, R. Zini, A. Jones, K. Zoi, A. Reiter, A. Duncombe, D. Pietra, E. Rumi, F. Cervantes, G. Barosi, M. Cazzola, N. C. Cross, A. Tefferi, Mutations and prognosis in primary myelofibrosis. *Leukemia* **27**, 1861-1869 (2013).

3. J. Xu, Z. Shao, D. Li, H. Xie, W. Kim, J. Huang, J. E. Taylor, L. Pinello, K. Glass, J. D. Jaffe, G. C. Yuan, S. H. Orkin, Developmental control of polycomb subunit composition by GATA factors mediates a switch to non-canonical functions. *Molecular cell* **57**, 304-316 (2015).

4. B. Xu, K. D. Konze, J. Jin, G. G. Wang, Targeting EZH2 and PRC2 dependence as novel anticancer therapy. *Experimental hematology*, (2015).

5. D. Pasini, P. A. Cloos, J. Walfridsson, L. Olsson, J. P. Bukowski, J. V. Johansen, M. Bak, N. Tommerup, J. Rappsilber, K. Helin, JARID2 regulates binding of the Polycomb repressive complex 2 to target genes in ES cells. *Nature* **464**, 306-310 (2010).

6. D. G. Gilliland, Hematologic malignancies. *Current opinion in hematology* **8**, 189-191 (2001).

7. A. H. Shih, O. Abdel-Wahab, J. P. Patel, R. L. Levine, The role of mutations in epigenetic regulators in myeloid malignancies. *Nature reviews. Cancer* **12**, 599-612 (2012).

8. R. D. Morin, N. A. Johnson, T. M. Severson, A. J. Mungall, J. An, R. Goya, J. E. Paul, M. Boyle, B. W. Woolcock, F. Kuchenbauer, D. Yap, R. K. Humphries, O. L. Griffith, S. Shah, H. Zhu, M. Kimbara, P. Shashkin, J. F. Charlot, M. Tcherpakov, R. Corbett, A. Tam, R. Varhol, D. Smailus, M. Moksa, Y. Zhao, A. Delaney, H. Qian, I. Birol, J. Schein, R. Moore, R. Holt, D. E. Horsman, J. M. Connors, S. Jones, S. Aparicio, M. Hirst, R. D. Gascoyne, M. A. Marra, Somatic mutations altering EZH2 (Tyr641) in follicular and diffuse large B-cell lymphomas of germinal-center origin. *Nature genetics* **42**, 181-185 (2010).

9. A. Murati, M. Brecqueville, R. Devillier, M. J. Mozziconacci, V. Gelsi-Boyer, D. Birnbaum, Myeloid malignancies: mutations, models and management. *BMC cancer* **12**, 304 (2012).

10. O. Abdel-Wahab, M. E. Figueroa, Interpreting new molecular genetics in myelodysplastic syndromes. *Hematology / the Education Program of the American Society of Hematology. American Society of Hematology. Education Program* **2012**, 56-64 (2012).

11. R. L. Levine, A. Pardanani, A. Tefferi, D. G. Gilliland, Role of JAK2 in the pathogenesis and therapy of myeloproliferative disorders. *Nature reviews. Cancer* **7**, 673-683 (2007).

12. O. Abdel-Wahab, R. L. Levine, Mutations in epigenetic modifiers in the pathogenesis and therapy of acute myeloid leukemia. *Blood* **121**, 3563-3572 (2013).

13. D. Noble, Conrad Waddington and the origin of epigenetics. *The Journal of experimental biology* **218**, 816-818 (2015).

14. P. Chi, C. D. Allis, G. G. Wang, Covalent histone modifications--miswritten, misinterpreted and mis-erased in human cancers. *Nature reviews. Cancer* **10**, 457-469 (2010).

15. B. D. Strahl, C. D. Allis, The language of covalent histone modifications. *Nature* **403**, 41-45 (2000).

16. M. A. Dawson, T. Kouzarides, Cancer epigenetics: from mechanism to therapy. *Cell* **150**, 12-27 (2012).

17. C. L. Fisher, J. Berger, F. Randazzo, H. W. Brock, A human homolog of Additional sex combs, ADDITIONAL SEX COMBS-LIKE 1, maps to chromosome 20q11. *Gene* **306**, 115-126 (2003).

18. M. Katoh, M. Katoh, Identification and characterization of ASXL2 gene in silico. *International journal of oncology* **23**, 845-850 (2003).

19. M. Katoh, M. Katoh, Identification and characterization of ASXL3 gene in silico. *International journal of oncology* **24**, 1617-1622 (2004).

20. M. Katoh, Functional and cancer genomics of ASXL family members. *British journal of cancer* **109**, 299-306 (2013).

21. L. Aravind, L. M. Iyer, The HARE-HTH and associated domains: novel modules in the coordination of epigenetic DNA and protein modifications. *Cell cycle* **11**, 119-131 (2012).

22. J. C. Scheuermann, A. G. de Ayala Alonso, K. Oktaba, N. Ly-Hartig, R. K. McGinty, S. Fraterman, M. Wilm, T. W. Muir, J. Muller, Histone H2A deubiquitinase activity of the Polycomb repressive complex PR-DUB. *Nature* **465**, 243-247 (2010).

23. L. Sanchez-Pulido, L. Kong, C. P. Ponting, A common ancestry for BAP1 and Uch37 regulators. *Bioinformatics* **28**, 1953-1956 (2012).

24. D. A. Sinclair, T. A. Milne, J. W. Hodgson, J. Shellard, C. A. Salinas, M. Kyba, F. Randazzo, H. W. Brock, The Additional sex combs gene of Drosophila encodes a chromatin protein that binds to shared and unique Polycomb group sites on polytene chromosomes. *Development* **125**, 1207-1216 (1998).

25. D. A. Sinclair, R. B. Campbell, F. Nicholls, E. Slade, H. W. Brock, Genetic analysis of the additional sex combs locus of Drosophila melanogaster. *Genetics* **130**, 817-825 (1992).

26. J. Simon, A. Chiang, W. Bender, Ten different Polycomb group genes are required for spatial control of the abdA and AbdB homeotic products. *Development* **114**, 493-505 (1992).

27. C. Davies, B. H. Yip, M. Fernandez-Mercado, P. S. Woll, X. Agirre, F. Prosper, S. E. Jacobsen, J. S. Wainscoat, A. Pellagatti, J. Boultwood, Silencing of ASXL1

impairs the granulomonocytic lineage potential of human CD34(+) progenitor cells. *British journal of haematology* **160**, 842-850 (2013).

28. J. Wang, Z. Li, Y. He, F. Pan, S. Chen, S. Rhodes, L. Nguyen, J. Yuan, L. Jiang, X. Yang, O. Weeks, Z. Liu, J. Zhou, H. Ni, C. L. Cai, M. Xu, F. C. Yang, Loss of Asxl1 leads to myelodysplastic syndrome-like disease in mice. *Blood* **123**, 541-553 (2014).

29. U. H. Park, S. K. Yoon, T. Park, E. J. Kim, S. J. Um, Additional sex comb-like (ASXL) proteins 1 and 2 play opposite roles in adipogenesis via reciprocal regulation of peroxisome proliferator-activated receptor {gamma}. *The Journal of biological chemistry* **286**, 1354-1363 (2011).

30. S. W. Lee, Y. S. Cho, J. M. Na, U. H. Park, M. Kang, E. J. Kim, S. J. Um, ASXL1 represses retinoic acid receptor-mediated transcription through associating with HP1 and LSD1. *The Journal of biological chemistry* **285**, 18-29 (2010).

31. Y. S. Cho, E. J. Kim, U. H. Park, H. S. Sin, S. J. Um, Additional sex comb-like 1 (ASXL1), in cooperation with SRC-1, acts as a ligand-dependent coactivator for retinoic acid receptor. *The Journal of biological chemistry* **281**, 17588-17598 (2006).

32. A. Hoischen, B. W. van Bon, B. Rodriguez-Santiago, C. Gilissen, L. E. Vissers, P. de Vries, I. Janssen, B. van Lier, R. Hastings, S. F. Smithson, R. Newbury-Ecob, S. Kjaergaard, J. Goodship, R. McGowan, D. Bartholdi, A. Rauch, M. Peippo, J. M. Cobben, D. Wieczorek, G. Gillessen-Kaesbach, J. A. Veltman, H. G. Brunner, B. B. de Vries, De novo nonsense mutations in ASXL1 cause Bohring-Opitz syndrome. *Nature genetics* **43**, 729-731 (2011).

33. O. Abdel-Wahab, A. Pardanani, J. Patel, M. Wadleigh, T. Lasho, A. Heguy, M. Beran, D. G. Gilliland, R. L. Levine, A. Tefferi, Concomitant analysis of EZH2 and ASXL1 mutations in myelofibrosis, chronic myelomonocytic leukemia and blast-phase myeloproliferative neoplasms. *Leukemia* **25**, 1200-1202 (2011).

34. V. Gelsi-Boyer, V. Trouplin, J. Adelaide, J. Bonansea, N. Cervera, N. Carbuccia, A. Lagarde, T. Prebet, M. Nezri, D. Sainty, S. Olschwang, L. Xerri, M. Chaffanet, M. J. Mozziconacci, N. Vey, D. Birnbaum, Mutations of polycomb-associated gene ASXL1 in myelodysplastic syndromes and chronic myelomonocytic leukaemia. *British journal of haematology* **145**, 788-800 (2009).

35. F. Thol, I. Friesen, F. Damm, H. Yun, E. M. Weissinger, J. Krauter, K. Wagner, A. Chaturvedi, A. Sharma, M. Wichmann, G. Gohring, C. Schumann, G. Bug, O. Ottmann, W. K. Hofmann, B. Schlegelberger, M. Heuser, A. Ganser, Prognostic significance of ASXL1 mutations in patients with myelodysplastic syndromes. *Journal of clinical oncology : official journal of the American Society of Clinical Oncology* **29**, 2499-2506 (2011).

36. R. Bejar, K. Stevenson, O. Abdel-Wahab, N. Galili, B. Nilsson, G. Garcia-Manero, H. Kantarjian, A. Raza, R. L. Levine, D. Neuberg, B. L. Ebert, Clinical effect of point mutations in myelodysplastic syndromes. *The New England journal of medicine* **364**, 2496-2506 (2011).

37. M. Meggendorfer, U. Bacher, T. Alpermann, C. Haferlach, W. Kern, C. Gambacorti-Passerini, T. Haferlach, S. Schnittger, SETBP1 mutations occur in 9% of MDS/MPN and in 4% of MPN cases and are strongly associated with

atypical CML, monosomy 7, isochromosome i(17)(q10), ASXL1 and CBL mutations. *Leukemia* **27**, 1852-1860 (2013).

38. O. Abdel-Wahab, T. Manshouri, J. Patel, K. Harris, J. Yao, C. Hedvat, A. Heguy, C. Bueso-Ramos, H. Kantarjian, R. L. Levine, S. Verstovsek, Genetic analysis of transforming events that convert chronic myeloproliferative neoplasms to leukemias. *Cancer research* **70**, 447-452 (2010).

39. K. H. Metzeler, H. Becker, K. Maharry, M. D. Radmacher, J. Kohlschmidt, K. Mrozek, D. Nicolet, S. P. Whitman, Y. Z. Wu, S. Schwind, B. L. Powell, T. H. Carter, M. Wetzler, J. O. Moore, J. E. Kolitz, M. R. Baer, A. J. Carroll, R. A. Larson, M. A. Caligiuri, G. Marcucci, C. D. Bloomfield, ASXL1 mutations identify a high-risk subgroup of older patients with primary cytogenetically normal AML within the ELN Favorable genetic category. *Blood* **118**, 6920-6929 (2011).

40. J. P. Patel, M. Gonen, M. E. Figueroa, H. Fernandez, Z. Sun, J. Racevskis, P. Van Vlierberghe, I. Dolgalev, S. Thomas, O. Aminova, K. Huberman, J. Cheng, A. Viale, N. D. Socci, A. Heguy, A. Cherry, G. Vance, R. R. Higgins, R. P. Ketterling, R. E. Gallagher, M. Litzow, M. R. van den Brink, H. M. Lazarus, J. M. Rowe, S. Luger, A. Ferrando, E. Paietta, M. S. Tallman, A. Melnick, O. Abdel-Wahab, R. L. Levine, Prognostic relevance of integrated genetic profiling in acute myeloid leukemia. *The New England journal of medicine* **366**, 1079-1089 (2012).

41. I. Yonal-Hindilerden, A. Daglar-Aday, B. Akadam-Teker, C. Yilmaz, M. Nalcaci, A. S. Yavuz, D. Sargin, Prognostic significance of ASXL1, JAK2V617F mutations and JAK2V617F allele burden in Philadelphia-negative myeloproliferative neoplasms. *Journal of blood medicine* **6**, 157-175 (2015).

42. D. Inoue, J. Kitaura, K. Togami, K. Nishimura, Y. Enomoto, T. Uchida, Y. Kagiyama, K. C. Kawabata, F. Nakahara, K. Izawa, T. Oki, A. Maehara, M. Isobe, A. Tsuchiya, Y. Harada, H. Harada, T. Ochiya, H. Aburatani, H. Kimura, F. Thol, M. Heuser, R. L. Levine, O. Abdel-Wahab, T. Kitamura, Myelodysplastic syndromes are induced by histone methylation-altering ASXL1 mutations. *The Journal of clinical investigation* **123**, 4627-4640 (2013).

43. A. Balasubramani, A. Larjo, J. A. Bassein, X. Chang, R. B. Hastie, S. M. Togher, H. Lahdesmaki, A. Rao, Cancer-associated ASXL1 mutations may act as gain-of-function mutations of the ASXL1-BAP1 complex. *Nature communications* **6**, 7307 (2015).

44. C. L. Fisher, F. Randazzo, R. K. Humphries, H. W. Brock, Characterization of Asxl1, a murine homolog of Additional sex combs, and analysis of the Asx-like gene family. *Gene* **369**, 109-118 (2006).

45. C. L. Fisher, N. Pineault, C. Brookes, C. D. Helgason, H. Ohta, C. Bodner, J. L. Hess, R. K. Humphries, H. W. Brock, Loss-of-function Additional sex combs like 1 mutations disrupt hematopoiesis but do not cause severe myelodysplasia or leukemia. *Blood* **115**, 38-46 (2010).

46. C. L. Fisher, I. Lee, S. Bloyer, S. Bozza, J. Chevalier, A. Dahl, C. Bodner, C. D. Helgason, J. L. Hess, R. K. Humphries, H. W. Brock, Additional sex combs-like 1 belongs to the enhancer of trithorax and polycomb group and genetically interacts with Cbx2 in mice. *Developmental biology* **337**, 9-15 (2010).

47. O. Abdel-Wahab, J. Gao, M. Adli, A. Dey, T. Trimarchi, Y. R. Chung, C. Kuscu, T. Hricik, D. Ndiaye-Lobry, L. M. Lafave, R. Koche, A. H. Shih, O. A. Guryanova, E.

Kim, S. Li, S. Pandey, J. Y. Shin, L. Telis, J. Liu, P. K. Bhatt, S. Monette, X. Zhao, C. E. Mason, C. Y. Park, B. E. Bernstein, I. Aifantis, R. L. Levine, Deletion of Asxl1 results in myelodysplasia and severe developmental defects in vivo. *The Journal of experimental medicine* **210**, 2641-2659 (2013).

48. M. A. Dawson, A. J. Bannister, B. Gottgens, S. D. Foster, T. Bartke, A. R. Green, T. Kouzarides, JAK2 phosphorylates histone H3Y41 and excludes HP1alpha from chromatin. *Nature* **461**, 819-822 (2009).

49. D. E. Jensen, M. Proctor, S. T. Marquis, H. P. Gardner, S. I. Ha, L. A. Chodosh, A. M. Ishov, N. Tommerup, H. Vissing, Y. Sekido, J. Minna, A. Borodovsky, D. C. Schultz, K. D. Wilkinson, G. G. Maul, N. Barlev, S. L. Berger, G. C. Prendergast, F. J. Rauscher, 3rd, BAP1: a novel ubiquitin hydrolase which binds to the BRCA1 RING finger and enhances BRCA1-mediated cell growth suppression. *Oncogene* **16**, 1097-1112 (1998).

50. M. Carbone, H. Yang, H. I. Pass, T. Krausz, J. R. Testa, G. Gaudino, BAP1 and cancer. *Nature reviews. Cancer* **13**, 153-159 (2013).

51. S. Misaghi, S. Ottosen, A. Izrael-Tomasevic, D. Arnott, M. Lamkanfi, J. Lee, J. Liu, K. O'Rourke, V. M. Dixit, A. C. Wilson, Association of C-terminal ubiquitin hydrolase BRCA1-associated protein 1 with cell cycle regulator host cell factor 1. *Molecular and cellular biology* **29**, 2181-2192 (2009).

52. K. H. Ventii, N. S. Devi, K. L. Friedrich, T. A. Chernova, M. Tighiouart, E. G. Van Meir, K. D. Wilkinson, BRCA1-associated protein-1 is a tumor suppressor that requires deubiquitinating activity and nuclear localization. *Cancer research* **68**, 6953-6962 (2008).

53. Y. Fang, D. Fu, X. Z. Shen, The potential role of ubiquitin c-terminal hydrolases in oncogenesis. *Biochimica et biophysica acta* **1806**, 1-6 (2010).

54. N. Mashtalir, S. Daou, H. Barbour, N. N. Sen, J. Gagnon, I. Hammond-Martel, H. H. Dar, M. Therrien, B. Affar el, Autodeubiquitination protects the tumor suppressor BAP1 from cytoplasmic sequestration mediated by the atypical ubiquitin ligase UBE2O. *Molecular cell* **54**, 392-406 (2014).

55. T. Wiesner, A. C. Obenauf, R. Murali, I. Fried, K. G. Griewank, P. Ulz, C. Windpassinger, W. Wackernagel, S. Loy, I. Wolf, A. Viale, A. E. Lash, M. Pirun, N. D. Socci, A. Rutten, G. Palmedo, D. Abramson, K. Offit, A. Ott, J. C. Becker, L. Cerroni, H. Kutzner, B. C. Bastian, M. R. Speicher, Germline mutations in BAP1 predispose to melanocytic tumors. *Nature genetics* **43**, 1018-1021 (2011).

56. C. N. Njauw, I. Kim, A. Piris, M. Gabree, M. Taylor, A. M. Lane, M. M. DeAngelis, E. Gragoudas, L. M. Duncan, H. Tsao, Germline BAP1 inactivation is preferentially associated with metastatic ocular melanoma and cutaneous-ocular melanoma families. *PloS one* **7**, e35295 (2012).

57. T. Wiesner, I. Fried, P. Ulz, E. Stacher, H. Popper, R. Murali, H. Kutzner, S. Lax, F. Smolle-Juttner, J. B. Geigl, M. R. Speicher, Toward an improved definition of the tumor spectrum associated with BAP1 germline mutations. *Journal of clinical oncology : official journal of the American Society of Clinical Oncology* **30**, e337-340 (2012).

58. J. R. Testa, M. Cheung, J. Pei, J. E. Below, Y. Tan, E. Sementino, N. J. Cox, A. U. Dogan, H. I. Pass, S. Trusa, M. Hesdorffer, M. Nasu, A. Powers, Z. Rivera, S. Comertpay, M. Tanji, G. Gaudino, H. Yang, M. Carbone, Germline BAP1

mutations predispose to malignant mesothelioma. *Nature genetics* **43**, 1022-1025 (2011).

59. M. H. Abdel-Rahman, R. Pilarski, C. M. Cebulla, J. B. Massengill, B. N. Christopher, G. Boru, P. Hovland, F. H. Davidorf, Germline BAP1 mutation predisposes to uveal melanoma, lung adenocarcinoma, meningioma, and other cancers. *Journal of medical genetics* **48**, 856-859 (2011).

60. M. Carbone, L. K. Ferris, F. Baumann, A. Napolitano, C. A. Lum, E. G. Flores, G. Gaudino, A. Powers, P. Bryant-Greenwood, T. Krausz, E. Hyjek, R. Tate, J. Friedberg, T. Weigel, H. I. Pass, H. Yang, BAP1 cancer syndrome: malignant mesothelioma, uveal and cutaneous melanoma, and MBAITs. *Journal of translational medicine* **10**, 179 (2012).

61. J. W. Harbour, M. D. Onken, E. D. Roberson, S. Duan, L. Cao, L. A. Worley, M. L. Council, K. A. Matatall, C. Helms, A. M. Bowcock, Frequent mutation of BAP1 in metastasizing uveal melanomas. *Science* **330**, 1410-1413 (2010).

62. K. A. Matatall, O. A. Agapova, M. D. Onken, L. A. Worley, A. M. Bowcock, J. W. Harbour, BAP1 deficiency causes loss of melanocytic cell identity in uveal melanoma. *BMC cancer* **13**, 371 (2013).

63. M. Bott, M. Brevet, B. S. Taylor, S. Shimizu, T. Ito, L. Wang, J. Creaney, R. A. Lake, M. F. Zakowski, B. Reva, C. Sander, R. Delsite, S. Powell, Q. Zhou, R. Shen, A. Olshen, V. Rusch, M. Ladanyi, The nuclear deubiquitinase BAP1 is commonly inactivated by somatic mutations and 3p21.1 losses in malignant pleural mesothelioma. *Nature genetics* **43**, 668-672 (2011).

64. Y. Yoshikawa, A. Sato, T. Tsujimura, M. Emi, T. Morinaga, K. Fukuoka, S. Yamada, A. Murakami, N. Kondo, S. Matsumoto, Y. Okumura, F. Tanaka, S. Hasegawa, T. Nakano, T. Hashimoto-Tamaoki, Frequent inactivation of the BAP1 gene in epithelioid-type malignant mesothelioma. *Cancer science* **103**, 868-874 (2012).

65. S. Pena-Llopis, S. Vega-Rubin-de-Celis, A. Liao, N. Leng, A. Pavia-Jimenez, S. Wang, T. Yamasaki, L. Zhrebker, S. Sivanand, P. Spence, L. Kinch, T. Hambuch, S. Jain, Y. Lotan, V. Margulis, A. I. Sagalowsky, P. B. Summerour, W. Kabbani, S. W. Wong, N. Grishin, M. Laurent, X. J. Xie, C. D. Haudenschild, M. T. Ross, D. R. Bentley, P. Kapur, J. Brugarolas, BAP1 loss defines a new class of renal cell carcinoma. *Nature genetics* **44**, 751-759 (2012).

66. A. A. Hakimi, I. Ostrovnaya, B. Reva, N. Schultz, Y. B. Chen, M. Gonen, H. Liu, S. Takeda, M. H. Voss, S. K. Tickoo, V. E. Reuter, P. Russo, E. H. Cheng, C. Sander, R. J. Motzer, J. J. Hsieh, R. C. C. C. G. A. R. N. i. cc, Adverse outcomes in clear cell renal cell carcinoma with mutations of 3p21 epigenetic regulators BAP1 and SETD2: a report by MSKCC and the KIRC TCGA research network. *Clinical cancer research : an official journal of the American Association for Cancer Research* **19**, 3259-3267 (2013).

67. Y. Jiao, T. M. Pawlik, R. A. Anders, F. M. Selaru, M. M. Streppel, D. J. Lucas, N. Niknafs, V. B. Guthrie, A. Maitra, P. Argani, G. J. Offerhaus, J. C. Roa, L. R. Roberts, G. J. Gores, I. Popescu, S. T. Alexandrescu, S. Dima, M. Fassan, M. Simbolo, A. Mafficini, P. Capelli, R. T. Lawlor, A. Ruzzenente, A. Guglielmi, G. Tortora, F. de Braud, A. Scarpa, W. Jarnagin, D. Klimstra, R. Karchin, V. E. Velculescu, R. H. Hruban, B. Vogelstein, K. W. Kinzler, N. Papadopoulos, L. D.

Wood, Exome sequencing identifies frequent inactivating mutations in BAP1, ARID1A and PBRM1 in intrahepatic cholangiocarcinomas. *Nature genetics* **45**, 1470-1473 (2013).

68.   J. J. Sacco, J. Kenyani, Z. Butt, R. Carter, H. Y. Chew, L. P. Cheeseman, S. Darling, M. Denny, S. Urbe, M. J. Clague, J. M. Coulson, Loss of the deubiquitylase BAP1 alters class I histone deacetylase expression and sensitivity of mesothelioma cells to HDAC inhibitors. *Oncotarget* **6**, 13757-13771 (2015).

69.   H. Nishikawa, W. Wu, A. Koike, R. Kojima, H. Gomi, M. Fukuda, T. Ohta, BRCA1-associated protein 1 interferes with BRCA1/BARD1 RING heterodimer activity. *Cancer research* **69**, 111-119 (2009).

70.   R. A. Greenberg, B. Sobhian, S. Pathania, S. B. Cantor, Y. Nakatani, D. M. Livingston, Multifactorial contributions to an acute DNA damage response by BRCA1/BARD1-containing complexes. *Genes & development* **20**, 34-46 (2006).

71.   H. Yu, H. Pak, I. Hammond-Martel, M. Ghram, A. Rodrigue, S. Daou, H. Barbour, L. Corbeil, J. Hebert, E. Drobetsky, J. Y. Masson, J. M. Di Noia, B. Affar el, Tumor suppressor and deubiquitinase BAP1 promotes DNA double-strand break repair. *Proceedings of the National Academy of Sciences of the United States of America* **111**, 285-290 (2014).

72.   S. Hakiri, H. Osada, F. Ishiguro, H. Murakami, Y. Murakami-Tonami, K. Yokoi, Y. Sekido, Functional differences between wild-type and mutant-type BAP1 tumor suppressor against malignant mesothelioma cells. *Cancer science*, (2015).

73.   Y. J. Machida, Y. Machida, A. A. Vashisht, J. A. Wohlschlegel, A. Dutta, The deubiquitinating enzyme BAP1 regulates cell growth via interaction with HCF-1. *The Journal of biological chemistry* **284**, 34179-34188 (2009).

74.   S. Tyagi, A. L. Chabes, J. Wysocka, W. Herr, E2F activation of S phase promoters via association with HCF-1 and the MLL family of histone H3K4 methyltransferases. *Molecular cell* **27**, 107-119 (2007).

75.   H. Yu, N. Mashtalir, S. Daou, I. Hammond-Martel, J. Ross, G. Sui, G. W. Hart, F. J. Rauscher, 3rd, E. Drobetsky, E. Milot, Y. Shi, B. Affar el, The ubiquitin carboxyl hydrolase BAP1 forms a ternary complex with YY1 and HCF-1 and is a critical regulator of gene expression. *Molecular and cellular biology* **30**, 5071-5085 (2010).

76.   A. Dey, D. Seshasayee, R. Noubade, D. M. French, J. Liu, M. S. Chaurushiya, D. S. Kirkpatrick, V. C. Pham, J. R. Lill, C. E. Bakalarski, J. Wu, L. Phu, P. Katavolos, L. M. LaFave, O. Abdel-Wahab, Z. Modrusan, S. Seshagiri, K. Dong, Z. Lin, M. Balazs, R. Suriben, K. Newton, S. Hymowitz, G. Garcia-Manero, F. Martin, R. L. Levine, V. M. Dixit, Loss of the tumor suppressor BAP1 causes myeloid transformation. *Science* **337**, 1541-1546 (2012).

77.   O. Abdel-Wahab, A. Dey, The ASXL-BAP1 axis: new factors in myelopoiesis, cancer and epigenetics. *Leukemia* **27**, 10-15 (2013).

78.   J. A. Hanover, M. W. Krause, D. C. Love, Bittersweet memories: linking metabolism to epigenetics through O-GlcNAcylation. *Nature reviews. Molecular cell biology* **13**, 312-321 (2012).

79.   M. E. Sowa, E. J. Bennett, S. P. Gygi, J. W. Harper, Defining the human deubiquitinating enzyme interaction landscape. *Cell* **138**, 389-403 (2009).

80.   J. Xu, Y. Kadariya, M. Cheung, J. Pei, J. Talarchek, E. Sementino, Y. Tan, C. W. Menges, K. Q. Cai, S. Litwin, H. Peng, J. Karar, F. J. Rauscher, J. R. Testa, Germline Mutation of Bap1 Accelerates Development of Asbestos-Induced Malignant Mesothelioma. *Cancer research*, (2014).

81.   W. K. Tse, B. Eisenhaber, S. H. Ho, Q. Ng, F. Eisenhaber, Y. J. Jiang, Genome-wide loss-of-function analysis of deubiquitylating enzymes for zebrafish development. *BMC genomics* **10**, 637 (2009).

82.   J. Ng, C. M. Hart, K. Morgan, J. A. Simon, A Drosophila ESC-E(Z) protein complex is distinct from other polycomb group complexes and contains covalently modified ESC. *Molecular and cellular biology* **20**, 3069-3078 (2000).

83.   R. Cao, L. Wang, H. Wang, L. Xia, H. Erdjument-Bromage, P. Tempst, R. S. Jones, Y. Zhang, Role of histone H3 lysine 27 methylation in Polycomb-group silencing. *Science* **298**, 1039-1043 (2002).

84.   K. Lund, P. D. Adams, M. Copland, EZH2 in normal and malignant hematopoiesis. *Leukemia* **28**, 44-49 (2014).

85.   H. Kim, K. Kang, J. Kim, AEBP2 as a potential targeting protein for Polycomb Repression Complex PRC2. *Nucleic acids research* **37**, 2940-2950 (2009).

86.   J. C. Peng, A. Valouev, T. Swigut, J. Zhang, Y. Zhao, A. Sidow, J. Wysocka, Jarid2/Jumonji coordinates control of PRC2 enzymatic activity and target gene occupancy in pluripotent cells. *Cell* **139**, 1290-1302 (2009).

87.   S. A. Jacobs, J. M. Harp, S. Devarakonda, Y. Kim, F. Rastinejad, S. Khorasanizadeh, The active site of the SET domain is constructed on a knot. *Nature structural biology* **9**, 833-838 (2002).

88.   T. L. Cha, B. P. Zhou, W. Xia, Y. Wu, C. C. Yang, C. T. Chen, B. Ping, A. P. Otte, M. C. Hung, Akt-mediated phosphorylation of EZH2 suppresses methylation of lysine 27 in histone H3. *Science* **310**, 306-310 (2005).

89.   S. Chen, L. R. Bohrer, A. N. Rai, Y. Pan, L. Gan, X. Zhou, A. Bagchi, J. A. Simon, H. Huang, Cyclin-dependent kinases regulate epigenetic gene silencing through phosphorylation of EZH2. *Nature cell biology* **12**, 1108-1114 (2010).

90.   T. Swigut, J. Wysocka, H3K27 demethylases, at long last. *Cell* **131**, 29-32 (2007).

91.   G. Deb, A. K. Singh, S. Gupta, EZH2: not EZHY (easy) to deal. *Molecular cancer research : MCR* **12**, 639-653 (2014).

92.   X. Shen, Y. Liu, Y. J. Hsu, Y. Fujiwara, J. Kim, X. Mao, G. C. Yuan, S. H. Orkin, EZH1 mediates methylation on histone H3 lysine 27 and complements EZH2 in maintaining stem cell identity and executing pluripotency. *Molecular cell* **32**, 491-502 (2008).

93.   E. Ezhkova, W. H. Lien, N. Stokes, H. A. Pasolli, J. M. Silva, E. Fuchs, EZH1 and EZH2 cogovern histone H3K27 trimethylation and are essential for hair follicle homeostasis and wound repair. *Genes & development* **25**, 485-498 (2011).

94.   L. Stojic, Z. Jasencakova, C. Prezioso, A. Stutzer, B. Bodega, D. Pasini, R. Klingberg, C. Mozzetta, R. Margueron, P. L. Puri, D. Schwarzer, K. Helin, W.

Fischle, V. Orlando, Chromatin regulated interchange between polycomb repressive complex 2 (PRC2)-Ezh2 and PRC2-Ezh1 complexes controls myogenin activation in skeletal muscle cells. *Epigenetics & chromatin* **4**, 16 (2011).

95. B. Henriquez, F. J. Bustos, R. Aguilar, A. Becerra, F. Simon, M. Montecino, B. van Zundert, Ezh1 and Ezh2 differentially regulate PSD-95 gene transcription in developing hippocampal neurons. *Molecular and cellular neurosciences* **57**, 130-143 (2013).

96. R. Margueron, G. Li, K. Sarma, A. Blais, J. Zavadil, C. L. Woodcock, B. D. Dynlacht, D. Reinberg, Ezh1 and Ezh2 maintain repressive chromatin through different mechanisms. *Molecular cell* **32**, 503-518 (2008).

97. I. Hidalgo, A. Herrera-Merchan, J. M. Ligos, L. Carramolino, J. Nunez, F. Martinez, O. Dominguez, M. Torres, S. Gonzalez, Ezh1 is required for hematopoietic stem cell maintenance and prevents senescence-like cell cycle arrest. *Cell stem cell* **11**, 649-662 (2012).

98. M. Mochizuki-Kashio, Y. Mishima, S. Miyagi, M. Negishi, A. Saraya, T. Konuma, J. Shinga, H. Koseki, A. Iwama, Dependency on the polycomb gene Ezh2 distinguishes fetal from adult hematopoietic stem cells. *Blood* **118**, 6553-6561 (2011).

99. T. Neff, A. U. Sinha, M. J. Kluk, N. Zhu, M. H. Khattab, L. Stein, H. Xie, S. H. Orkin, S. A. Armstrong, Polycomb repressive complex 2 is required for MLL-AF9 leukemia. *Proceedings of the National Academy of Sciences of the United States of America* **109**, 5028-5033 (2012).

100. H. Xie, J. Xu, J. H. Hsu, M. Nguyen, Y. Fujiwara, C. Peng, S. H. Orkin, Polycomb repressive complex 2 regulates normal hematopoietic stem cell function in a developmental-stage-specific manner. *Cell stem cell* **14**, 68-80 (2014).

101. C. Bodor, V. Grossmann, N. Popov, J. Okosun, C. O'Riain, K. Tan, J. Marzec, S. Araf, J. Wang, A. M. Lee, A. Clear, S. Montoto, J. Matthews, S. Iqbal, H. Rajnai, A. Rosenwald, G. Ott, E. Campo, L. M. Rimsza, E. B. Smeland, W. C. Chan, R. M. Braziel, L. M. Staudt, G. Wright, T. A. Lister, O. Elemento, R. Hills, J. G. Gribben, C. Chelala, A. Matolcsy, A. Kohlmann, T. Haferlach, R. D. Gascoyne, J. Fitzgibbon, EZH2 mutations are frequent and represent an early event in follicular lymphoma. *Blood* **122**, 3165-3168 (2013).

102. M. T. McCabe, A. P. Graves, G. Ganji, E. Diaz, W. S. Halsey, Y. Jiang, K. N. Smitheman, H. M. Ott, M. B. Pappalardi, K. E. Allen, S. B. Chen, A. Della Pietra, 3rd, E. Dul, A. M. Hughes, S. A. Gilbert, S. H. Thrall, P. J. Tummino, R. G. Kruger, M. Brandt, B. Schwartz, C. L. Creasy, Mutation of A677 in histone methyltransferase EZH2 in human B-cell lymphoma promotes hypertrimethylation of histone H3 on lysine 27 (H3K27). *Proceedings of the National Academy of Sciences of the United States of America* **109**, 2989-2994 (2012).

103. D. Zingg, J. Debbache, S. M. Schaefer, E. Tuncer, S. C. Frommel, P. Cheng, N. Arenas-Ramirez, J. Haeusel, Y. Zhang, M. Bonalli, M. T. McCabe, C. L. Creasy, M. P. Levesque, O. Boyman, R. Santoro, O. Shakhova, R. Dummer, L. Sommer, The epigenetic modifier EZH2 controls melanoma growth and metastasis through

silencing of distinct tumour suppressors. *Nature communications* **6**, 6051 (2015).

104. K. Xu, Z. J. Wu, A. C. Groner, H. H. He, C. Cai, R. T. Lis, X. Wu, E. C. Stack, M. Loda, T. Liu, H. Xu, L. Cato, J. E. Thornton, R. I. Gregory, C. Morrissey, R. L. Vessella, R. Montironi, C. Magi-Galluzzi, P. W. Kantoff, S. P. Balk, X. S. Liu, M. Brown, EZH2 oncogenic activity in castration-resistant prostate cancer cells is Polycomb-independent. *Science* **338**, 1465-1469 (2012).

105. S. Varambally, S. M. Dhanasekaran, M. Zhou, T. R. Barrette, C. Kumar-Sinha, M. G. Sanda, D. Ghosh, K. J. Pienta, R. G. Sewalt, A. P. Otte, M. A. Rubin, A. M. Chinnaiyan, The polycomb group protein EZH2 is involved in progression of prostate cancer. *Nature* **419**, 624-629 (2002).

106. C. G. Kleer, Q. Cao, S. Varambally, R. Shen, I. Ota, S. A. Tomlins, D. Ghosh, R. G. Sewalt, A. P. Otte, D. F. Hayes, M. S. Sabel, D. Livant, S. J. Weiss, M. A. Rubin, A. M. Chinnaiyan, EZH2 is a marker of aggressive breast cancer and promotes neoplastic transformation of breast epithelial cells. *Proceedings of the National Academy of Sciences of the United States of America* **100**, 11606-11611 (2003).

107. T. Sato, A. Kaneda, S. Tsuji, T. Isagawa, S. Yamamoto, T. Fujita, R. Yamanaka, Y. Tanaka, T. Nukiwa, V. E. Marquez, Y. Ishikawa, M. Ichinose, H. Aburatani, PRC2 overexpression and PRC2-target gene repression relating to poorer prognosis in small cell lung cancer. *Scientific reports* **3**, 1911 (2013).

108. T. Ernst, A. J. Chase, J. Score, C. E. Hidalgo-Curtis, C. Bryant, A. V. Jones, K. Waghorn, K. Zoi, F. M. Ross, A. Reiter, A. Hochhaus, H. G. Drexler, A. Duncombe, F. Cervantes, D. Oscier, J. Boultwood, F. H. Grand, N. C. Cross, Inactivating mutations of the histone methyltransferase gene EZH2 in myeloid disorders. *Nature genetics* **42**, 722-726 (2010).

109. G. Nikoloski, S. M. Langemeijer, R. P. Kuiper, R. Knops, M. Massop, E. R. Tonnissen, A. van der Heijden, T. N. Scheele, P. Vandenberghe, T. de Witte, B. A. van der Reijden, J. H. Jansen, Somatic mutations of the histone methyltransferase gene EZH2 in myelodysplastic syndromes. *Nature genetics* **42**, 665-667 (2010).

110. S. N. Khan, A. M. Jankowska, R. Mahfouz, A. J. Dunbar, Y. Sugimoto, N. Hosono, Z. Hu, V. Cheriyath, S. Vatolin, B. Przychodzen, F. J. Reu, Y. Saunthararajah, C. O'Keefe, M. A. Sekeres, A. F. List, A. R. Moliterno, M. A. McDevitt, J. P. Maciejewski, H. Makishima, Multiple mechanisms deregulate EZH2 and histone H3 lysine 27 epigenetic changes in myeloid malignancies. *Leukemia* **27**, 1301-1309 (2013).

111. P. Ntziachristos, A. Tsirigos, P. Van Vlierberghe, J. Nedjic, T. Trimarchi, M. S. Flaherty, D. Ferres-Marco, V. da Ros, Z. Tang, J. Siegle, P. Asp, M. Hadler, I. Rigo, K. De Keersmaecker, J. Patel, T. Huynh, F. Utro, S. Poglio, J. B. Samon, E. Paietta, J. Racevskis, J. M. Rowe, R. Rabadan, R. L. Levine, S. Brown, F. Pflumio, M. Dominguez, A. Ferrando, I. Aifantis, Genetic inactivation of the polycomb repressive complex 2 in T cell acute lymphoblastic leukemia. *Nature medicine* **18**, 298-301 (2012).

112. Q. Cao, J. Yu, S. M. Dhanasekaran, J. H. Kim, R. S. Mani, S. A. Tomlins, R. Mehra, B. Laxman, X. Cao, J. Yu, C. G. Kleer, S. Varambally, A. M. Chinnaiyan,

Repression of E-cadherin by the polycomb group protein EZH2 in cancer. *Oncogene* **27**, 7274-7284 (2008).

113. A. Herrera-Merchan, L. Arranz, J. M. Ligos, A. de Molina, O. Dominguez, S. Gonzalez, Ectopic expression of the histone methyltransferase Ezh2 in haematopoietic stem cells causes myeloproliferative disease. *Nature communications* **3**, 623 (2012).

114. W. Beguelin, R. Popovic, M. Teater, Y. Jiang, K. L. Bunting, M. Rosen, H. Shen, S. N. Yang, L. Wang, T. Ezponda, E. Martinez-Garcia, H. Zhang, Y. Zheng, S. K. Verma, M. T. McCabe, H. M. Ott, G. S. Van Aller, R. G. Kruger, Y. Liu, C. F. McHugh, D. W. Scott, Y. R. Chung, N. Kelleher, R. Shaknovich, C. L. Creasy, R. D. Gascoyne, K. K. Wong, L. Cerchietti, R. L. Levine, O. Abdel-Wahab, J. D. Licht, O. Elemento, A. M. Melnick, EZH2 is required for germinal center formation and somatic EZH2 mutations promote lymphoid transformation. *Cancer cell* **23**, 677-692 (2013).

115. D. O'Carroll, S. Erhardt, M. Pagani, S. C. Barton, M. A. Surani, T. Jenuwein, The polycomb-group gene Ezh2 is required for early mouse development. *Molecular and cellular biology* **21**, 4330-4336 (2001).

116. I. H. Su, A. Basavaraj, A. N. Krutchinsky, O. Hobert, A. Ullrich, B. T. Chait, A. Tarakhovsky, Ezh2 controls B cell development through histone H3 methylation and Igh rearrangement. *Nature immunology* **4**, 124-131 (2003).

117. C. Simon, J. Chagraoui, J. Krosl, P. Gendron, B. Wilhelm, S. Lemieux, G. Boucher, P. Chagnon, S. Drouin, R. Lambert, C. Rondeau, A. Bilodeau, S. Lavallee, M. Sauvageau, J. Hebert, G. Sauvageau, A key role for EZH2 and associated genes in mouse and human adult T-cell acute leukemia. *Genes & development* **26**, 651-656 (2012).

118. T. Muto, G. Sashida, M. Oshima, G. R. Wendt, M. Mochizuki-Kashio, Y. Nagata, M. Sanada, S. Miyagi, A. Saraya, A. Kamio, G. Nagae, C. Nakaseko, K. Yokote, K. Shimoda, H. Koseki, Y. Suzuki, S. Sugano, H. Aburatani, S. Ogawa, A. Iwama, Concurrent loss of Ezh2 and Tet2 cooperates in the pathogenesis of myelodysplastic disorders. *The Journal of experimental medicine* **210**, 2627-2639 (2013).

119. S. C. Lee, S. Miller, C. Hyland, M. Kauppi, M. Lebois, L. Di Rago, D. Metcalf, S. A. Kinkel, E. C. Josefsson, M. E. Blewitt, I. J. Majewski, W. S. Alexander, Polycomb repressive complex 2 component Suz12 is required for hematopoietic stem cell function and lymphopoiesis. *Blood*, (2015).

120. J. Tan, X. Yang, L. Zhuang, X. Jiang, W. Chen, P. L. Lee, R. K. Karuturi, P. B. Tan, E. T. Liu, Q. Yu, Pharmacologic disruption of Polycomb-repressive complex 2-mediated gene repression selectively induces apoptosis in cancer cells. *Genes & development* **21**, 1050-1063 (2007).

121. W. Qi, H. Chan, L. Teng, L. Li, S. Chuai, R. Zhang, J. Zeng, M. Li, H. Fan, Y. Lin, J. Gu, O. Ardayfio, J. H. Zhang, X. Yan, J. Fang, Y. Mi, M. Zhang, T. Zhou, G. Feng, Z. Chen, G. Li, T. Yang, K. Zhao, X. Liu, Z. Yu, C. X. Lu, P. Atadja, E. Li, Selective inhibition of Ezh2 by a small molecule inhibitor blocks tumor cells proliferation. *Proceedings of the National Academy of Sciences of the United States of America* **109**, 21360-21365 (2012).

122. S. K. Knutson, T. J. Wigle, N. M. Warholic, C. J. Sneeringer, C. J. Allain, C. R. Klaus, J. D. Sacks, A. Raimondi, C. R. Majer, J. Song, M. P. Scott, L. Jin, J. J. Smith, E. J. Olhava, R. Chesworth, M. P. Moyer, V. M. Richon, R. A. Copeland, H. Keilhack, R. M. Pollock, K. W. Kuntz, A selective inhibitor of EZH2 blocks H3K27 methylation and kills mutant lymphoma cells. *Nature chemical biology* **8**, 890-896 (2012).

123. M. T. McCabe, H. M. Ott, G. Ganji, S. Korenchuk, C. Thompson, G. S. Van Aller, Y. Liu, A. P. Graves, A. Della Pietra, 3rd, E. Diaz, L. V. LaFrance, M. Mellinger, C. Duquenne, X. Tian, R. G. Kruger, C. F. McHugh, M. Brandt, W. H. Miller, D. Dhanak, S. K. Verma, P. J. Tummino, C. L. Creasy, EZH2 inhibition as a therapeutic strategy for lymphoma with EZH2-activating mutations. *Nature* **492**, 108-112 (2012).

124. S. K. Knutson, S. Kawano, Y. Minoshima, N. M. Warholic, K. C. Huang, Y. Xiao, T. Kadowaki, M. Uesugi, G. Kuznetsov, N. Kumar, T. J. Wigle, C. R. Klaus, C. J. Allain, A. Raimondi, N. J. Waters, J. J. Smith, M. Porter-Scott, R. Chesworth, M. P. Moyer, R. A. Copeland, V. M. Richon, T. Uenaka, R. M. Pollock, K. W. Kuntz, A. Yokoi, H. Keilhack, Selective inhibition of EZH2 by EPZ-6438 leads to potent antitumor activity in EZH2-mutant non-Hodgkin lymphoma. *Molecular cancer therapeutics* **13**, 842-854 (2014).

125. J. E. Campbell, K. W. Kuntz, S. K. Knutson, N. M. Warholic, H. Keilhack, T. J. Wigle, A. Raimondi, C. R. Klaus, N. Rioux, A. Yokoi, S. Kawano, Y. Minoshima, H. Choi, M. Porter Scott, N. J. Waters, J. J. Smith, R. Chesworth, M. P. Moyer, R. A. Copeland, EPZ011989, A Potent, Orally-Available EZH2 Inhibitor with Robust in

Vivo Activity. *ACS Med Chem Lett* **6**, 491-495 (2015).

126. K. D. Konze, A. Ma, F. Li, D. Barsyte-Lovejoy, T. Parton, C. J. Macnevin, F. Liu, C. Gao, X. P. Huang, E. Kuznetsova, M. Rougie, A. Jiang, S. G. Pattenden, J. L. Norris, L. I. James, B. L. Roth, P. J. Brown, S. V. Frye, C. H. Arrowsmith, K. M. Hahn, G. G. Wang, M. Vedadi, J. Jin, An orally bioavailable chemical probe of the Lysine Methyltransferases EZH2 and EZH1. *ACS chemical biology* **8**, 1324-1334 (2013).

127. W. Kim, G. H. Bird, T. Neff, G. Guo, M. A. Kerenyi, L. D. Walensky, S. H. Orkin, Targeted disruption of the EZH2-EED complex inhibits EZH2-dependent cancer. *Nature chemical biology* **9**, 643-650 (2013).

128. A. Scelfo, A. Piunti, D. Pasini, The controversial role of the Polycomb group proteins in transcription and cancer: how much do we not understand Polycomb proteins? *The FEBS journal* **282**, 1703-1722 (2015).

129. J. Qin, W. A. Whyte, E. Anderssen, E. Apostolou, H. H. Chen, S. Akbarian, R. T. Bronson, K. Hochedlinger, S. Ramaswamy, R. A. Young, H. Hock, The polycomb group protein L3mbtl2 assembles an atypical PRC1-family complex that is essential in pluripotent stem cells and early development. *Cell stem cell* **11**, 319-332 (2012).

130. Y. Guo, N. Nady, C. Qi, A. Allali-Hassani, H. Zhu, P. Pan, M. A. Adams-Cioaba, M. F. Amaya, A. Dong, M. Vedadi, M. Schapira, R. J. Read, C. H. Arrowsmith, J. Min, Methylation-state-specific recognition of histones by the MBT repeat protein L3MBTL2. *Nucleic acids research* **37**, 2204-2210 (2009).

131. M. Pratcorona, S. Abbas, M. A. Sanders, J. E. Koenders, F. G. Kavelaars, C. A. Erpelinck-Verschueren, A. Zeilemakers, B. Lowenberg, P. J. Valk, Acquired mutations in ASXL1 in acute myeloid leukemia: prevalence and prognostic value. *Haematologica* **97**, 388-392 (2012).

132. C. Gaebler, S. Stanzl-Tschegg, G. Heinze, B. Holper, T. Milne, G. Berger, V. Vecsei, Fatigue strength of locking screws and prototypes used in small-diameter tibial nails: a biomechanical study. *The Journal of trauma* **47**, 379-384 (1999).

133. D. Huesken, J. Lange, C. Mickanin, J. Weiler, F. Asselbergs, J. Warner, B. Meloon, S. Engel, A. Rosenberg, D. Cohen, M. Labow, M. Reinhardt, F. Natt, J. Hall, Design of a genome-wide siRNA library using an artificial neural network. *Nature biotechnology* **23**, 995-1001 (2005).

134. R. A. Dickins, M. T. Hemann, J. T. Zilfou, D. R. Simpson, I. Ibarra, G. J. Hannon, S. W. Lowe, Probing tumor phenotypes using stable and regulated synthetic microRNA precursors. *Nature genetics* **37**, 1289-1295 (2005).

135. A. G. Muntean, J. Tan, K. Sitwala, Y. Huang, J. Bronstein, J. A. Connelly, V. Basrur, K. S. Elenitoba-Johnson, J. L. Hess, The PAF complex synergizes with MLL fusion proteins at HOX loci to promote leukemogenesis. *Cancer cell* **17**, 609-621 (2010).

136. N. C. Riddle, A. Minoda, P. V. Kharchenko, A. A. Alekseyenko, Y. B. Schwartz, M. Y. Tolstorukov, A. A. Gorchakov, J. D. Jaffe, C. Kennedy, D. Linder-Basso, S. E. Peach, G. Shanower, H. Zheng, M. I. Kuroda, V. Pirrotta, P. J. Park, S. C. Elgin, G. H. Karpen, Plasticity in patterns of histone modifications and chromosomal proteins in Drosophila heterochromatin. *Genome research* **21**, 147-163 (2011).

137. M. E. Figueroa, M. Reimers, R. F. Thompson, K. Ye, Y. Li, R. R. Selzer, J. Fridriksson, E. Paietta, P. Wiernik, R. D. Green, J. M. Greally, A. Melnick, An integrative genomic and epigenomic approach for the study of transcriptional regulation. *PloS one* **3**, e1882 (2008).

138. B. E. Bernstein, T. S. Mikkelsen, X. Xie, M. Kamal, D. J. Huebert, J. Cuff, B. Fry, A. Meissner, M. Wernig, K. Plath, R. Jaenisch, A. Wagschal, R. Feil, S. L. Schreiber, E. S. Lander, A bivalent chromatin structure marks key developmental genes in embryonic stem cells. *Cell* **125**, 315-326 (2006).

139. T. S. Mikkelsen, M. Ku, D. B. Jaffe, B. Issac, E. Lieberman, G. Giannoukos, P. Alvarez, W. Brockman, T. K. Kim, R. P. Koche, W. Lee, E. Mendenhall, A. O'Donovan, A. Presser, C. Russ, X. Xie, A. Meissner, M. Wernig, R. Jaenisch, C. Nusbaum, E. S. Lander, B. E. Bernstein, Genome-wide maps of chromatin state in pluripotent and lineage-committed cells. *Nature* **448**, 553-560 (2007).

140. P. Koppikar, O. Abdel-Wahab, C. Hedvat, S. Marubayashi, J. Patel, A. Goel, N. Kucine, J. R. Gardner, A. P. Combs, K. Vaddi, P. J. Haley, T. C. Burn, M. Rupar, J. F. Bromberg, M. L. Heaney, E. de Stanchina, J. S. Fridman, R. L. Levine, Efficacy of the JAK2 inhibitor INCB16562 in a murine model of MPLW515L-induced thrombocytosis and myelofibrosis. *Blood* **115**, 2919-2927 (2010).

141. N. P. Dantuma, T. A. Groothuis, F. A. Salomons, J. Neefjes, A dynamic ubiquitin equilibrium couples proteasomal activity to chromatin remodeling. *The Journal of cell biology* **173**, 19-26 (2006).

142. A. R. Kumar, Q. Li, W. A. Hudson, W. Chen, T. Sam, Q. Yao, E. A. Lund, B. Wu, B. J. Kowal, J. H. Kersey, A role for MEIS1 in MLL-fusion gene leukemia. *Blood* **113**, 1756-1758 (2009).
143. A. Takeda, C. Goolsby, N. R. Yaseen, NUP98-HOXA9 induces long-term proliferation and blocks differentiation of primary human CD34+ hematopoietic cells. *Cancer research* **66**, 6628-6637 (2006).
144. K. L. MacKenzie, A. Dolnikov, M. Millington, Y. Shounan, G. Symonds, Mutant N-ras induces myeloproliferative disorders and apoptosis in bone marrow repopulated mice. *Blood* **93**, 2043-2056 (1999).
145. B. S. Braun, J. A. Archard, J. A. Van Ziffle, D. A. Tuveson, T. E. Jacks, K. Shannon, Somatic activation of a conditional KrasG12D allele causes ineffective erythropoiesis in vivo. *Blood* **108**, 2041-2044 (2006).
146. R. L. Darley, T. G. Hoy, P. Baines, R. A. Padua, A. K. Burnett, Mutant N-RAS induces erythroid lineage dysplasia in human CD34+ cells. *The Journal of experimental medicine* **185**, 1337-1347 (1997).
147. J. Zhang, M. Socolovsky, A. W. Gross, H. F. Lodish, Role of Ras signaling in erythroid differentiation of mouse fetal liver cells: functional analysis by a flow cytometry-based novel culture system. *Blood* **102**, 3938-3946 (2003).
148. B. S. Braun, D. A. Tuveson, N. Kong, D. T. Le, S. C. Kogan, J. Rozmus, M. M. Le Beau, T. E. Jacks, K. M. Shannon, Somatic activation of oncogenic Kras in hematopoietic cells initiates a rapidly fatal myeloproliferative disorder. *Proceedings of the National Academy of Sciences of the United States of America* **101**, 597-602 (2004).
149. T. C. Somervaille, M. L. Cleary, Identification and characterization of leukemia stem cells in murine MLL-AF9 acute myeloid leukemia. *Cancer cell* **10**, 257-268 (2006).
150. K. Moran-Crusio, L. Reavie, A. Shih, O. Abdel-Wahab, D. Ndiaye-Lobry, C. Lobry, M. E. Figueroa, A. Vasanthakumar, J. Patel, X. Zhao, F. Perna, S. Pandey, J. Madzo, C. Song, Q. Dai, C. He, S. Ibrahim, M. Beran, J. Zavadil, S. D. Nimer, A. Melnick, L. A. Godley, I. Aifantis, R. L. Levine, Tet2 loss leads to increased hematopoietic stem cell self-renewal and myeloid transformation. *Cancer cell* **20**, 11-24 (2011).
151. A. Mullally, S. W. Lane, B. Ball, C. Megerdichian, R. Okabe, F. Al-Shahrour, M. Paktinat, J. E. Haydu, E. Housman, A. M. Lord, G. Wernig, M. G. Kharas, T. Mercher, J. L. Kutok, D. G. Gilliland, B. L. Ebert, Physiological Jak2V617F expression causes a lethal myeloproliferative neoplasm with differential effects on hematopoietic stem and progenitor cells. *Cancer cell* **17**, 584-596 (2010).
152. A. P. Bracken, K. Helin, Polycomb group proteins: navigators of lineage pathways led astray in cancer. *Nature reviews. Cancer* **9**, 773-784 (2009).
153. R. Margueron, D. Reinberg, The Polycomb complex PRC2 and its mark in life. *Nature* **469**, 343-349 (2011).
154. M. Sauvageau, G. Sauvageau, Polycomb group proteins: multi-faceted regulators of somatic stem cells and cancer. *Cell stem cell* **7**, 299-313 (2010).
155. J. Score, C. Hidalgo-Curtis, A. V. Jones, N. Winkelmann, A. Skinner, D. Ward, K. Zoi, T. Ernst, F. Stegelmann, K. Dohner, A. Chase, N. C. Cross, Inactivation of

polycomb repressive complex 2 components in myeloproliferative and myelodysplastic/myeloproliferative neoplasms. *Blood* **119**, 1208-1213 (2012).

156. D. Landeira, S. Sauer, R. Poot, M. Dvorkina, L. Mazzarella, H. F. Jorgensen, C. F. Pereira, M. Leleu, F. M. Piccolo, M. Spivakov, E. Brookes, A. Pombo, C. Fisher, W. C. Skarnes, T. Snoek, K. Bezstarosti, J. Demmers, R. J. Klose, M. Casanova, L. Tavares, N. Brockdorff, M. Merkenschlager, A. G. Fisher, Jarid2 is a PRC2 component in embryonic stem cells required for multi-lineage differentiation and recruitment of PRC1 and RNA Polymerase II to developmental regulators. *Nature cell biology* **12**, 618-624 (2010).

157. X. Shen, W. Kim, Y. Fujiwara, M. D. Simon, Y. Liu, M. R. Mysliwiec, G. C. Yuan, Y. Lee, S. H. Orkin, Jumonji modulates polycomb activity and self-renewal versus differentiation of stem cells. *Cell* **139**, 1303-1314 (2009).

158. H. J. Lawrence, G. Sauvageau, R. K. Humphries, C. Largman, The role of HOX homeobox genes in normal and leukemic hematopoiesis. *Stem cells* **14**, 281-291 (1996).

159. E. Kroon, J. Krosl, U. Thorsteinsdottir, S. Baban, A. M. Buchberg, G. Sauvageau, Hoxa9 transforms primary bone marrow cells through specific collaboration with Meis1a but not Pbx1b. *The EMBO journal* **17**, 3714-3725 (1998).

160. G. L. Dalgliesh, K. Furge, C. Greenman, L. Chen, G. Bignell, A. Butler, H. Davies, S. Edkins, C. Hardy, C. Latimer, J. Teague, J. Andrews, S. Barthorpe, D. Beare, G. Buck, P. J. Campbell, S. Forbes, M. Jia, D. Jones, H. Knott, C. Y. Kok, K. W. Lau, C. Leroy, M. L. Lin, D. J. McBride, M. Maddison, S. Maguire, K. McLay, A. Menzies, T. Mironenko, L. Mulderrig, L. Mudie, S. O'Meara, E. Pleasance, A. Rajasingham, R. Shepherd, R. Smith, L. Stebbings, P. Stephens, G. Tang, P. S. Tarpey, K. Turrell, K. J. Dykema, S. K. Khoo, D. Petillo, B. Wondergem, J. Anema, R. J. Kahnoski, B. T. Teh, M. R. Stratton, P. A. Futreal, Systematic sequencing of renal carcinoma reveals inactivation of histone modifying genes. *Nature* **463**, 360-363 (2010).

161. T. J. Ley, L. Ding, M. J. Walter, M. D. McLellan, T. Lamprecht, D. E. Larson, C. Kandoth, J. E. Payton, J. Baty, J. Welch, C. C. Harris, C. F. Lichti, R. R. Townsend, R. S. Fulton, D. J. Dooling, D. C. Koboldt, H. Schmidt, Q. Zhang, J. R. Osborne, L. Lin, M. O'Laughlin, J. F. McMichael, K. D. Delehaunty, S. D. McGrath, L. A. Fulton, V. J. Magrini, T. L. Vickery, J. Hundal, L. L. Cook, J. J. Conyers, G. W. Swift, J. P. Reed, P. A. Alldredge, T. Wylie, J. Walker, J. Kalicki, M. A. Watson, S. Heath, W. D. Shannon, N. Varghese, R. Nagarajan, P. Westervelt, M. H. Tomasson, D. C. Link, T. A. Graubert, J. F. DiPersio, E. R. Mardis, R. K. Wilson, DNMT3A mutations in acute myeloid leukemia. *The New England journal of medicine* **363**, 2424-2433 (2010).

162. R. D. Morin, M. Mendez-Lago, A. J. Mungall, R. Goya, K. L. Mungall, R. D. Corbett, N. A. Johnson, T. M. Severson, R. Chiu, M. Field, S. Jackman, M. Krzywinski, D. W. Scott, D. L. Trinh, J. Tamura-Wells, S. Li, M. R. Firme, S. Rogic, M. Griffith, S. Chan, O. Yakovenko, I. M. Meyer, E. Y. Zhao, D. Smailus, M. Moksa, S. Chittaranjan, L. Rimsza, A. Brooks-Wilson, J. J. Spinelli, S. Ben-Neriah, B. Meissner, B. Woolcock, M. Boyle, H. McDonald, A. Tam, Y. Zhao, A. Delaney, T. Zeng, K. Tse, Y. Butterfield, I. Birol, R. Holt, J. Schein, D. E.

Horsman, R. Moore, S. J. Jones, J. M. Connors, M. Hirst, R. D. Gascoyne, M. A. Marra, Frequent mutation of histone-modifying genes in non-Hodgkin lymphoma. *Nature* **476**, 298-303 (2011).

163. L. Pasqualucci, V. Trifonov, G. Fabbri, J. Ma, D. Rossi, A. Chiarenza, V. A. Wells, A. Grunn, M. Messina, O. Elliot, J. Chan, G. Bhagat, A. Chadburn, G. Gaidano, C. G. Mullighan, R. Rabadan, R. Dalla-Favera, Analysis of the coding genome of diffuse large B-cell lymphoma. *Nature genetics* **43**, 830-837 (2011).

164. E. R. Mardis, L. Ding, D. J. Dooling, D. E. Larson, M. D. McLellan, K. Chen, D. C. Koboldt, R. S. Fulton, K. D. Delehaunty, S. D. McGrath, L. A. Fulton, D. P. Locke, V. J. Magrini, R. M. Abbott, T. L. Vickery, J. S. Reed, J. S. Robinson, T. Wylie, S. M. Smith, L. Carmichael, J. M. Eldred, C. C. Harris, J. Walker, J. B. Peck, F. Du, A. F. Dukes, G. E. Sanderson, A. M. Brummett, E. Clark, J. F. McMichael, R. J. Meyer, J. K. Schindler, C. S. Pohl, J. W. Wallis, X. Shi, L. Lin, H. Schmidt, Y. Tang, C. Haipek, M. E. Wiechert, J. V. Ivy, J. Kalicki, G. Elliott, R. E. Ries, J. E. Payton, P. Westervelt, M. H. Tomasson, M. A. Watson, J. Baty, S. Heath, W. D. Shannon, R. Nagarajan, D. C. Link, M. J. Walter, T. A. Graubert, J. F. DiPersio, R. K. Wilson, T. J. Ley, Recurring mutations found by sequencing an acute myeloid leukemia genome. *The New England journal of medicine* **361**, 1058-1066 (2009).

165. D. Rohle, J. Popovici-Muller, N. Palaskas, S. Turcan, C. Grommes, C. Campos, J. Tsoi, O. Clark, B. Oldrini, E. Komisopoulou, K. Kunii, A. Pedraza, S. Schalm, L. Silverman, A. Miller, F. Wang, H. Yang, Y. Chen, A. Kernytsky, M. K. Rosenblum, W. Liu, S. A. Biller, S. M. Su, C. W. Brennan, T. A. Chan, T. G. Graeber, K. E. Yen, I. K. Mellinghoff, An inhibitor of mutant IDH1 delays growth and promotes differentiation of glioma cells. *Science* **340**, 626-630 (2013).

166. F. Delhommeau, S. Dupont, V. Della Valle, C. James, S. Trannoy, A. Masse, O. Kosmider, J. P. Le Couedic, F. Robert, A. Alberdi, Y. Lecluse, I. Plo, F. J. Dreyfus, C. Marzac, N. Casadevall, C. Lacombe, S. P. Romana, P. Dessen, J. Soulier, F. Viguie, M. Fontenay, W. Vainchenker, O. A. Bernard, Mutation in TET2 in myeloid cancers. *The New England journal of medicine* **360**, 2289-2301 (2009).

167. S. M. Langemeijer, R. P. Kuiper, M. Berends, R. Knops, M. G. Aslanyan, M. Massop, E. Stevens-Linders, P. van Hoogen, A. G. van Kessel, R. A. Raymakers, E. J. Kamping, G. E. Verhoef, E. Verburgh, A. Hagemeijer, P. Vandenberghe, T. de Witte, B. A. van der Reijden, J. H. Jansen, Acquired mutations in TET2 are common in myelodysplastic syndromes. *Nature genetics* **41**, 838-842 (2009).

168. N. Ahuja, H. Easwaran, S. B. Baylin, Harnessing the potential of epigenetic therapy to target solid tumors. *The Journal of clinical investigation* **124**, 56-63 (2014).

169. O. Abdel-Wahab, M. Adli, L. M. LaFave, J. Gao, T. Hricik, A. H. Shih, S. Pandey, J. P. Patel, Y. R. Chung, R. Koche, F. Perna, X. Zhao, J. E. Taylor, C. Y. Park, M. Carroll, A. Melnick, S. D. Nimer, J. D. Jaffe, I. Aifantis, B. E. Bernstein, R. L. Levine, ASXL1 mutations promote myeloid transformation through loss of PRC2-mediated gene repression. *Cancer cell* **22**, 180-193 (2012).

170. W. C. Skarnes, B. Rosen, A. P. West, M. Koutsourakis, W. Bushell, V. Iyer, A. O. Mujica, M. Thomas, J. Harrow, T. Cox, D. Jackson, J. Severin, P. Biggs, J. Fu, M.

Nefedov, P. J. de Jong, A. F. Stewart, A. Bradley, A conditional knockout resource for the genome-wide study of mouse gene function. *Nature* **474**, 337-342 (2011).

171. M. I. Love, W. Huber, S. Anders, Moderated estimation of fold change and dispersion for RNA-seq data with DESeq2. *Genome biology* **15**, 550 (2014).

172. M. B. Suraokar, M. I. Nunez, L. Diao, C. W. Chow, D. Kim, C. Behrens, H. Lin, S. Lee, G. Raso, C. Moran, D. Rice, R. Mehran, J. J. Lee, H. I. Pass, J. Wang, A. A. Momin, B. P. James, A. Corvalan, K. Coombes, A. Tsao, Wistuba, II, Expression profiling stratifies mesothelioma tumors and signifies deregulation of spindle checkpoint pathway and microtubule network with therapeutic implications. *Annals of oncology : official journal of the European Society for Medical Oncology / ESMO* **25**, 1184-1192 (2014).

173. B. A. Garcia, S. Mollah, B. M. Ueberheide, S. A. Busby, T. L. Muratore, J. Shabanowitz, D. F. Hunt, Chemical derivatization of histones for facilitated analysis by mass spectrometry. *Nature protocols* **2**, 933-938 (2007).

174. B. MacLean, D. M. Tomazela, N. Shulman, M. Chambers, G. L. Finney, B. Frewen, R. Kern, D. L. Tabb, D. C. Liebler, M. J. MacCoss, Skyline: an open source document editor for creating and analyzing targeted proteomics experiments. *Bioinformatics* **26**, 966-968 (2010).

175. A. V. Krivtsov, Z. Feng, M. E. Lemieux, J. Faber, S. Vempati, A. U. Sinha, X. Xia, J. Jesneck, A. P. Bracken, L. B. Silverman, J. L. Kutok, A. L. Kung, S. A. Armstrong, H3K79 methylation profiles define murine and human MLL-AF4 leukemias. *Cancer cell* **14**, 355-368 (2008).

176. H. O'Geen, L. Echipare, P. J. Farnham, Using ChIP-seq technology to generate high-resolution profiles of histone modifications. *Methods in molecular biology* **791**, 265-286 (2011).

177. Y. T. Phung, D. Barbone, V. C. Broaddus, M. Ho, Rapid generation of in vitro multicellular spheroids for the study of monoclonal antibody therapy. *Journal of Cancer* **2**, 507-514 (2011).

178. J. L. Hess, C. B. Bittner, D. T. Zeisig, C. Bach, U. Fuchs, A. Borkhardt, J. Frampton, R. K. Slany, c-Myb is an essential downstream target for homeobox-mediated transformation of hematopoietic cells. *Blood* **108**, 297-304 (2006).

179. A. P. Bracken, N. Dietrich, D. Pasini, K. H. Hansen, K. Helin, Genome-wide mapping of Polycomb target genes unravels their roles in cell fate transitions. *Genes & development* **20**, 1123-1136 (2006).

180. D. Lara-Astiaso, A. Weiner, E. Lorenzo-Vivas, I. Zaretsky, D. A. Jaitin, E. David, H. Keren-Shaul, A. Mildner, D. Winter, S. Jung, N. Friedman, I. Amit, Immunogenetics. Chromatin state dynamics during blood formation. *Science* **345**, 943-949 (2014).

181. K. Nishioka, J. C. Rice, K. Sarma, H. Erdjument-Bromage, J. Werner, Y. Wang, S. Chuikov, P. Valenzuela, P. Tempst, R. Steward, J. T. Lis, C. D. Allis, D. Reinberg, PR-Set7 is a nucleosome-specific methyltransferase that modifies lysine 20 of histone H4 and is associated with silent chromatin. *Molecular cell* **9**, 1201-1213 (2002).

182. G. Blum, G. Ibanez, X. Rao, D. Shum, C. Radu, H. Djaballah, J. C. Rice, M. Luo, Small-molecule inhibitors of SETD8 with cellular activity. *ACS chemical biology* **9**, 2471-2478 (2014).

183. P. Trojer, A. R. Cao, Z. Gao, Y. Li, J. Zhang, X. Xu, G. Li, R. Losson, H. Erdjument-Bromage, P. Tempst, P. J. Farnham, D. Reinberg, L3MBTL2 protein acts in concert with PcG protein-mediated monoubiquitination of H2A to establish a repressive chromatin structure. *Molecular cell* **42**, 438-450 (2011).

184. P. Trojer, G. Li, R. J. Sims, 3rd, A. Vaquero, N. Kalakonda, P. Boccuni, D. Lee, H. Erdjument-Bromage, P. Tempst, S. D. Nimer, Y. H. Wang, D. Reinberg, L3MBTL1, a histone-methylation-dependent chromatin lock. *Cell* **129**, 915-928 (2007).

185. J. Qin, D. Van Buren, H. S. Huang, L. Zhong, R. Mostoslavsky, S. Akbarian, H. Hock, Chromatin protein L3MBTL1 is dispensable for development and tumor suppression in mice. *The Journal of biological chemistry* **285**, 27767-27775 (2010).

186. C. Stielow, B. Stielow, F. Finkernagel, M. Scharfe, M. Jarek, G. Suske, SUMOylation of the polycomb group protein L3MBTL2 facilitates repression of its target genes. *Nucleic acids research* **42**, 3044-3058 (2014).

187. N. Herranz, D. Pasini, V. M. Diaz, C. Franci, A. Gutierrez, N. Dave, M. Escriva, I. Hernandez-Munoz, L. Di Croce, K. Helin, A. Garcia de Herreros, S. Peiro, Polycomb complex 2 is required for E-cadherin repression by the Snail1 transcription factor. *Molecular and cellular biology* **28**, 4772-4781 (2008).

188. I. Alimova, D. K. Birks, P. S. Harris, J. A. Knipstein, S. Venkataraman, V. E. Marquez, N. K. Foreman, R. Vibhakar, Inhibition of EZH2 suppresses self-renewal and induces radiation sensitivity in atypical rhabdoid teratoid tumor cells. *Neuro-oncology* **15**, 149-160 (2013).

189. M. D. Leiserson, F. Vandin, H. T. Wu, J. R. Dobson, J. V. Eldridge, J. L. Thomas, A. Papoutsaki, Y. Kim, B. Niu, M. McLellan, M. S. Lawrence, A. Gonzalez-Perez, D. Tamborero, Y. Cheng, G. A. Ryslik, N. Lopez-Bigas, G. Getz, L. Ding, B. J. Raphael, Pan-cancer network analysis identifies combinations of rare somatic mutations across pathways and protein complexes. *Nature genetics* **47**, 106-114 (2015).